PROJECT:

Development of Operational SFMR Validation and Processing Tools

NOAA Award No.:

NA07OAR4590426

DOCUMENT TITLE:

Final Report

Date: 27 February 2009 (Original)

Author: James Carswell and Dan Robinson, RSS
Eric Uhlhorn, NOAA / AOML / HRD

Update: 12 February 2010

TABLE OF CONTENTS

TABLE OF FIGURES

TABLE OF TABLES

1.0 Introduction

This document serves as the final report for the work performed and accomplishments of the Joint Hurricane Test Bed (JHT) project entitled, "Development of Operational SFMR Validation and Processing Tools." This project was a two year joint effort between Remote Sensing Solutions and the NOAA Hurricane Research Division (HRD). The NOAA Co-Principal Investigator was originally Dr. Peter Black. During the first year of the project, Dr. Black retired. Dr. Eric Uhlhorn of NOAA HRD assumed his role as the NOAA Co-PI. Because of difficulties experienced by HRD in hiring a CIMAS staff member, much their work was delayed.

1.1 Applicable Documents

The following documents serve as a reference to this work:

1. JHT Proposal: "Development of Operational SFMR Validation and Processing Tools".
2. JHT Project: Development of Operational SFMR Validation and Processing Tools – Year One Annual Report.

1.2 Document Breakdown

Section 1 contains the introduction. Section 2 reviews the work performed, results obtained and recommended actions to take. Appendix 1 provides details on original development of the new absorption model for the SFMR that was reported on in 2007. Appendix 2 through 4 described the file formats used by the real-time display application.

2.0 Work Performed and Accomplishments

2.1 Validation of Absorption Model

Dr. Carswell of RSS developed a new absorption model for the SFMR retrieval process and recommended in 2007 to the JHT Steering Committee that this new model be used for the operational retrieval process. The model being used at that time, and the model still being used today, over estimates the absorption due to precipitation. As a result, the rain rate retrievals produced by the SFMR retrieval processor under predict the true rain rate, and more importantly, the surface emission in the presence of precipitation is under estimated by the retrieval process. Thus, the retrieved surface wind speed underestimates the true wind speed in the presence of precipitation, and this under estimation (i.e. bias – not a random error) depends on both the wind speed and rain rate within the observed scene. Appendix 1 provides the details to the original analysis and development of the new model and its performance. Below the form of the model is shown:

$$K = \alpha\left(f^{R_m R_r^{Fe}}\right)\left(R_r^{R_e}\right) \qquad (1)$$

where,

R_r = rain rate (mm/hr)

$\square$ = 1.87×10^{-6} Np / km (constant)
f = frequency (GHz)
R_m = rain multiplier coefficient
R_e = rain exponent coefficient
F_e = frequency exponent coefficient

RSS derived new values for R_m, R_e and F_e. They were 2.8, 0.7 and 0.0756, respectively.

Dr. Peter Black (employed by HRD at the time) and Dr. Frank Marks expressed concerns about the new absorption model being proposed by RSS. HRD stated that they would further evaluate the model and make a recommendation. RSS was never provided details as to their concerns. Nevertheless, RSS continued to collect further data to validate and/or refine the new absorption model. A summary of the results are given below that provide clear evidence that the proposed absorption model is correct and consistent with other wind and precipitation sensors.

2.1.1 Validation of Rain Rate Retrievals

RSS and University of Massachusetts (UMass) upgraded the Imaging Wind and Rain Airborne Profiler in 2007 (now call AWRAP) to significantly enhance its sensitivity at C-band. With the modifications, the AWRAP system could measure rain rates on the order of 1 mm/hr and could penetrate to the surface even in the most intense rains in the eyewall. As a result an extensive set of coincident C-band volume reflectivity and ocean surface backscatter measurements and SFMR retrievals was collected in 2008. These C-band volume backscatter profiles were mapped to a 500-m along track grid in order to provide high resolution volume backscatter measurements that could matched and aligned to the SFMR sample volume and temporal sampling (both instruments were deployed on the same aircraft – N42RF). RSS derived wind speed and rain rate retrievals from the SFMR brightness temperature measurements using both the new and operational absorption models. The coincident rain rate retrievals were paired with the coincident IWRAP C-band volume reflectivity measurements (i.e. reflectivity factor, Z) for flights on 31 August 2008, 6 September 2008 and 7 September 2008. The reflectivity factor measurements were binned according to the SFMR rain rate estimates into 5 mm/hr bins. The average and standard deviation of the reflectivity factor measurements (linear scale) within each bin, as well as the mean rain rate for that bin, were calculated. The results are plotted in Figure 1. The solid circles are the average reflectivity factor value for each bin and the vertical lines are the standard deviation of the reflectivity factor measurements within the bin. The number above each line is the number of measurements within the bin. Note each reflectivity factor measurement is comprised of more than 4000 independent profiles assuming a 1 msec decorrelation time. Two Z-R models are over plotted. The dashed curve is the model used operationally prior to 2008 ($Z=300R^{1.4}$). In 2008, the WSR-88D Tropical Cyclone Operations Plan (date 5/12/2008, section 7d) changed its operational model for estimating precipitation to $Z=250R^{1.2}$ in order to provide more accurate estimates of tropical precipitation. This new model is shown by the solid black line. Two fits were performed to the measurements. For fit 1 (green curve) both the rain multiplier and exponent were solved for through a linear regression. For fit 2 (red curve), the rain

multiplier was set to 250 and the only the exponent was derived. In both cases, the derived Z-R relationships are essentially the same as the operational Z-R model for tropical precipitation.

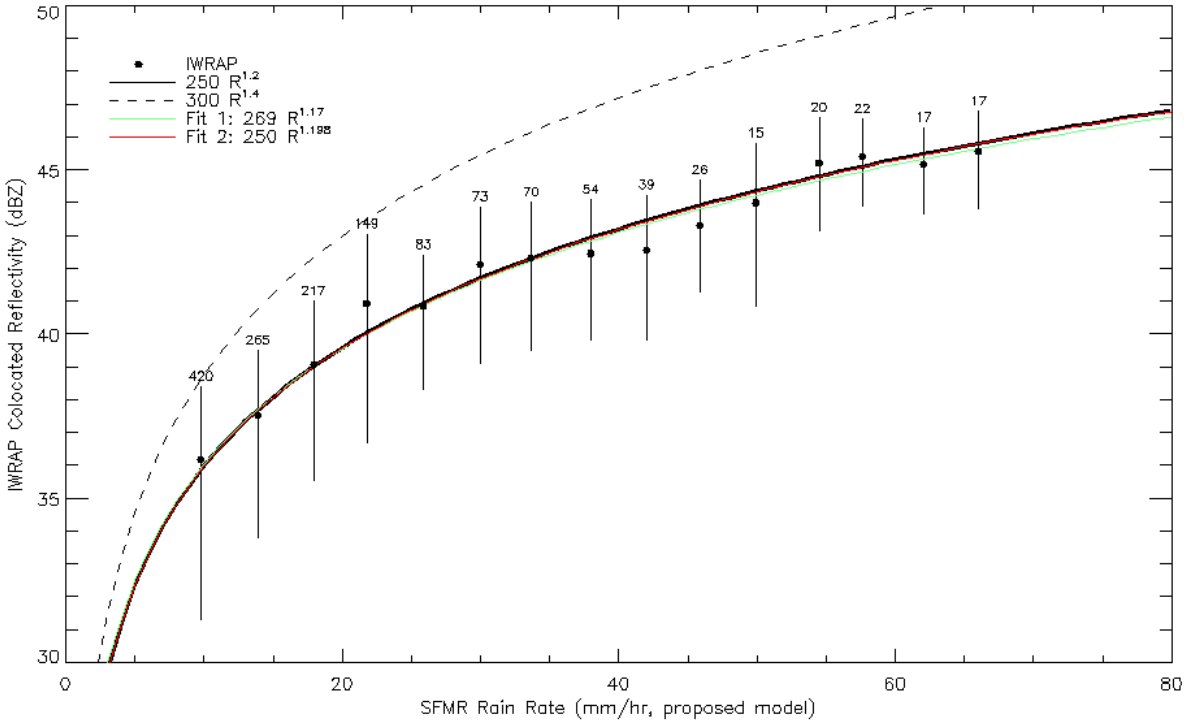

Figure 1: AWRAP coincident reflectivity measurements are averaged into 5 mm/hr rain rate bins based on the SFMR rain rate retrievals using the new absorption model. The solid circles represent the mean reflectivity factor and the vertical lines the standard deviation for the measurements within each bin. The black dashed and solid line are the old and new (2008) operational Z-R models for deriving tropical precipitation. The green and red curves are Z-R curves fit to the data. The rain multiplier and exponent were both derived for the green curve. The rain multiplier was set to 250 and the rain exponent derived for the red curve.

This strong agreement yet another independent verification of the new absorption model RSS proposed. That is, with the rain retrievals derived using the new absorption model result in the exact same Z-R relationship that was implemented operationally in 2008 for tropical precipitation retrievals.

For completeness the same comparison was performed using the rain rate retrievals derived with the old (or current) absorption model and shown in Figure 2. To no surprise, the resulting Z-R relationship agrees with the older operational Z-R model (not quite as well as the new absorption model agrees with the new operational Z-R model), which was found to significantly under predict the true precipitation rate. In both figures, the exact same set of Z measurements is used. The new operational Z-R retrieval algorithm was never used to derive the new absorption model coefficients, so this is a fully independent validation.

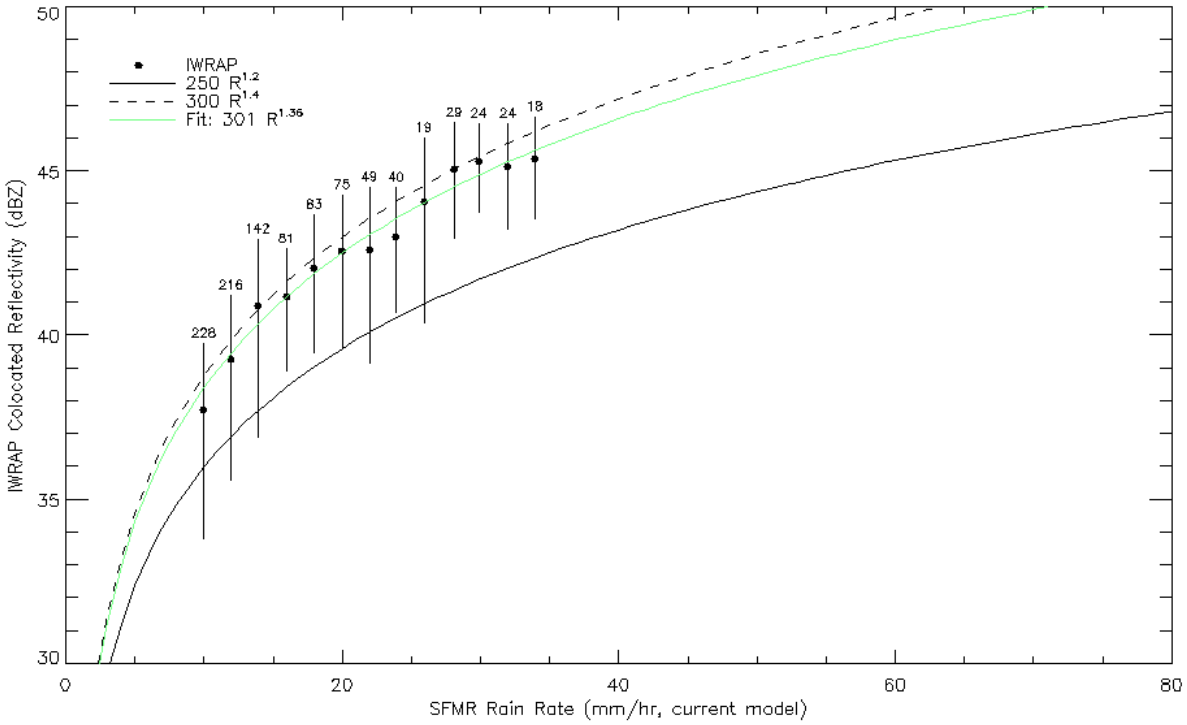

Figure 2: Same as figure 1 except the SFMR rain rate retrieval is derived using the old absorption model. The green curve is the fit to the data. Because of the rain rates using the old absorption model span less than half the range with the new model (i.e. under predict the rain rate) the rate rate bin was reduced in half to 2.5 mm/hr.

2.2 Ocean Surface Wind Speed Retrieval Error

As stated above, the real problem is that if the SFMR retrieval process underestimates the precipitation due to errors in its absorption model, the SFMR retrieval process will also under estimate the surface emissivity, and thus under estimate the ocean surface wind speed. In Appendix 1, diagrams are shown to illustrate the error in the wind speed retrieval as a function of the wind speed and rain rate conditions. To further illustrate this error, the error in the ocean surface wind speed for the measurements collected during these 2008 mission is plotted versus the SFMR rain rate retrieval in **Error! Reference source not found.** Panel (a) plots the error using the SFMR rain rate retrieval. In this plot the rain rate is that which is derived using the old absorption model. This is done so that if someone wants to compare to the archived measurements, they can use this plot. When no rain is present, there is no error. As the rain rate increases the SFMR retrievals using the old absorption model under estimate the ocean surface wind speed. The amount of under estimation depends on the wind speed as well. For these data however, the high rain rates only occurred at hurricane force winds. As shown by the figure, significant wind speed errors were encounter in 2008 because the old absorption model was used, and this model over estimates the absorption due to precipitation.

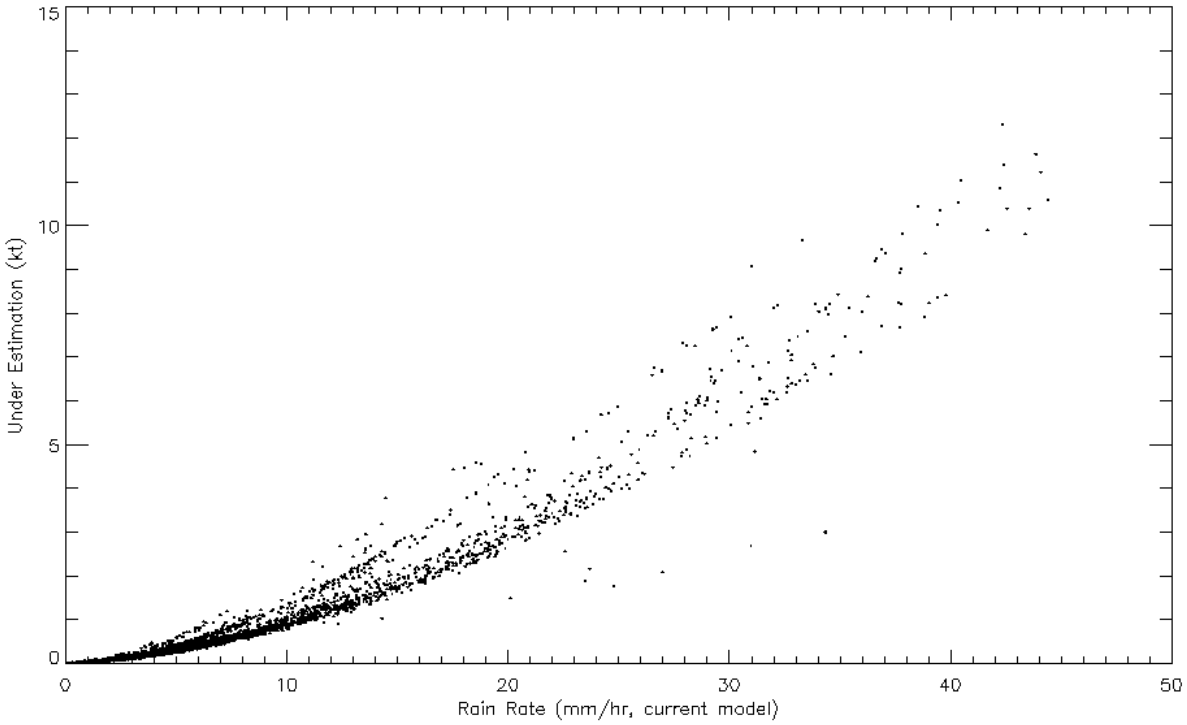

Figure 3: SFMR ocean surface wind speed retrieval error (true wind speed - retrieved wind speed) plotted versus the SFMR rain rate retrieval that was derived using the old absorption model. The data shown is from the exact same set of measurements shown in the figures.

To further illustrate the error in the SFMR wind speed retrievals, the AWRAP along track mean ocean surface normalized radar cross section (A0) was collocated with the SFMR oceans surface wind speed retrievals that were derived using the old and new absorption models. Figure 4 plots the A0 measurements collected at 50 degrees incidence and horizontal polarization versus the SFMR wind speed retrievals derived using the old absorption model. As with the reflectivity factor measurements, the A0 measurements were binned into 2 m/s bins (~ 4kt bins) and the mean A0 and wind speed value determined for each bin. The standard deviation of the A0 measurements within each bin is shown by the vertical line and the number of points indicated. The black curve is the C-band NRCS geophysical model function (IWRAP GMF) derived by Esteban et. al, 2006. The red curve is a fit to the A0 measurements. At the higher wind speeds where significant precipitation was present, the A0 values seem to be much higher than the model function predicts. This is an artifact of the SFMR wind speed retrievals being under estimated. Note that the IWRAP GMF was derived in rain free conditions. Figure 5 plots the same measurements except the SFMR retrievals were derived using the new absorption model. The A0 measurements are now in much closer agreement with the IWRAP GMF. This is further documentation of the errors introduced by the errors in the old absorption model and evidence that the new absorption model is correct.

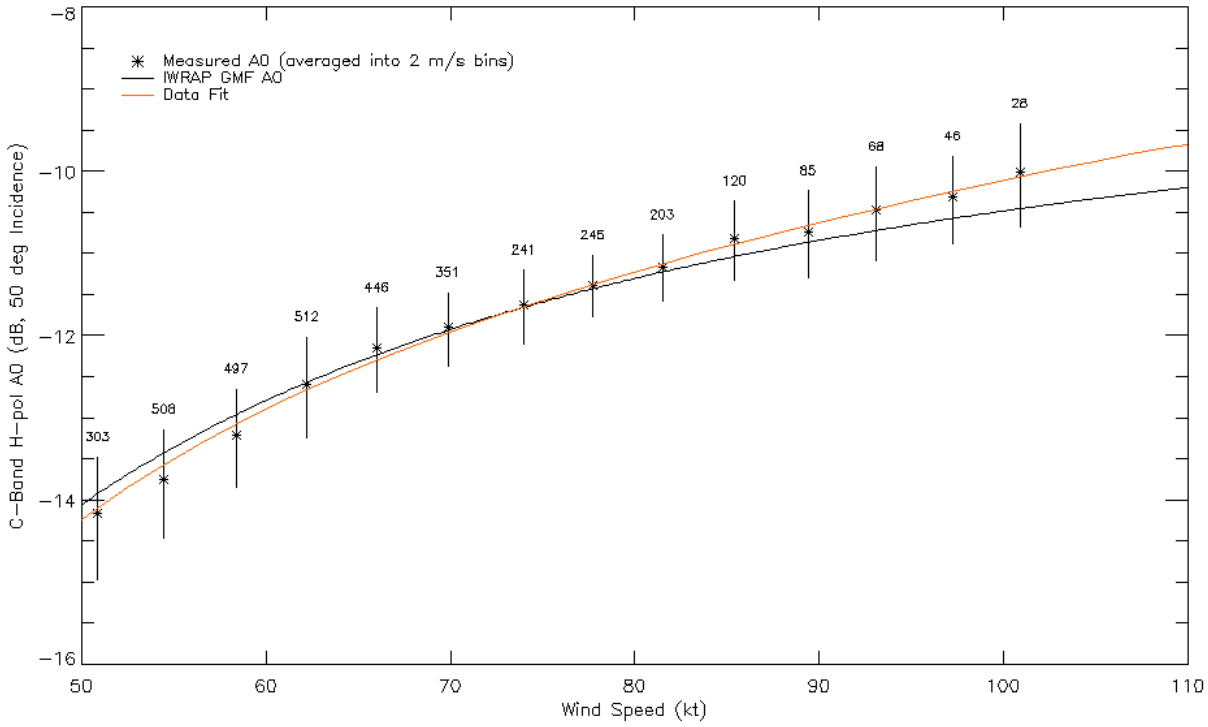

Figure 4: C-band mean NRCS measurements collected at 50 degrees incidence and horizontal polarization from missions on 31 August 2008, 6 September 2008 and 7 September 2008 are binned and averaged according to the collocated SFMR wind speed retrievals derived using the old absorption model and plotted. The black curve is the IWRAP NRCS GMF. The red curve is a fit to the measurements.

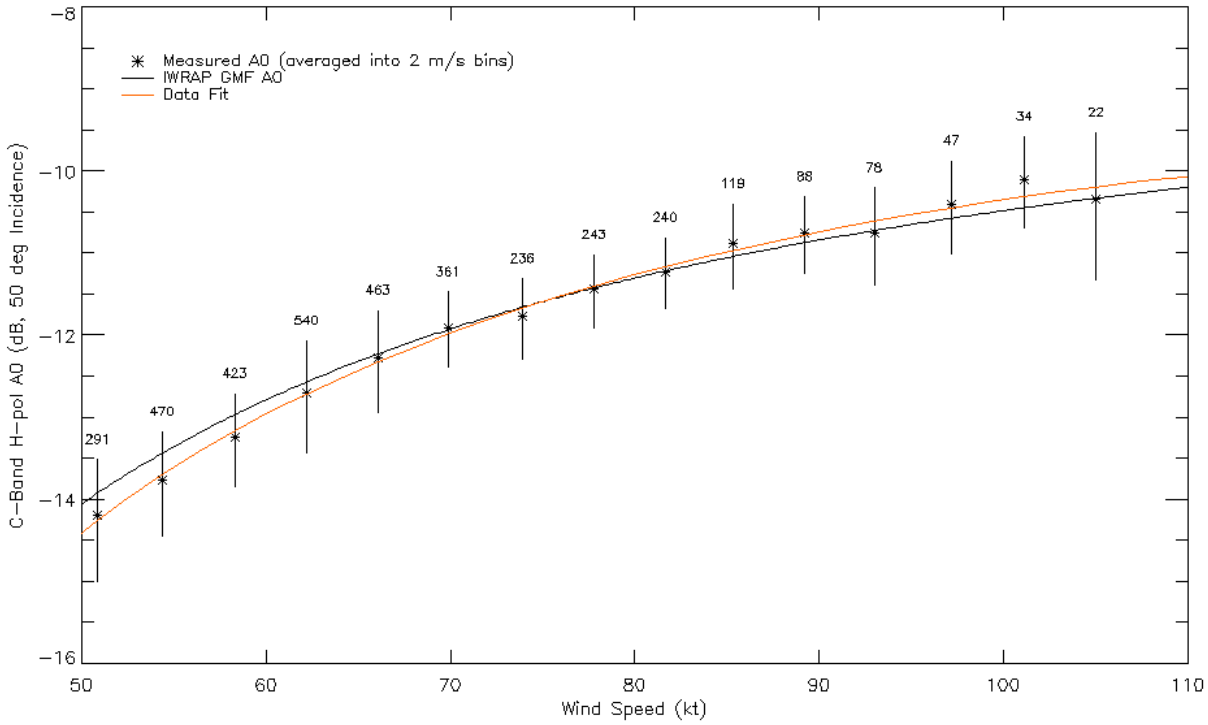

Figure 5: Same as figure 4 except the SFMR wind speed retrievals were derived using the new absorption model. The A0 measurements are in close agreement with the IWRAP NRCS GMF.

These data and analyzes clearly document that the new absorption model derived by RSS for the SFMR is much more accurate and is consistent with the operational models and measurements. The errors in the SFMR ocean surface wind speed retrievals are significant at hurricane force winds and the absorption model used in the operational retrieval algorithm should be replaced by the model proposed here.

2.3 Real-time Reconnaissance Data Processor Application

Remote Sensing Solutions designed, implemented and deployed a real-time reconnaissance data processor application. The primary objective of this data processor application is to collect and process the aircraft reconnaissance observations as soon they become available. A secondary objective is to create a complete archive of these data for use during post season analysis. Note that this application can also be run at any point on any computer to automatically build an identical data archive on that system. Specially, the application:

1) Gathers all reconnaissance high density observation (HDOB) and dropsonde files currently present and any new files as soon as they become available.
2) Extracts and quality controls the observations contained within these reconnaissance files.
3) Organizes the observations by storm (mission type when not storm).
4) Calculates the storm relative coordinates for each observation.
5) Colocates high density observations with dropsonde profile data.
6) Stores the observations and their storm relative coordinates into NetCDF files for viewing by the RSS Real-time Data Display Application (discussed in section 2.4).
7) Stores the collocated data in separate storm based NetCDF files.

This processor is designed to run unattended, 24 hours a day – 7 days a week (24/7). Since the application is Python-based, it can run on Linux, UNIX, MacIntosh, and Windows based computers. The only requirements are that the computer it resides on has Internet access to communicate with the servers receiving the posted reconnaissance and center fix data files, Python 2.3 or later, and the proper NetCDF libraries to handle archiving of processed data. The intent is to run this application at National Hurricane Center (NHC), but it could also be deployed at other Weather Field Offices (WFOs).

Figure 6 presents the flow chart of this application. The green boxes indicate python applications, the red boxes are data files in their original format and the yellow boxes are NetCDF files containing the quality controlled processed data.

The application consists of four main layers:

Layer 1: Initial acquisition

Layer 2: Quality control, parsing and location processing

Layer 3: Collocation processing

Layer 4: Storm Relative Processing

Note that Layer 0 will be discussed in section 2.3.9. It handles the automatic posting of the Air Force raw SFMR data files to NHC for use in post analysis and detailed validation studies. In the sub sections to follow, each layer will be discussed.

To minimize code changes and software maintenance from year to year associated with format changes in the reconnaissance data files and other data files, the processor has been developed such that only the parsing code in Layer 2 will need to be updated. The output of this second layer is a series of standard NetCDF files that all following applications read. Thus the second layer buffers all following layers and stages from format changes in the reconnaissance and other data files.

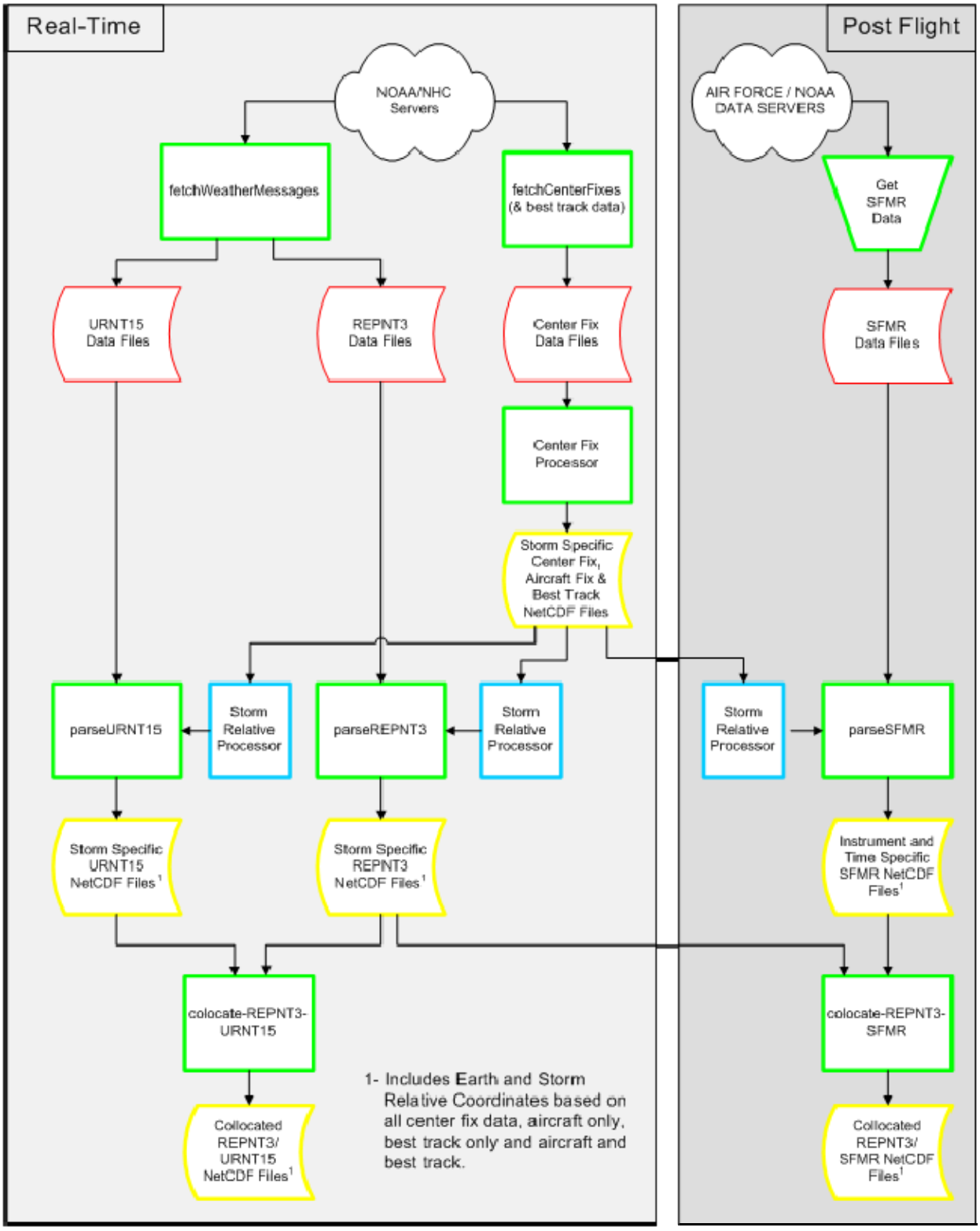

Figure 6: Flow chart of real-time and post flight processing. See section 2.3.9 for layer 0 application that automates the transmission of Air Force SFMR raw data files.

2.3.1 Version Control

The real-time reconnaissance data processor application, as well as all other code / applications described in this report, is maintained under a subversion version control repository at Remote Sensing Solutions. Access to this repository is achieved through a SSL URL. The applications and code deployed at NHC are a “working copy” of the code maintained by this version control system. During development and testing, as NHC hurricane specialists and staff members requested changes, new features, or found problems; Remote Sensing Solutions developers made the appropriate changes in the code base and committed the updated versions into the repository. NHC (Jose Salazar) then only had to issue a simply command, svn update, and the code and applications at NHC were automatically updated. Since the repository is posted on a SSL encrypted website, no special arrangements in terms of the NHC network or firewall had to be made to access the Remote Sensing Solutions repository, nor was Remote Sensing Solutions required to have access to the server which the applications and code were deployed on. This enabled seamless development and testing.

2.3.2 Layer 1 - Initial Acquisition

Layer 1 acquires and locally archives reconnaissance high density observation and dropsonde data files. It also gathers center fix and best track files that are used by the storm relative processor. This initial acquisition layer consists of two python applications: fetchWeatherMessages.py and fetchCenterFixes.py. Their functions are described below.

2.3.2.1 Weather Messages

The application, fetchWeatherMessages.py, automatically detects and retrieves reconnaissance data files as they are posted to the NOAA web site:

Error! Hyperlink reference not valid.

It then also stores the files in a local archive. The file types include, but are not limited to, HDOB (URNT15), REPNT2 and REPNT3. An XML configuration file governs the operation of this application by specifying the data types it should fetch and their relative location within the archive. It also allows the user to specify other parameters, such as the year. Normally, this application fetches data from the current year (i.e. assumes real-time operation), but it can also retrieve files from past years (using a different URL). This feature allows users to automatically build full archives of the reconnaissance data when desired. The primary data server from which it retrieves these data files is ‘ratfish’. NHC personnel instructed us to use this server as it would provide reliable, 24/7 access. The data server is a configurable variable within the application, and thus can be easily changed if the server address is changed in the future.

In its normal running mode, the application queries the website every 30 seconds and auto-discovers any new files that have been posted. Once new files are detected, the application retrieves these files and writes each to the local archive. The application can be run unattended, 24/7. Remote Sensing Solutions has run this application on several Linux-based servers throughout the 2007 and 2008 hurricane season without fault.

2.3.2.2 Center Fixes

The application, fetchCenterFixes.py, retrieves center fix data files posted at:

ftp://ftp.nhc.noaa.gov/atcf/fix

and best track files posted at:

ftp://ftp.nhc.noaa.gov/atcf/btk

This application detects any new or modified files that are posted for the specified year and downloads each to its local archive. Normally it runs in a loop back mode checking for new data every two minutes. It is designed to run unattended, 24/7. It was run full-time during the 2007 and 2008 hurricane seasons without fault. This application also has a switch so that if instructed by the Real-time Display Application, it will download all modified files associated with a particular storm. This feature was added so that hurricane specialists who were working on post season best tracks could modify the best track file for a particular storm and visualize the impact these modifications had on the storm relative display of the reconnaissance data (radial plots and latitude/longitude maps).

2.3.3 Layer 2 – QOC, Parsing & Storm Relative Processing

Layer 2 serves three primary purposes. It implements a buffer zone to handle changes in reconnaissance and other data formats. Each year recommendations are implemented that potentially modify the structure and/or format of the reconnaissance data files, storm files and data servers. To prevent these changes from propagating through the entire real-time reconnaissance data processor application and subsequent applications, and to increase the IO efficiency of the third layer and later processing stages, layer 2 parses the files retrieved by layer 1, which are in the format specified by the National Hurricane Operations Plan (NHOP) document, and stores the parsed information in standard formats within NetCDF files. In this manner, layer 3 applications and later stages are unaffected by format changes in the initial files (e.g. those regulated by NHOP). With NetCDF files, later applications can be written to automatically configure themselves and self generate read procedures to access data within the NetCDF files. The applications can efficiently access subsets of these files (i.e. individual variables) with block reads rather than complicated pointer manipulation and single reads. This significantly reduces software development and maintenance time and improves run time efficiency.

Each parser also follows a QOC rule-set to detect, and correct or remove, any errors in the original files such that later applications are not impacted. It has been our experience that the reconnaissance files contain several errors and that significant coding is required to catch and correct these errors. Identifying errors in layer 2 significantly reduces the amount of QOC monitoring and handling in layer 3 applications and beyond, thus improving their performance and simplifying their development. We found that the QOC rule-set developed during the 2007 season required only a few small additions in 2008 to handle all error cases experienced.

Currently, layer 2 consists of three main applications: center fix processor, URNT15 parser and the REPNT3 parser. Future expansion of this layer may include parsers for other reconnaissance data or other data types that are needed for the processing stages that follow. The center fix processor, URNT15 parser and REPNT3 parser are described below.

2.3.3.1 Center Fix Processor

The center fix processor monitors the center fix file archive (i.e. center fix and best track files) created by the level 1 application, fetchCenterFixes.py. When new data arrives, it passes the data through the quality control procedure, extracts the new center fix estimates (i.e. time, latitude, longitude, etc), interpolates to 30 second intervals between fixes and writes the data to NetCDF files. Four NetCDF files are generated for each storm.

Table 1 describes the data used to derive each of these files and Appendix 1 provides a description of the NetCDF file format. Four different files were generated to address different needs or requests from NHC specialists. As will be shown later, the display application can display the observations based storm relative coordinates that are derived from all center fix data, aircraft center fixes only, best track center fixes only and a combination of aircraft and best track center fixes.

Table 1: Description of the NetCDF Center Fix File Types

File Name	Data Contained
<centerFix>-<storm name>[1].nc	All fixes in atfc/fix files.
<bestTrack>-<storm name>[1].nc	Best track fix locations from atfc/btk files.
<aircraft>-<storm name>[1].nc	Aircraft only (AIRC) fixes from atfc/fix files.
<airc_bst>-<storm name>[1].nc	Aircraft and best track fixes.

[1]: <storm name> is the assigned storm name or mission type (e.g. IKE)

Although the TD number is available for the center fix files, the consensus was to use the storm name to uniquely label the output NetCDF files. This also provides consistency with the reconnaissance data which does not always contain the TD number but does contain the storm name. A table is used by the application to relate the TD number and storm name. A future update to the application would automate the generation of this table by accessing a site that publishes the TD number and storm name relationship. Note that the names are known in advance, therefore only the TD number must be supplied, or adjusted if a tropical depression occurs but does not develop into a storm. This application also extrapolates the center fix data 30 minutes beyond the last fix by using the last known storm motion. A flag in these files indicates whether the data point is an actual data point from the original file, or whether it has been interpolated or extrapolated. For the actual data points, the flag also indicates its source (i.e. AIRC, DVTS, BEST, etc.). Values that are extrapolated are replaced when new center fixes arrive that cover the extrapolated time frame. Extrapolation is needed

to ensure that the storm relative processor for the reconnaissance data processors obtains the information it needs.

This application has been running without fault at Remote Sensing Solutions since the 2007 hurricane season, and was deployed at NHC during the 2008 hurricane season.

2.3.4 Storm Relative Processor

The storm relative processor was built as a python module to enable its use by all parsers to map their data into a storm relative coordinate system. At each run, this module updates its center fix locations contained within the files listed in Table 1. For each observation (i.e. SFMR wind speed, dropsonde wind measurement, etc), the storm relative processor identifies the center fix location that is closest in time using an efficient index method. It calculates the radial distance and angle from the center fix location at the time the data point was acquired to the data point location (i.e. storm relative coordinate system). It does this for each of the four center fix data types. The processor passes this storm relative positions back to the calling program so that they can be stored along with the observation in the observation's NetCDF file (e.g. URNT15-<storm name>.nc). In this manner, the reconnaissance observations can be mapped to a center fix location at any point in time by mapping the storm relative coordinate system to that center fix location. The data may also be displayed in terms of storm quadrant and radial distance from the storm's center fix location.

During operation, the storm relative processor continues to check for updated center fix data. It then updates coordinates that were based on extrapolated values as soon as the actual values are available in the center fix file created in layer 1. Recall that the layer 1 application extrapolates data 30 minutes beyond the last center fix to ensure that a center fix location is always available. Once again, when it does extrapolate, a flag is set to notify the storm relative processor that the value is extrapolated, not measured.

To illustrate the storm relative processing, Figure 7 displays an image derived from the Real-time Display Application (image capture of display – mouse click function). The data shown contains all reconnaissance observations of Hurricane IKE that were collected within a +/- 24 hour window of 12 September 12Z. The SFMR wind speed and flight level wind speed observations are plotted in the upper left panel as a function of time and overlaid on the GIS view. Also shown in the panels counter clockwise from the wind speed time series plot are the SFMR rain rate estimates, extrapolated surface pressure, aircraft altitude (more than one aircraft was present at a time), flight level air temperature and flight level dew point. Note that the purpose here is not to show these plots in detail, as their detailed view will be shown later, but to show the storm relative processor capability. To this end, Figure 8 plots the same data with the GIS view displaying the wind speed measurements plotted using the storm relative coordinates (derived from all aircraft center fix messages and interpolated in time) mapped to the center fix at the time stated above. Figure 9 zooms in further on the GIS storm relative view and also plots the wind speed as a function of the radial distance from the storm center for each quadrant of the storm (NW – upper left, NE – upper right, SW – middle left and SE – middle right). As these figures reveal, much more information can be

derived about the storm structure (i.e. hurricane force winds by quadrant) from the storm relative processed data, and the storm relative processor is functioning very well. The radial plots provide a quick graphical tool to determine the hurricane wind radii as a function of the storm quadrant. They also demonstrate how well the storm relative processor is performing. If it was in error, one would see wind speed radial profiles approach 0 m/s (i.e. center of the storm) at a radius greater than the eye. None are present.

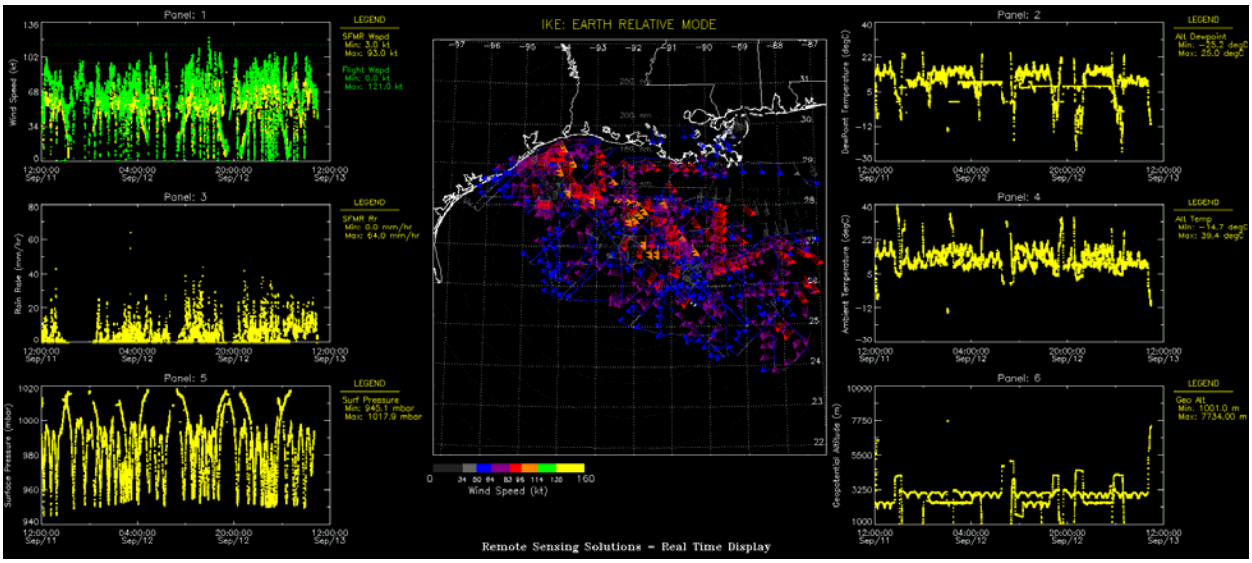

Figure 7: Image generated from the Real-time Display Application. Observations shown are of Hurricane Ike over a 48 hour period centered at 12Z on 12 September 2008.

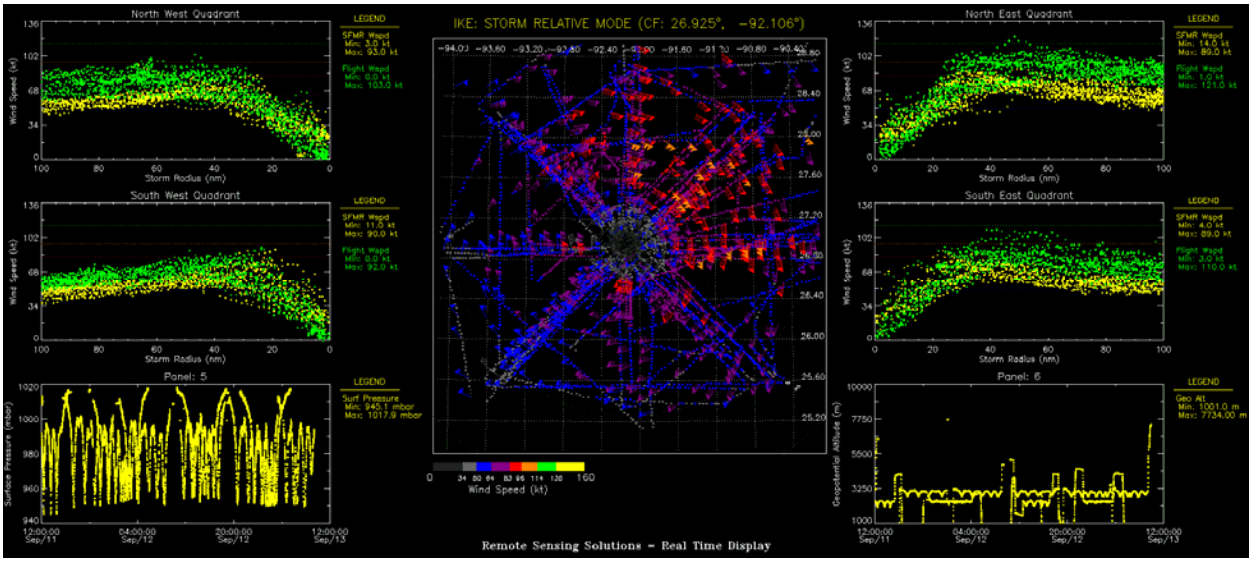

Figure 8: Same as Figure 7 but the GIS view is showing the observations using the storm relative coordinates and the center fix location at 12Z on 12 September 2008.

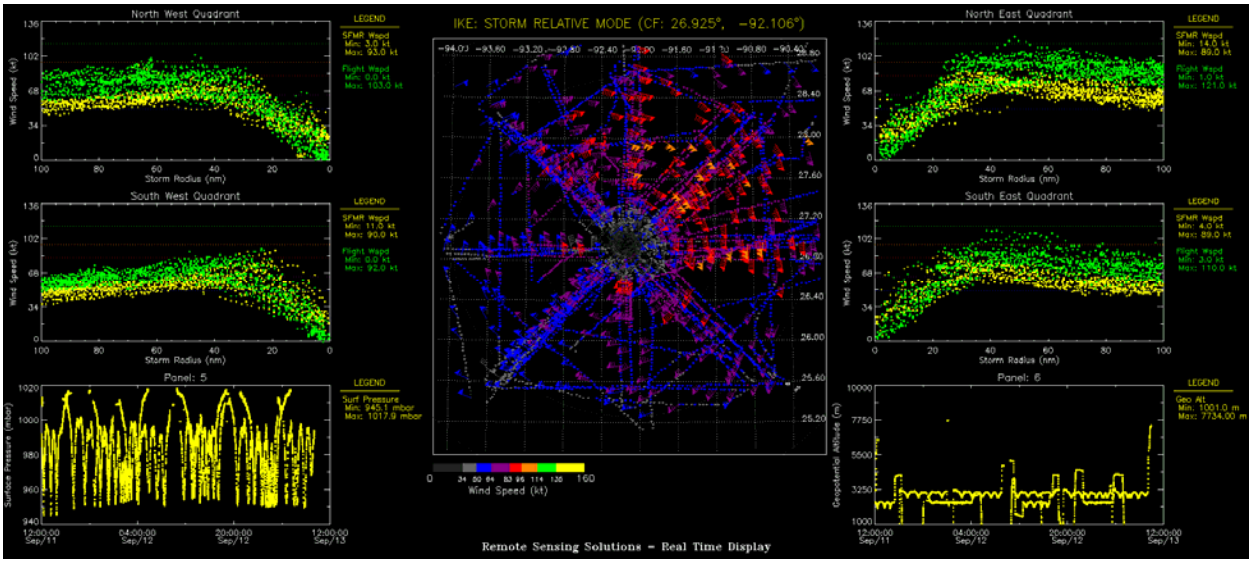

Figure 9: Same data shown in Figure 7 except radial plots of the SFMR and flight level wind speed observations for each storm quadrant are plotted and the data in the GIS view is plotted based on their storm relative coordinates and center fix at 12Z on 12 September 2008. GIS view can be zoomed in to 4 degrees and all data shown since the storm motion has been removed.

2.3.5 URNT15 Parser

The URNT15 parser application monitors the high density observations files (i.e. URNT15) in the local archive detecting the presence of any new files. When a new file appears, the parser reads this file and determines which TD number or storm it belongs to. Following a specific rule-set, it quality controls the data within the file, extracts each parameter into its NetCDF variable, calls the storm relative processing function to determine the storm relative coordinates for each point and writes the variables and storm relative coordinates to output the storm NetCDF file. Appendix 2 describes the format of this NetCDF and the data it contains. Note that all information, including its source (i.e. aircraft), is stored with the observations. The NetCDF file naming structure follows that described for the center fix files. For example all URNT15 data that were collected from missions through “Dean” are stored in the URNT15-DEAN.nc file.

As with previously built applications, this module runs continuously in an unattended mode (24/7). It has a variable timing loop that by default is set to 30 seconds (the minimal reporting interval). Remote Sensing Solutions has run this application throughout the 2007 and 2008 hurricane seasons to ensure its performance and ability to trap and handle errors in the original files. It has been running without fault since early September 2007. It was deployed at NHC during the 2008 hurricane season and has operated without fault since then.

2.3.6 REPNT3 Parser

The REPNT3 parser application is built and runs similarly to the URNT15 parser application except that it parses the GPS dropsonde data rather than the high density observations. Currently this parser only extracts Part A - the standard levels. If needed,

it could be modified to parse Part B of these files as well. Similar to the previous parser, it also calculates the storm relative coordinate system for each data point and stores the parsed data in NetCDF files sorted by splash time and organized by storm name. Appendix 3 describes the format of these NetCDF files. The application is designed to run unattended, 24/7, and by default checks for new files every 30 seconds. Remote Sensing Solutions has run this application since the 2007 hurricane season to ensure it handles all errors in the original files. It has been running without fault since September. It was deployed at NHC during the 2008 hurricane season.

2.3.7 Layer 3 – Collocation Processing

To provide real-time validation of the SFMR retrievals and a data archive that can be used for more in-depth analysis following the hurricane season, a collocation processor was designed and built. Similar to applications in layers 1 and 2, this processor is designed to run unattended, 24/7. Its primary objective is to discover all URNT15 and REPNT3 data that are within a specified distance and time window of one another. Note that the main criterion is distance since the aircraft moves quickly from the dropsonde and the wind field changes quickly in the radial direction (direction most often flown by the aircraft). The time filter serves as a means to prevent later flight legs that may over fly the splash point from being used. The splash location and splash time of the REPNT3 are used for this collocation since the SFMR measures the surface wind.

Monitoring the parsed URNT15 and REPNT3 files, this application detects when new data are present. It then determines if the new data are collocated within the specified distance and time window. For each data point that meets this criterion, the URNT15 and REPNT3 variables for that point are written to a collocation NetCDF file. These collocation files are organized by storm name. Along with the data, the distance and time separation between the URNT15 and REPNT3 data is stored so that later applications can use a stricter window if needed. Appendix 4 describes the format of these NetCDF files.

Remote Sensing Solutions has run this application during the 2007 hurricane season, and it continues to run without fault. Figure 10 plots the flight track for a mission through Hurricane DEAN on 19 August, 2007. The location of the SFMR retrievals is shown by the black and green dots. The green dots indicate those points that met the collocation criteria of 15 km and 1 hour within the splash location (red dots) and time of a GPS dropsonde measurement. The black circles show the 15 km radius circle around the splash location. For reference, time stamps are given at the blue triangles and the observation number for each dropsonde is given. As this figure shows, the collocation process (and all the other processes discussed above) are performing as intended.

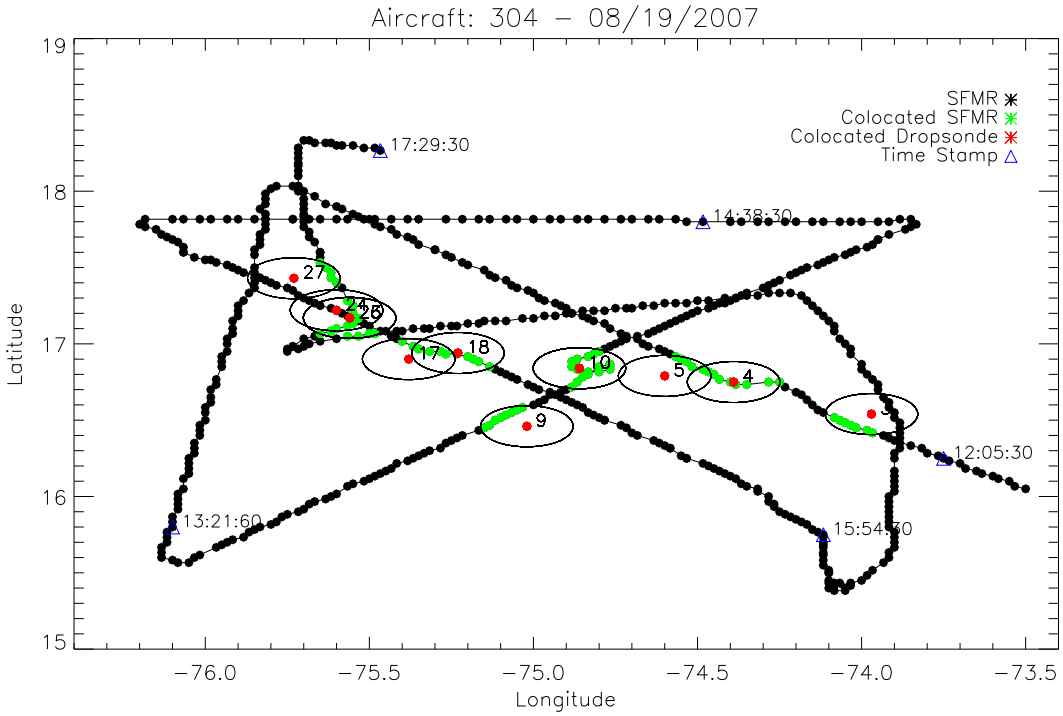

Figure 10: Flight track on 19 August 2007 through Hurricane Dean is plotted. The black and green dots show the SFMR measurement locations with green indicating those found to be within 15 km and 1 hour of a GPS dropsonde splash location (red dots). A 15 km radius circle around each splash location is drawn and the observation number given. Time stamps along the flight track are marked by the blue triangles as a reference.

2.3.8 Layer 4 – Storm Relative NAWIPS File Creation

A need originally existed for viewing storm relative data via the NAWIPS system. Generating files that can be ingested directly into NAWIPS would allow for visualization of these data sets while leveraging an existing and familiar visualization tool. NAWIPS currently does not provide storm relative processing. To meet this need and overcome NAWIPS' limitations, Remote Sensing Solutions created an application that uses the storm relative coordinates within the NetCDF URNT15 and REPTN3 data files to create GEMPAK ship files at specific (programmable) time intervals that contain the storm relative observations mapped to the center fix time of the file. It filtered the observations based on a configurable time (e.g. +/- 6 hours). Essentially this removed the storm motion for the aircraft measurements allowing them to represent a spatial snapshot in time of the tropical storm or cyclone as was depicted in Figure 8 and Figure 9. The application was written in Python for operating system portability and has been run and unit tested successfully at RSS. It is designed to run unattended 24/7 and continuously monitors the system for new NetCDF data files for automatic processing. Because the NAWIPS system development was frozen, this application was not deployed at NHC, but could easily be in the future.

2.3.9 Layer 0 – Air Force Raw SFMR Data Availability

Layer 0 provides a common mechanism for making diverse post processing data sets, such as raw SFMR data, available in a common location. This layer consists of a single python application: ftpDataFiles.py which is described below.

Automated Data File FTP

The application, ftpDataFiles.py, automatically pushes files from a local PC to a remote server so that they can be accessed by the layer 1 applications described above. The application was written to allow for the automated transfer of raw SFMR files, but is capable of transferring files of any type and therefore will not require modification to transfer files containing data from other sources in the future.

The application allows for three transfer options which provide flexibility with regard to making alterations to the data set. The application provides the option to transfer all files from the local machine; transfer only files that have not been transferred; or transfer only files that are not already on the server. Files written to the server are logged by the application and a status report for each time the application is executed is written to both the local computer as well as to the server. Writing these files to the server affords the ability to remotely check the transfer status and troubleshoot any issues. The status file names include the execution time to assist in matching each status file to a specific program execution instance and also to prevent the status files from being overwritten so that historical status is kept. Status files are written to a unique directory to ensure that they are not confused with data files.

This application was deployed on an Air Force computer and successfully run. It is configured to run 24/7. Air Force personnel only need to place SFMR data files in a directory on the computer's Desktop. The application then recognizes new files are present and transfers each to a FTP server within NHC. As mentioned above, log files monitoring the status are also sent to the server and kept locally for notifying the proper personnel if any errors occur.

2.4 Remote Sensing Solutions Real-time (& Analysis) Display Application

Remote Sensing Solutions developed, tested and deployed the real-time data display application and associated processing applications at NHC. Several workshops were held at NHC during this project to train and solicit feedback from NHC hurricane specialists and other personnel.

The Real-time Display Application provides the hurricane specialists (or end users) with the ability to visualize and interact with the reconnaissance observations contained within the NetCDF files described above. Built into its functionality is also the capability to display the high bandwidth data originating from the NOAA aircraft (i.e. 1 Hz data stream) and the capability to expand the application for the display of radar and satellite data as well. The display application is capable of running in a real-time mode, which maintains an update rate of once per second, to ensure the latest data is available to

the user. It also allows the user to visualize observations from the current or previous storms storm at any point in time where data is available. This allows the forecasters to use this tool for post season analysis as well as for gathering real-time information about the current system or systems of concern. The entire suite of applications was installed on a server which was deployed at NHC with a large (27 inch) LCD display for forecasters to use at their discretion. The PI, James Carswell, worked with Jose Salazar and Brian Mahar to deploy the system at NHC, and the code base has been kept up to date via version control. Feedback from hurricane specialists, Jose and Brian, was sought throughout the project and modifications to the system were made. Note that recently, the entire application and code base was transferred to a different server (muskie) that is deployed in the forecast area at NHC.

The following sections of this report summarize the application's capabilities.

2.4.1 Login Graphical User Interface (GUI)

A requirement for this project was to enable an efficient means for a hurricane specialist to visualize reconnaissance observations from a specific storm and in a predefined manner so that he/she would not be required to configure the display every time. At the same time, the ability to reconfigure the display and save display settings under different user names and mission types was required. To address these requirements, an initial login graphical interface was constructed. Figure 11 shows this login GUI. It is broken into three panels: Data Selection, Display Configuration and Action.

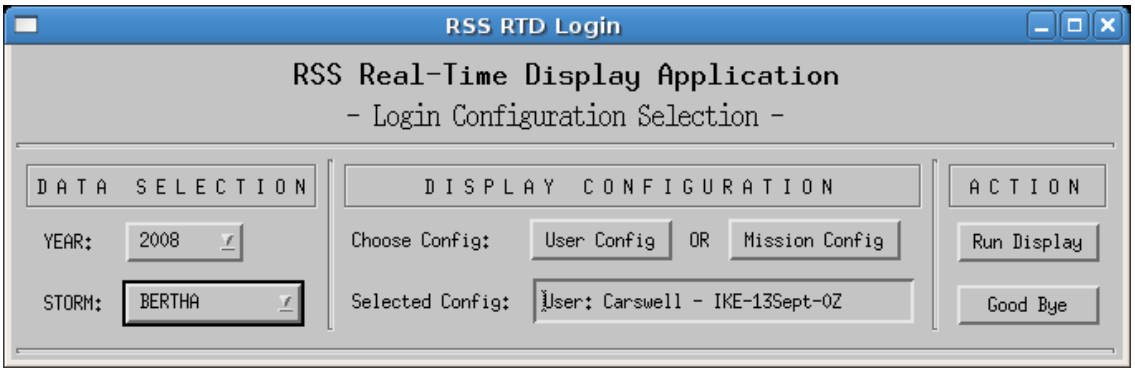

Figure 11: RSS RTD Login Graphical Interface

2.4.1.1 Data Selection

The Data Selection panel (on the left side of the image) provides users with the ability to select the data (i.e. storm or mission) that they wish to visual and interact with. Selecting the desired storm is performed using the two drop down lists labeled YEAR and STORM. The content of each list is dynamically created based on the data that resides on the server. In this manner, the code base does not require manual update of a storm names list, and the user is always presented with most recent list. Figure 12 shows a screen capture of the login GUI with the Storm dropdown listbox active and displaying the available storms. In this instance the user is selecting the data set associated with Hurricane Ike. Note that storms Bertha through Kyle are displayed. If the application was run today, it would list storms through hurricane Paloma. Because storms, such as

Josephine, were never flown, no data file exists for these storms and therefore are not presented in the list. The lower listings from “LOW “ to “WAVE” are missions that were flown and labeled accordingly in the URNT3 data files. These could be filtered out if desired.

2.4.1.2 Display Configuration

In the middle panel (Figure 11), the user can select the configuration to be accessed upon startup of the display application. The user may instead choose to recall a previously saved configuration. This capability was requested by hurricane specialists during a meeting RSS held at NHC during the spring of 2008. The requirement was that configurations be broken into two categories, “user” and “mission”. The user configurations would allow individuals to save their settings so that the display application would startup configured to their previous or desired settings. Likewise, a user could select from a set of default or defined mission settings (i.e. synoptic, ingest, center fix, etc). The configurations are filtered by the main name and then by a secondary tag. The secondary tag allows users to save different settings under separate profiles that he or she creates.

.

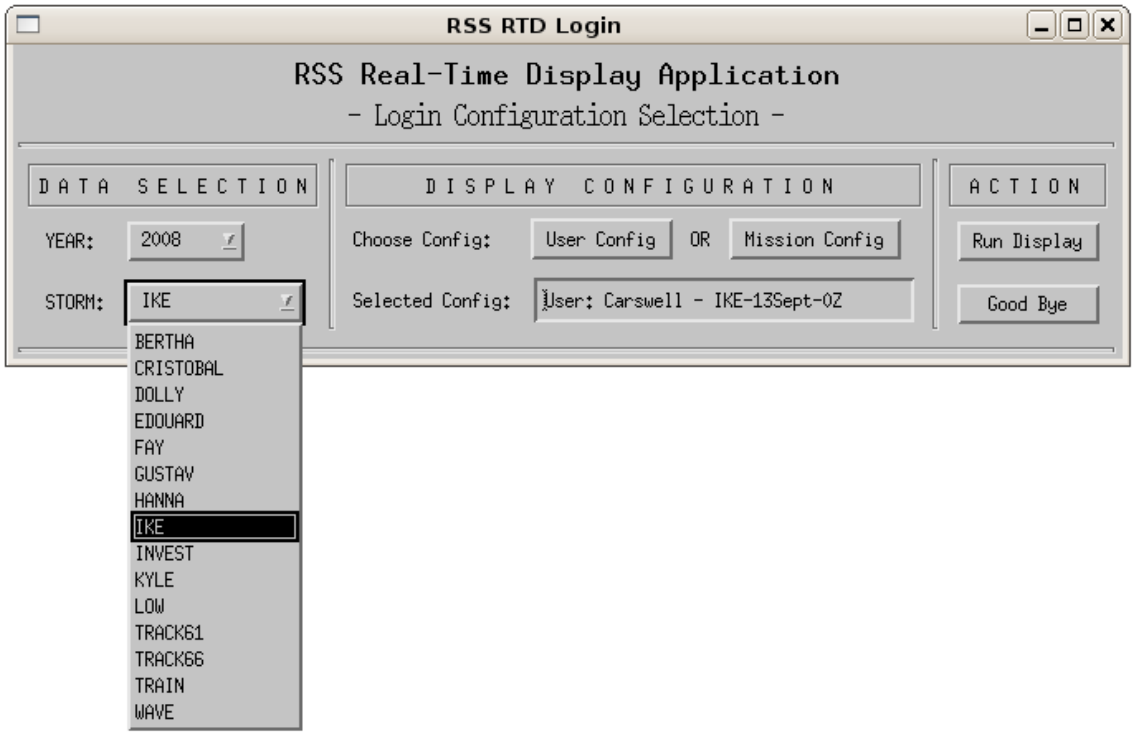

Figure 12: RSS RTD Login Graphical Interface – Storm drop down list.

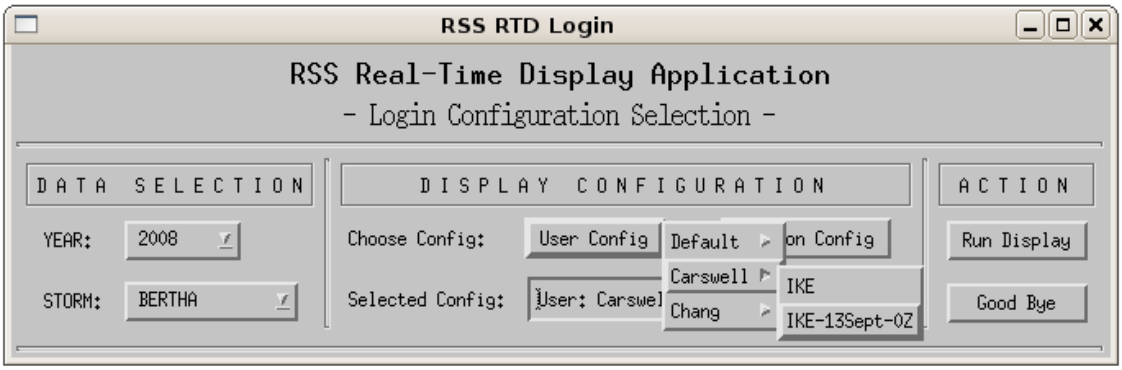

Figure 13: RSS RTD Login GUI - User Configuration drop down list.

Figure 13 shows a screen capture with the User Config button depressed. A drop down listbox presents a list of user configurations (Default, Carswell, Chang). In this example, the user has selected Carswell and is automatically presented with profiles under Carswell (IKE, IKE-13Sept-0Z). Besides allowing a user to immediately bring the display up in a default configuration so that he/she is not forced to make changes to the display application's configuration on each visit, a user can save the state of the display he or she is currently viewing, and then at a later date retrieve those settings (i.e. later in the day or during a post season when performing the best track analysis), and immediately display the data again for that particular moment in time and space that he/she was interested in. The settings can also be shared with other users and groups, such as HRD or RSS. This feature could be useful in the case that an anomaly is spotted with the SFMR sensor. The user can save the configuration of the display application that was employed when this anomaly was spotted. The configuration will in essence automatically document the anomaly and allow RSS and HRD personnel, through the configuration file, to immediately see the anomaly, by simply using the same configuration while simultaneously viewing the data.

The configuration files are persisted under a version control file system. The ability to commit these files to the repository can be easily added to the application via a button in the control GUI. Then authorized users at RSS and/or HRD can at any point simply issue an update command and the configuration files will be updated, and if not originally present, be automatically downloaded without the need for a person to manually send them. Note during the testing phase when a user discovered a problem or wanted to suggest a change, the user saved the configuration file. At Remote Sensing Solutions, we then updated our working copy through the repository and the configuration file was present. We could then see the exact same data and display as the user had been viewing. This enabled issues to be addressed very quickly and new features based on suggestions be rapidly incorporated into the system.

2.4.1.3 Action

The right panel (Figure 11) contains the action buttons. Depressing "Run Display" will launch the display application with the selected configuration and selected data set. Depressing the "Good Bye" button will terminate the application.

2.4.2 Display Application

As mentioned, a meeting was held in the spring of 2008 at NHC. James Carswell briefed several hurricane specialists and NHC staff on the potential capabilities of a real-time display application and demonstrated a prototype system. Based on the input from this mini-workshop, RSS created the Real-time Display Application and Control GUI. Several follow-on workshops were held to train NHC personnel on new features and solicit further feedback. The final application and its features are discussed below.

The display application has several views and many features to allow the users to interact with the data and quickly extract the desired information. The main display is broken into seven panels, three on the right, three on the left and one in the center. Figure 14 shows the display application (upper section) and user interface GUI that controls display configuration (lower section). The data shown in this screen capture are from NOAA and USAF flights through Hurricane Ike just prior to landfall (6 hour time window centered at 0Z on 13 September 2008). The data is plotted in the more conventional style – Earth relative GIS and time series. More details will be given below, but essentially, the left and right panels can display data either in a time series or storm quadrant-radial view (time-series shown) and the center panel presents a GIS view that overlays the data based on where the information was collected ("Earth relative view" shown) or in a storm relative view that removes the storm motion from the data and plots the data at a particular center fix time (i.e. center fix location) to produce a spatial snapshot in time.

2.4.2.1 Panel Plots

The left and right panels, labeled Panel 1 through Panel 6, present the selected data in a time series or radial plot format. The basic controls for these panels fall on the left side of the control GUI (lower section of the display) under the label, "Time-Radial Plot Configuration" and towards the right under "Parameter Configuration". In the current example shown in Figure 14, the panels are configured to display time series data. This is accomplished by setting the "Time Series" button in the control GUI. It is important to emphasis, once again, that the configurations are preset to the "proper" values through the configuration selection in the login GUI so that a user is not required to spend time configuring the display each time. The user is able to finely tune the display through the configuration GUI when time permits or conditions warrant.

The observations shown in the display are filtered in time. There are essentially two modes, real-time and historical, that can be seamlessly toggled between. Any change to the configuration occurs within less than a second providing the user with no apparent delay. If the "Center Time" button is selected, the data will be filtered in time around the time specified by Center Time fields in the control GUI. The time window is set by the "Window" field and is centered on the center time. When the center time button is not selected, all observations falling within the time window of the last observation point collected are displayed. As new data arrives the plots shift accordingly.

2.4.2.1.1 Panel Plots: Time Series

In Figure 14, “Center Time” has been selected and set to 0Z on 13 September 2008. In this case, with the time window set to 6 hr, all observations collected between 21 Z on 12 Sept 2008 and 3 Z on 13 Sept 2008 are shown. If 3Z had not yet been reached, then incoming data falling within that window would be displayed as it arrives. Below the time series and radial plot settings, the user can select which parameter he/she wants to display for each panel. The list is automatically populated by the data that is available. In this example, wind speed (flight level and SFMR) is plotted in Panel 1, dew point temperature in Panel 2, SFMR rain rate in Panel 3, ambient temperature in Panel 4, extrapolated surface pressure in Panel 5 and geo-potential altitude in Panel 6. In the last panel, it can easily be seen that two aircraft are present during the time window selected (a NOAA aircraft and an Air Force aircraft).

For each panel plot, the minimum and maximum values are displayed in the legend. These values are automatically calculated and updated as new data is ingested, or the data filtering is changed. Note in the case where center time is not selected (i.e. real-time mode), as new observations arrive, the plots are updated within one second of the data arrival. This ensures that the display content is current.

2.4.2.1.2 Map Panel Point

If the user selects the “Map Panel Point” button under mouse actions next to the panel parameter selection area in the configuration GUI, as he/she moves the mouse over any of the panel plots, a vertical line follows the location of the mouse. The line and the associated time on the x-axis is displayed on all panel plots and the value of the observations at that time is shown in the legend of each plot. At the same time, the location of the observations at that time is shown on the GIS view. The user can quickly identify where in time and space an observation occurred and what the other observations are at that time. If the mouse is held for a few seconds over that location, the line turns from white to green and the user can depress the mouse button to freeze its location. Figure 15 shows an example. The settings and observations are the same as in the previous plot, as the user has frozen the map panel data line at 23:25:30 on 12 Sept. At this point the flight level wind speed has reached a local maximum of 100 kt and the SFMR wind speed observation is 78 kt. On the GIS display the location is shown by the crosshair. The observations were collocated in the northeast quadrant at about 30 km for the center of the storm. The values for the other observations are also shown in the legend of each panel (Selected Values). To unfreeze the line, the user must only depress the mouse button again.

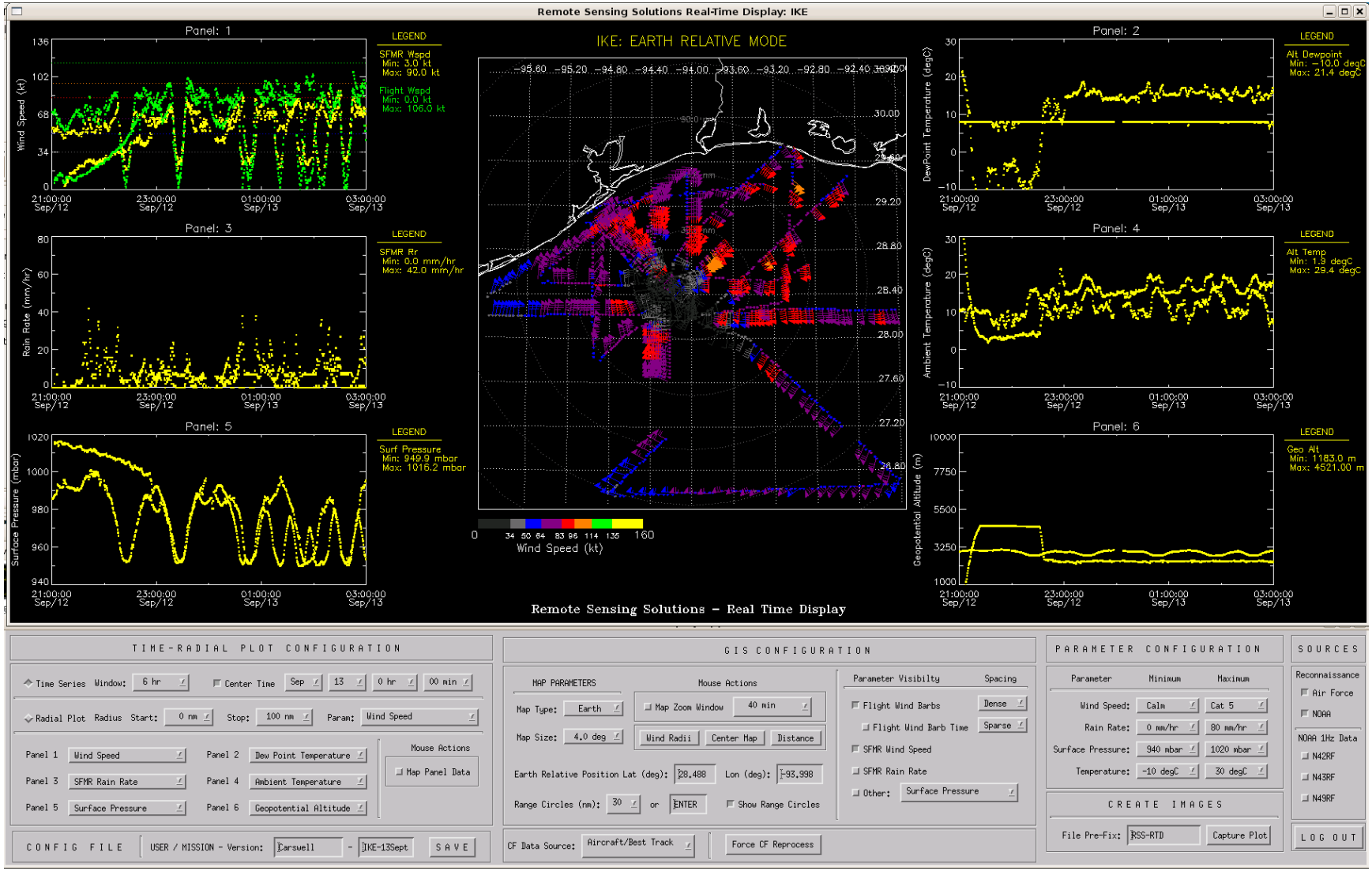

Figure 14: Real-time Display Application - Hurricane IKE on 13 September 2008 at 0Z , six hour time window. Earth relative GIS and time series panels are plotted. Panels 1 through 6 display flight level and SFMR winds, flight level dew point, SFMR rain rate, flight level ambient temperature, extrapolated surface pressure and aircraft geopotential altitude. Flight level wind barbs and SFMR wind speeds are overlaid on GIS view.

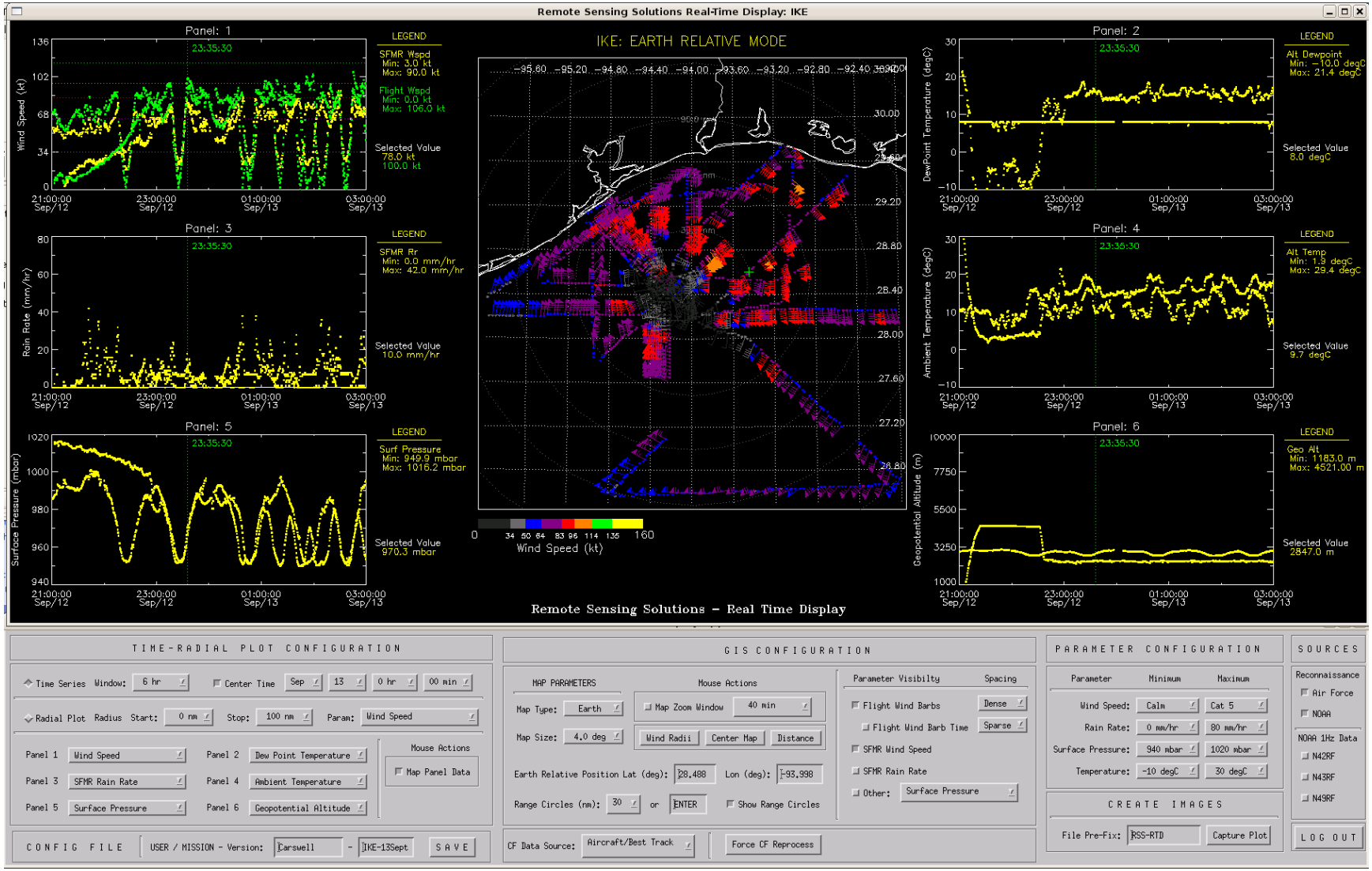

Figure 15: Real-time Display Application - Hurricane Ike on 13 September 2008 at 0Z. Example of "Map Panel Data" feature.

2.4.2.1.3 Parameter Scales

The scale of each panel is control by the parameter scales. This control resides under "Parameter Configuration" in the control GUI. Similar to the other lists shown in this GUI, these can easily be altered by simply changing the lists in the application.

2.4.2.1.4 Panel Plot: Storm Quadrant Radial

The observations can be toggled from time series to radial plots to allow the user to evaluate an observation as a function of radial distance from the center of the storm and by storm quadrant. This is especially useful when trying to determine the hurricane force wind radii in each storm quadrant. The user selects the Radial Plot button. In this mode, Panel 1 represents the Northwest quadrant, Panel 2 represents the Northeast quadrant, Panel 3 represents the Southwest quadrant and Panel 4 represents the Southeast quadrant. Panels 5 and 6 remain as time series plots. In radial mode, only one parameter is shown at a time. Figure 16 displays an example. The same data that was shown in Figure 14 is now plotted in radial format. The GUI hides the parameter selection for panels 1 through 4 and uses the selected parameter specified in the radial plot selection area. The user can toggle between time series and radial displays by clicking the radial and time series buttons and the display is updated in less than one second. The settings for both modes are automatically recalled. The user can apply additional filtering by specifying the radial window, in this case set to 100 nm. The start radius can also be selected. As with the time series plots, the minimum and maximum values are displayed in the legend for each quadrant immediately providing the user with the maximum wind speeds for each quadrant.

2.4.2.2 GIS View

As already mentioned, the center panel displays the selected data on a latitude-longitude map (i.e. GIS View). The GIS view offers a few different modes and several configurations and actions.

2.4.2.2.1 GIS View Mode

There are three viewing modes the user can select from:

- ***Earth Relative***: Selected observations are overlaid based on the collection location (i.e. latitude and longitude of observation). The center of the map is set by the user. This is a conventional GIS view.
- ***Center:*** Same as Earth Relative except the center of the map is set to be the mean latitude and longitude of the selected observations. This allows the GIS window to be quickly located over the selected data and the map will move with the data.
- ***Storm Relative:*** Using the storm relative coordinates of the observations, they are mapped around the center fix location for the specified center fix time. In this manner the storm motion during the period over which the observations were collected is removed from the data giving a spatial view of the observations at an instant in time.

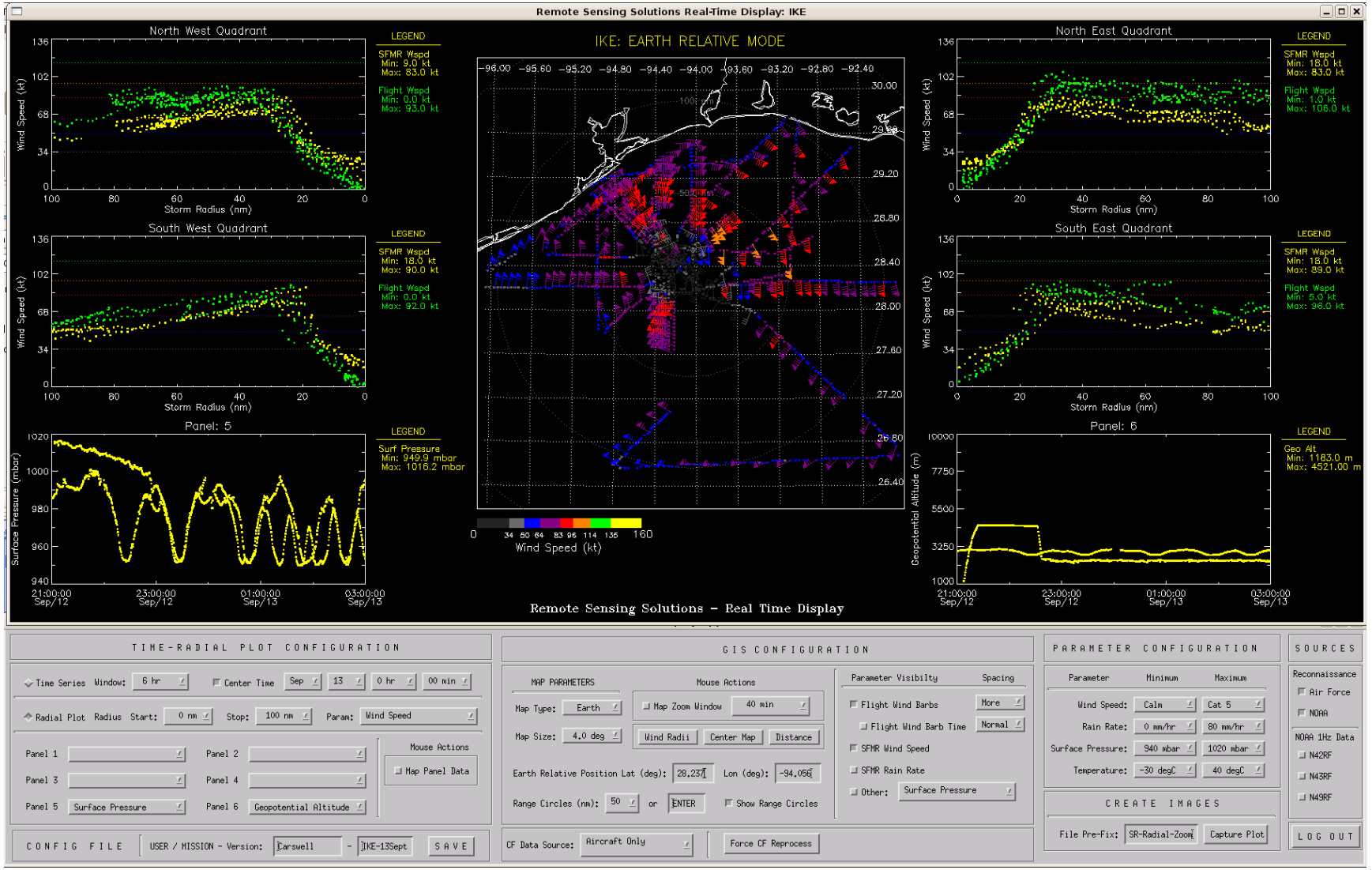

Figure 16: Real-time Display Application – Hurricane IKE on 13 September 2008 at 0Z (radial panels).

Previous figures showed the observations display in an “Earth Relative” mode in the GIS view. Figure 17 shows the same data as Figure 16 except that the GIS view is now in Storm Relative mode. Clearly the storm structure can be more easily seen since the motion of the storm over the six hours the data was acquired has been removed. This allows the user to more readily determine the strength of the storm as a function of the storm quadrant and to determine the wind radii and other important characterizations.

2.4.2.2.2 Map Parameters

Several features of the map can be configured if required. They are:

- **Map Size**: A drop down list allows the user to change the size of the GIS view. In the examples shown above the map size has been set to 4 degrees.
- **Center Position**: In Earth Relative mode, the center location for the map can be manually entered.
- **Range Circles**: Range circles can be turned on and off. A drop down list allows the user to choose the interval or the user can manual enter in the interval.

2.4.2.2.3 Mouse Actions

Map Zoom Window

The hurricane specialists requested the ability to mouse-over observations on the GIS view and have the application display the value of the observations. To accommodate this request, the application now has the Map Zoom Window feature. The user can select a time window next to the Map Zoom Window box from a drop down list. When the Map Zoom Window box is selected and the user places the mouse over the GIS view, the closest observation to the mouse location is determined. Using its time stamp, the observations shown in the panels are filtered to within the specified time window. As the user moves the mouse along the observations (white cross hair shows location), the panel plots are rapidly updated. If the mouse is left stationary for a few seconds, the crosshair on the GIS view will turn from white to green and the user can freeze the displays by clicking the mouse in the same manner as the Map Panel Data feature. Once frozen, the crosshair becomes an asterisk and the mouse can be moved without affecting the plots (plots are still updated when new data arrives).

Figure 18 shows this feature. The mouse location is in the southeast quadrant and shown by the green asterisks. The selected observational point is from a southeast to northwest leg. The panel plots show the observations in a time series format. From panel 1, the wind speed profile of the hurricane eyewall on this flight leg can clearly be seen. Selecting the radial plot button, the panels can be switched to radial plots without affecting other settings. Figure 19 shows the same data with the radial plot function enabled. Note that since the leg was a southeast to northwest leg, no data is shown in the northeast and southwest quadrants since the aircraft was not in these areas within 45 minutes of the selected observation (time window was set to 90 minutes).

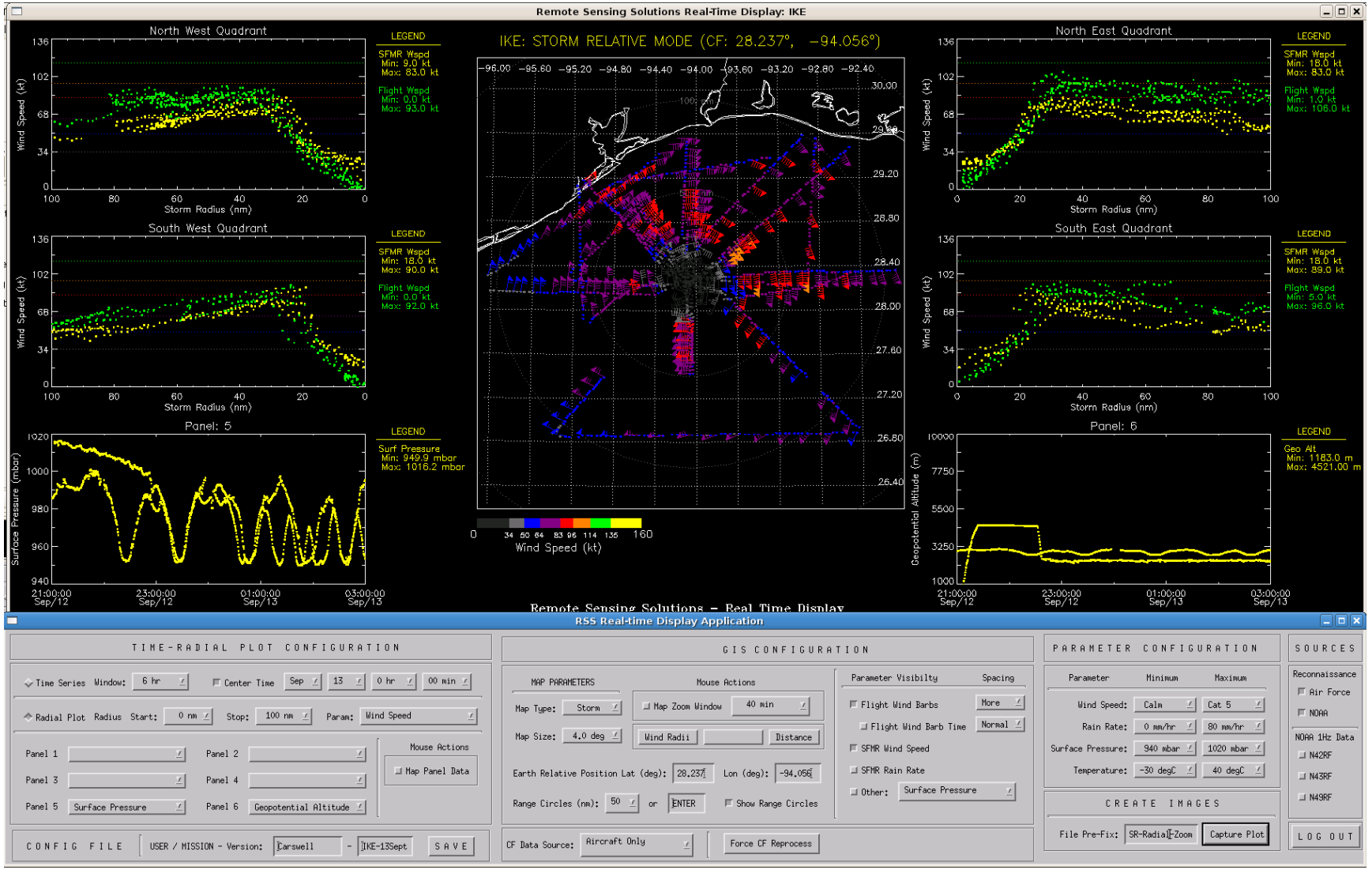

Figure 17: Same as previous figure except the GIS View is shown in Storm Relative mode.

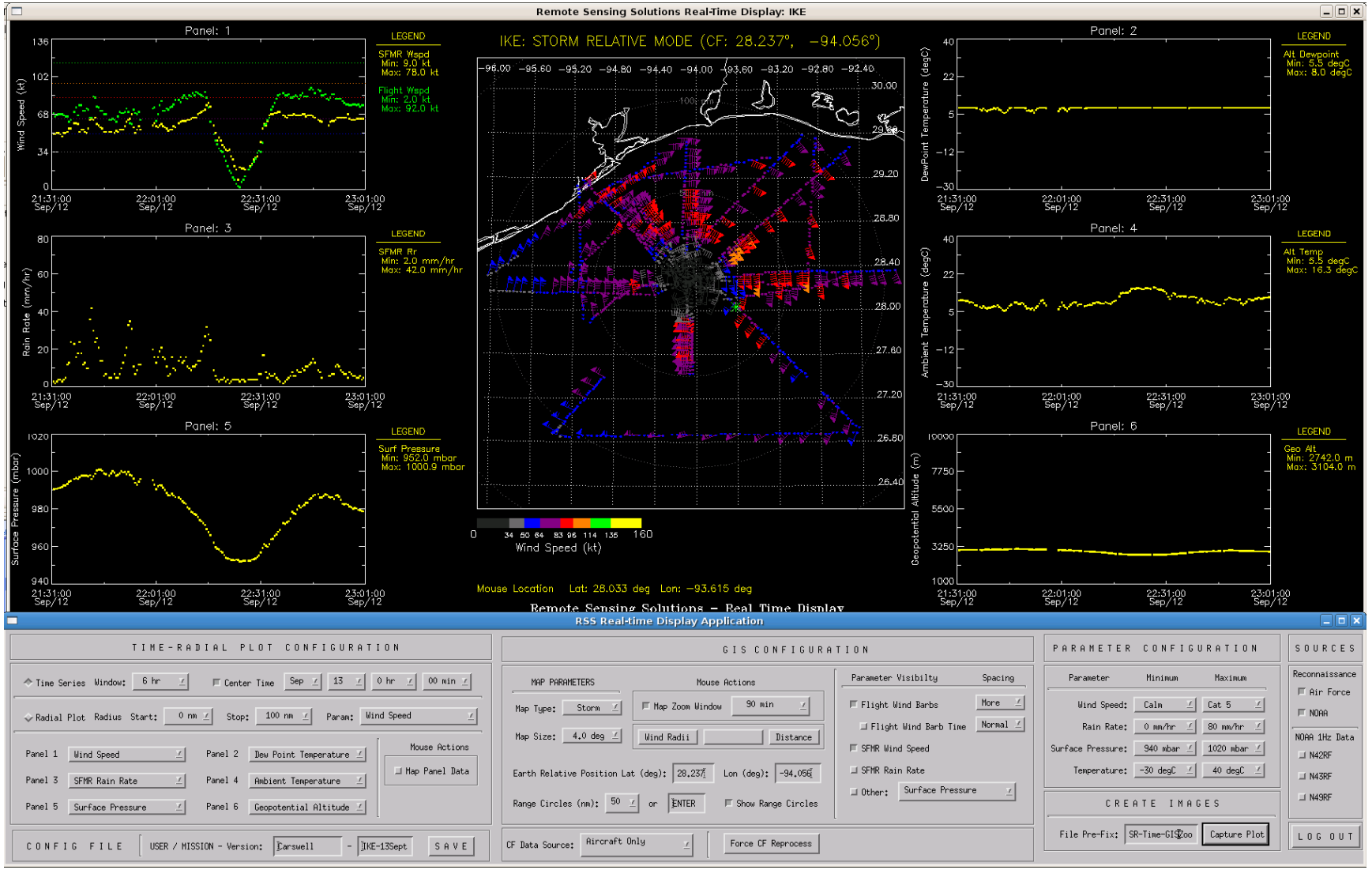

Figure 18 same as Figure 17 except Map Zoom Window has been selected with a 90 minute time window and the panel plots are shown in time series mode. The green asterisk at approximately 28.2 degrees latitude and -93.4 deg longitude shows the position of the mouse. The panel plots plot data that is within +/- 45 minutes of the observation collection time of the point selected. Note that one can move the mouse and the panel plots update at a 5 Hz rate as the mouse is moved.

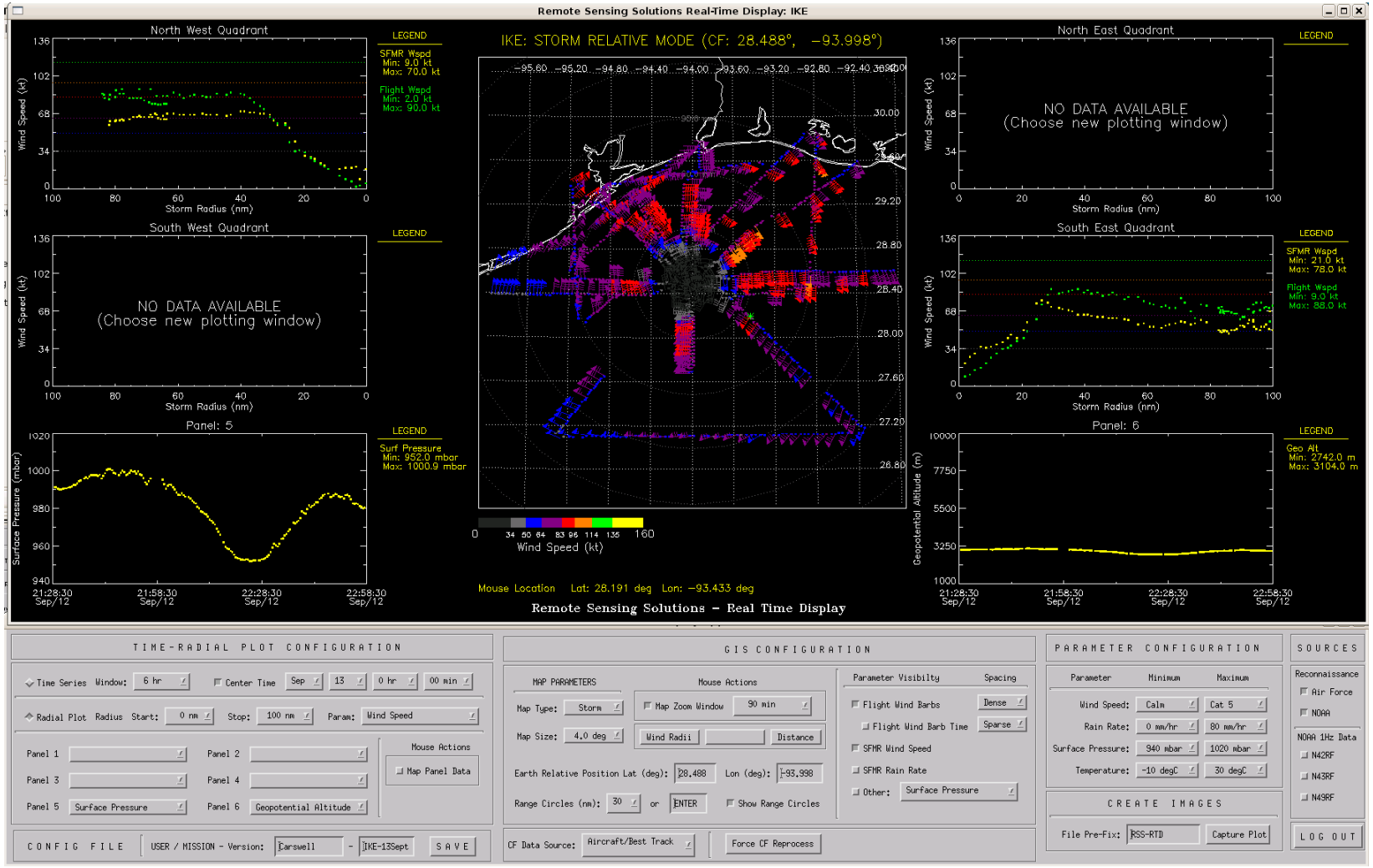

Figure 19 Figure 18 except the panel plots are in radial plot mode. As can be seen by this figure, the aircraft was traveling in the northwest direction and the flight leg within +/- 45 minutes of the observation point closest to the mouse travelled from the southeast quadrant to the northwest quadrant of Hurricane Ike. Panels 5 and 6 are still shown as time-series plots.

2.4.2.2.4 Parameter Visibility

Any of the parameters can be displayed on the GIS view. The parameter visibility panel allows the user to turn the visibility of the observations on or off. The default values are the flight level wind barbs and the SFMR estimates, but any other observation can be selected and displayed by choosing another and using the drop down box. Time stamps for association with the flight level wind barbs can also be toggled on and off. The density of the wind barbs and the time stamps can be selected as well.

2.4.2.2.5 Center Fix Data

The hurricane specialists, as previously mentioned, requested the ability to calculate the storm relative coordinates based on different sources. The display application configuration allows the user to choose which source is used in calculating the storm relative coordinates. Note that the actual processor discussed previously calculates the storm relative coordinates for all sources. This feature is only a filter that selects which source is used for display purposes. The “Force CF Reprocess” button is there for post analysis. The hurricane specialists can change the best track file and then depress this button. The application will then instruct the processor to immediately fetch the new best track data file (as well as the other center fix files) for the selected storm and will reprocess all the storm relative coordinates for the selected storm. This will enable the hurricane specialist to evaluate, in a graphical manner, how well the new best track values (post season values) agree with the observations.

2.4.2.3 Saving Configuration

The user can save his/her settings by using the “SAVE” button (lower left part of configuration GUI). For the configuration the user can change the user / mission name and the version or profile field. Once a configuration is saved, the login GUI will present it upon next login.

2.4.2.4 Other Settings /Features

Finally, the user can toggle observations from the Air Force and NOAA aircraft by turning on and off the selection for the Air Force and NOAA aircraft (far upper right panel on the configuration GUI). The user can also create an image of the display simply by clicking the “Capture Plot” button. A unique time stamp is put on the file so that the user does not have to supply a unique name. The user can supply a file pre-fix if desired. Finally, the user can return to the login GUI by depressing the “LOG OUT” button.

2.5 SFMR Validation Algorithm

As part of this project, a key capability that must be developed and implemented is the ability to validate and detect errors in the SFMR calibration and stability. As detailed in our previous JHT project, “Operational SFMR-NAWIPS Airborne Processing and Data Distribution Products”, which focused on the NOAA SFMR, small calibration errors in the SFMR translate to significant errors in the SFMR wind speed estimates. For the Air Force SFMR units, ProSensing, Inc, the manufacturer, performs a laboratory calibration. The instrument is then installed and a calibration flight in low to moderate wind conditions is flown. GPS dropsonde surface wind observations and buoy-based wind observations are compared against the SFMR wind estimates. If the SFMR wind observations are found to disagree from the buoy and dropsonde measurements, the SFMR calibration offset parameter is tuned to eliminate this error. Although this approach will remove significantly large errors, it still does not provide the necessary accuracy to ensure an acceptable maximum level of uncertainty in the SFMR retrievals. Part of the problem exists in the wind speed retrievals being compared to the in situ wind speed measurements as the sole criteria. For a small range of wind and rain conditions, the calibration bias for the SFMR can be tuned to produce reasonable wind comparisons, but residual error in the calibration may and probably will still exist. That is, some of the channels may produce higher brightness temperature measurements and other channels lower brightness temperature measurements compared to the model function. For the limited set of wind / rain conditions sampled, these errors can offset each other thereby erroneously producing wind retrievals that agree with the in situ measurements. However, under different wind and rain conditions, these errors can produce significant errors in the SFMR wind speed retrievals. To ensure this scenario is eliminated, an approach to validate the calibration of the SFMR that accounts for both the wind and rain contributions is required.

Remote Sensing Solutions has developed such an analysis approach. The novel part of this approach is that it does not require in situ wind or rain estimates and uses a parameter already calculated within the retrieval process. With a minor modification to the real-time processor, this calibration-validation approach could be implemented on the operational SFMR systems. The premise of the approach is: If the instrument calibration is properly tuned to the model function, then the measurements should agree in the mean with the predicted brightness temperatures that are based on the retrievals. In fact, the retrieval process itself tries to accomplish this objective. It adjusts its wind speed and rain rate estimates to minimize the error between the six frequency brightness temperature measurements (per channel) and the predicted brightness temperature values derived using the SFMR model function.

To illustrate, RSS’ SFMR simulator was used to produce a set of SFMR measurements for wind and rain conditions ranging from 0 to 80 m/s and 0 to 80 mm/hr. The standard deviation of the simulated brightness temperature measurements was set to 0.5 K. and 200 realizations at each wind speed and rain rate level were produced. The simulated measurements were passed through the SFMR retrieval process and wind speed and rain rate estimates derived. These estimates showed a zero mean bias since a

calibration bias was not introduced. The wind and rain retrievals were then passed back through the SFMR brightness temperature model function to produce a set of predicted brightness temperature measurements. For each channel the difference between the measured and predicted brightness temperature measurement was calculated. Figure 20 plots a histogram of this difference in terms of percent of occurrence as a function of the error for each channel. As expected, each channel has a zero mean bias indicating that there is no calibration error.

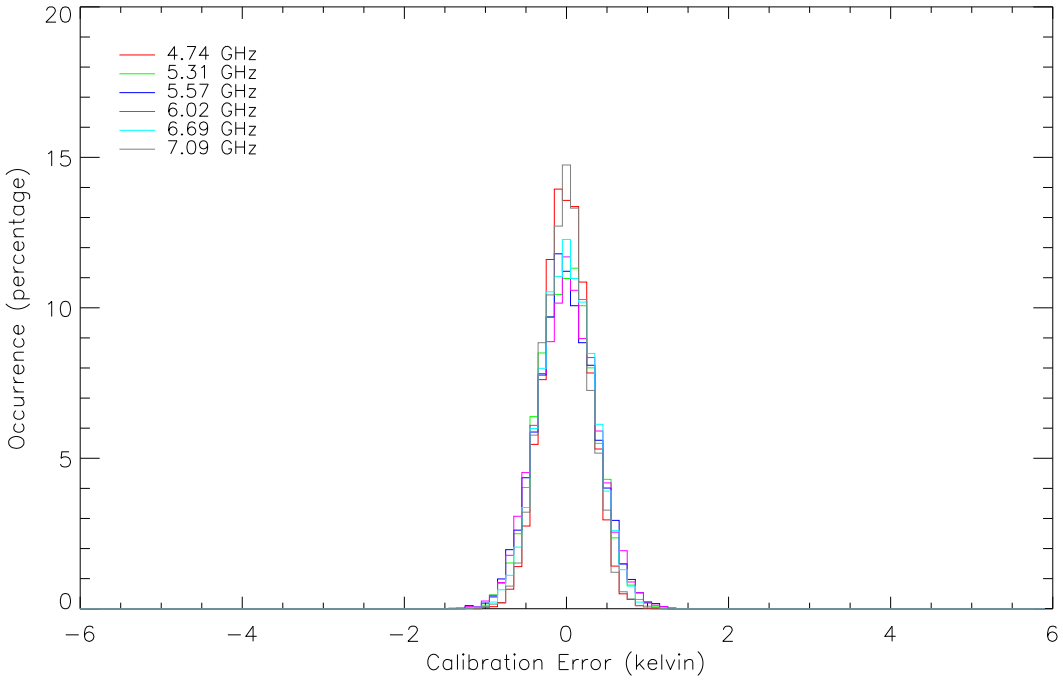

Figure 20: Histogram of the difference between the measured Tb and the predicted Tb for each channel is shown. The calibration error for all channels is set to zero.

Following the same procedure, a calibration error was introduced into the second highest frequency channel (-1 K error). The retrieval process was run and the predicted brightness temperatures derived from the retrievals. Figure 21 presents the error histogram. In this case, channel 5 clearly shows a negative bias. Because the retrieval process believes the measurements to be true and attempts to minimize the error between the measured and predicted brightness temperatures, its wind speed retrievals for this case are slightly high and the rain rate retrievals slightly low. The error in channel 5 spreads into adjacent channels with channel 6 having a slightly high bias. In any event, this approach clearly detects calibration errors. Further it does not require any in situ wind measurements nor does it require specific wind or rain conditions. In fact, it can be run continuously during all missions to monitor the calibration and health of the instrument. Additionally, as mentioned previously, any calculated difference within the retrieval process could be made available as a quality control and calibration validation tool.

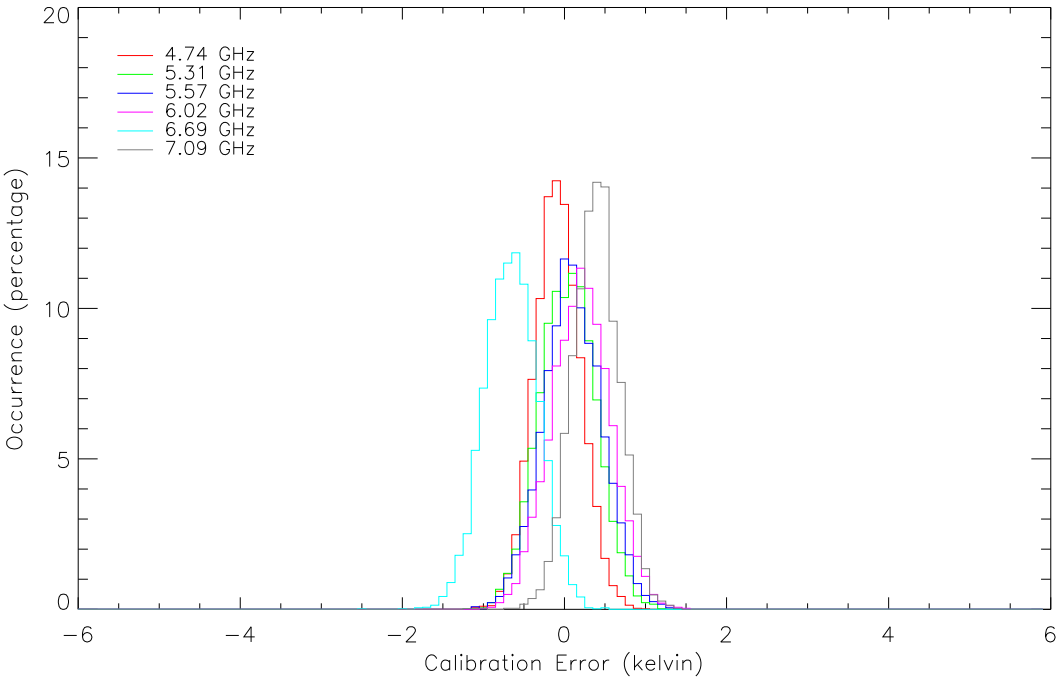

Figure 21: Same as Figure 20 except a -1K calibration error was introduced into channel 5.

Applying this analysis to SFMR observations collected from missions through Hurricane Dean, Figure 22 through Figure 24 plot the SFMR calibration errors for each channel derived from measurements on the 16th, 17th and 18th of August, 2007. These plots show that channel 5 is biased low and channel 6 is biased high, which is exactly as shown in the above simulation. Also present are small errors in the lower channels. As mentioned previously, these calibration errors will result in errors in the retrieved wind speed. To show the stability of this approach, the errors calculated on the 16th were removed from the measurements on the 17th and 18th and the error histograms recalculated. The results are shown in Figure 25 and Figure 26. As these figures show, the same errors are seen on all three flights.

Using both this new analysis approach to provide guidance along with the existing calibration tuning procedures, it should be possible to remove the calibration errors of the SFMR.

Another advantage of this approach is its ability to be run continuously in order to provide feedback on the performance of each SFMR. In the event that an instrument's measurements begin to drift or one of its channels begins to fail, this analysis will immediately detect the problem. In fact, by setting a simple threshold (such as an absolute bias less then 0.2K), a simple indicator for each channel can notify the operator that the threshold has been crossed. If the error is found to originate from a single channel, that channel can be disabled. Therefore, the detection of this error state during a flight will allow the operator to immediately address this issue after the flight. Note that all information to implement this approach resides within the SFMR instrument

itself, meaning the operator and/or end user is not required to possess a detailed understanding of the SFMR operations and the remote sensing theory behind the process in order to effectively use this information.

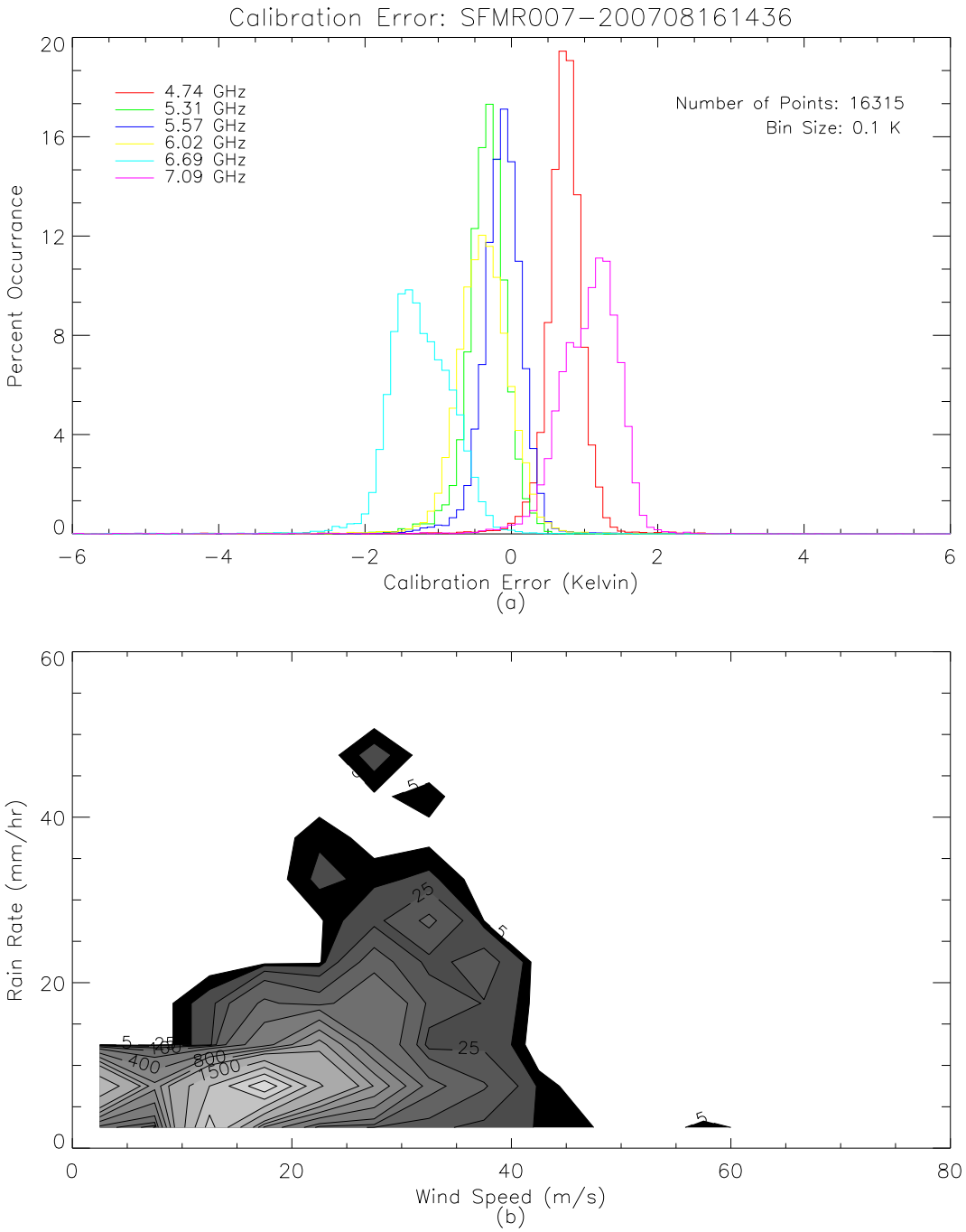

Figure 22: Panel (a) plots a histogram of the calibration error for SFMR007 during a mission through Dean on 16 August 2007. Panel (b) presents a 2-D histogram of the retrieved wind speeds and rain rates for this flight to provide an estimate of the conditions sampled. Note that because a calibration error exists, the wind and rain observations will also be in error.

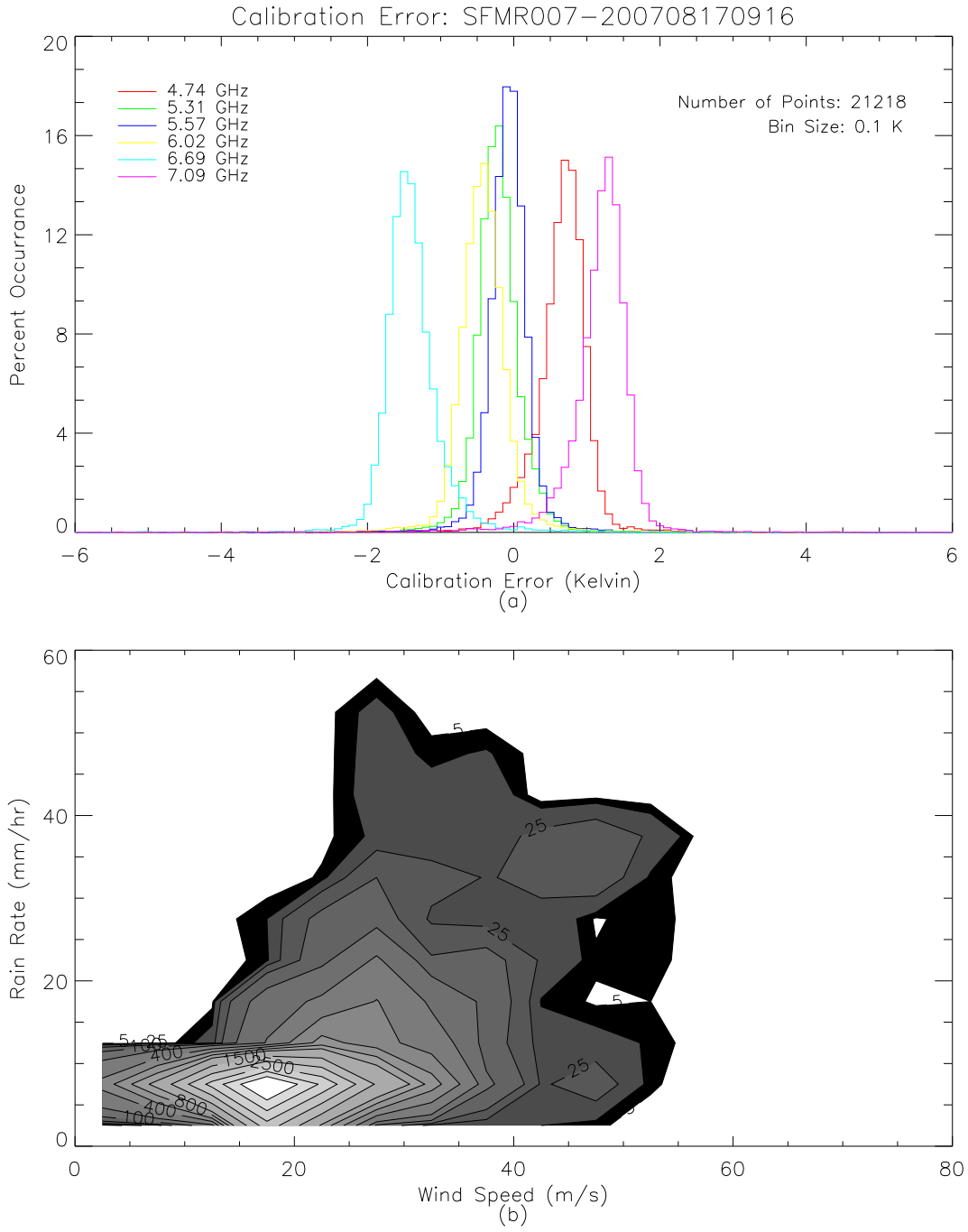

Figure 23 Panel (a) plots a histogram of the calibration error for SFMR007 during a mission through Dean on 17 August 2007. Panel (b) presents a 2-D histogram of the retrieved wind speeds and rain rates for this flight to provide an estimate of the conditions sampled. Note that because a calibration error exists, the wind and rain observations will also be in error.

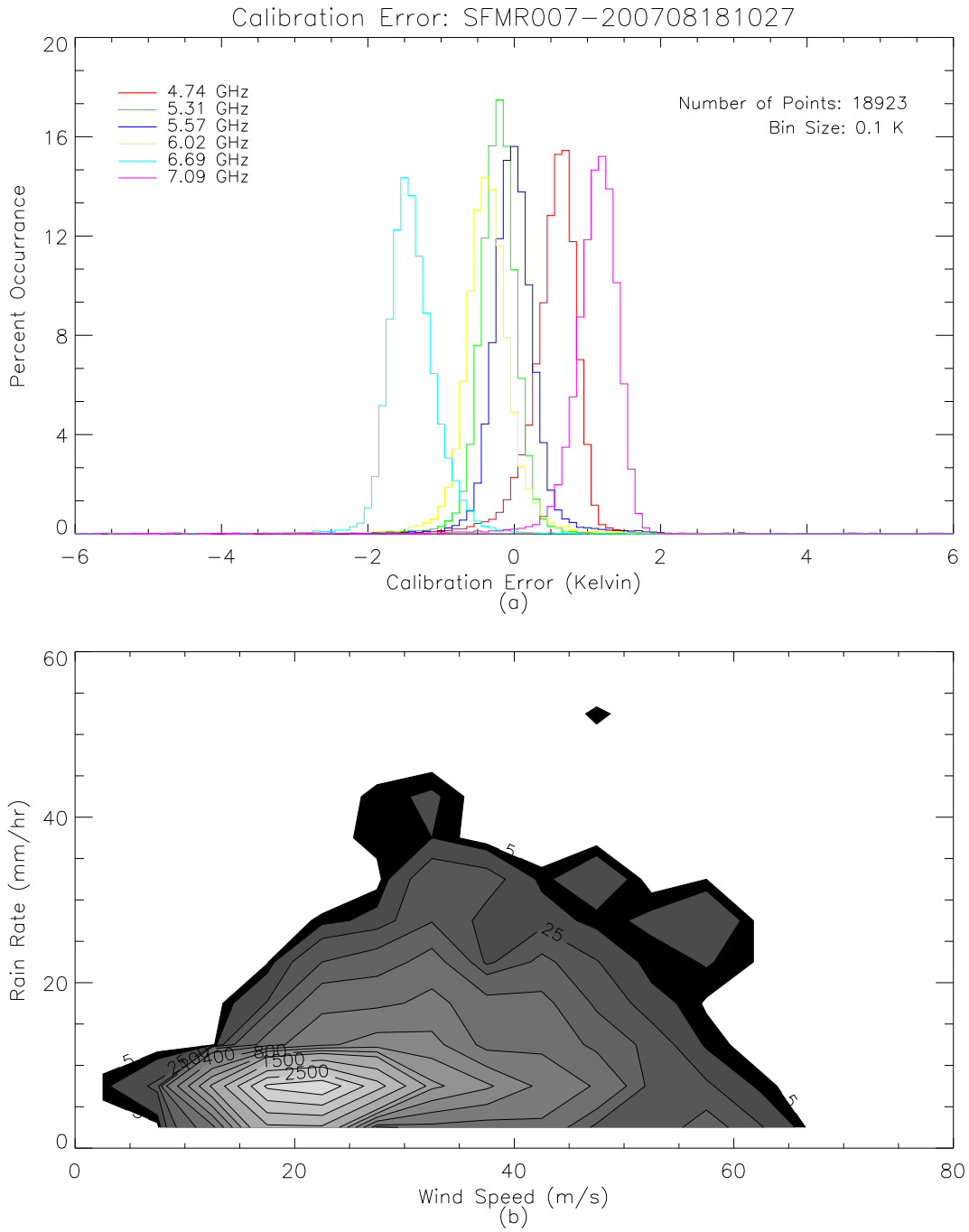

Figure 24 Panel (a) plots a histogram of the calibration error for SFMR007 during a mission through Dean on 18 August 2007. Panel (b) presents a 2-D histogram of the retrieved wind speeds and rain rates for this flight to provide an estimate of the conditions sampled. Note that because a calibration error exists, the wind and rain observations will also be in error

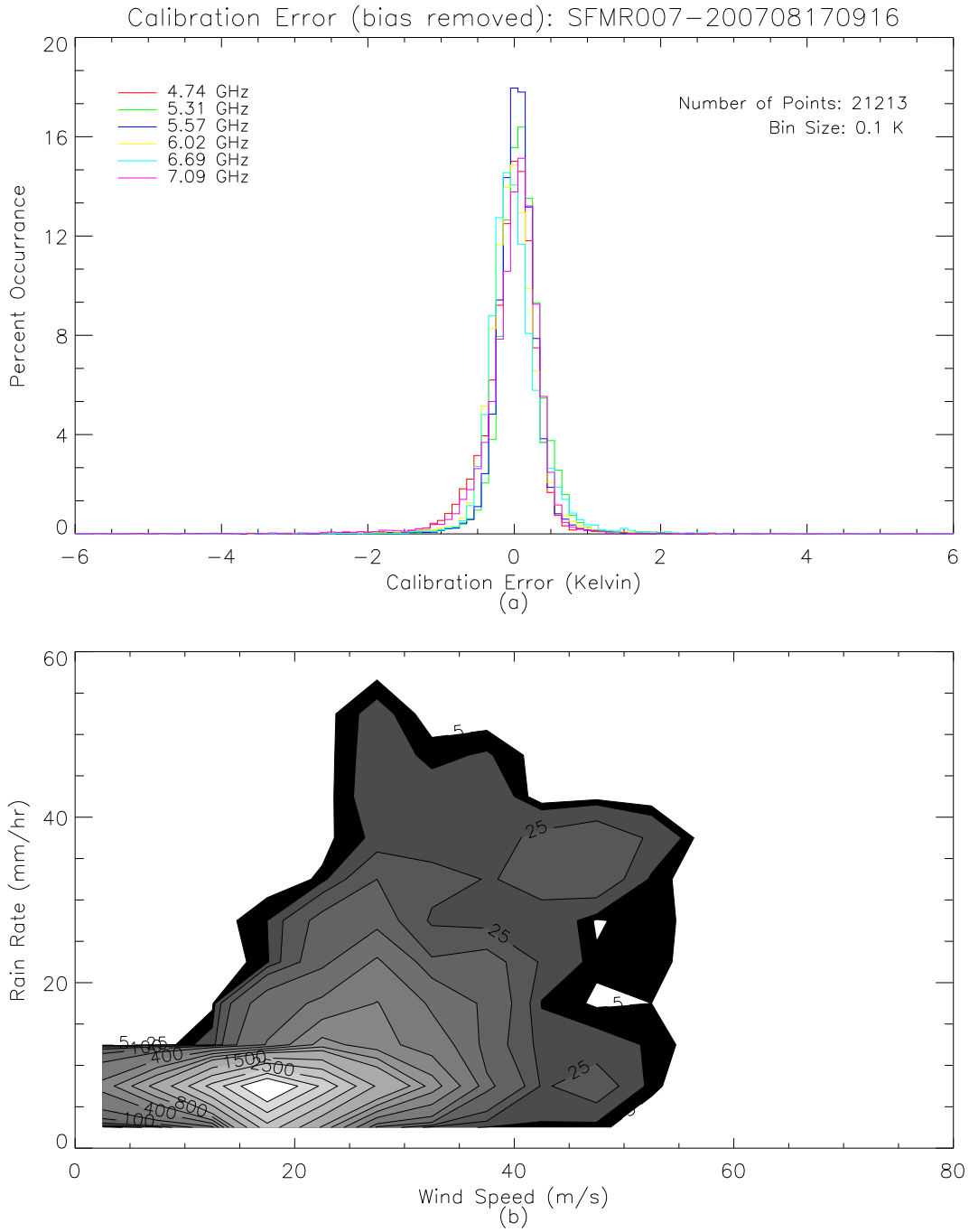

Figure 25: Same as Figure 23 except the mean errors calculated from the 16 August 2007 flight are used to correct the measurements. The errors now have a zero mean for all channels.

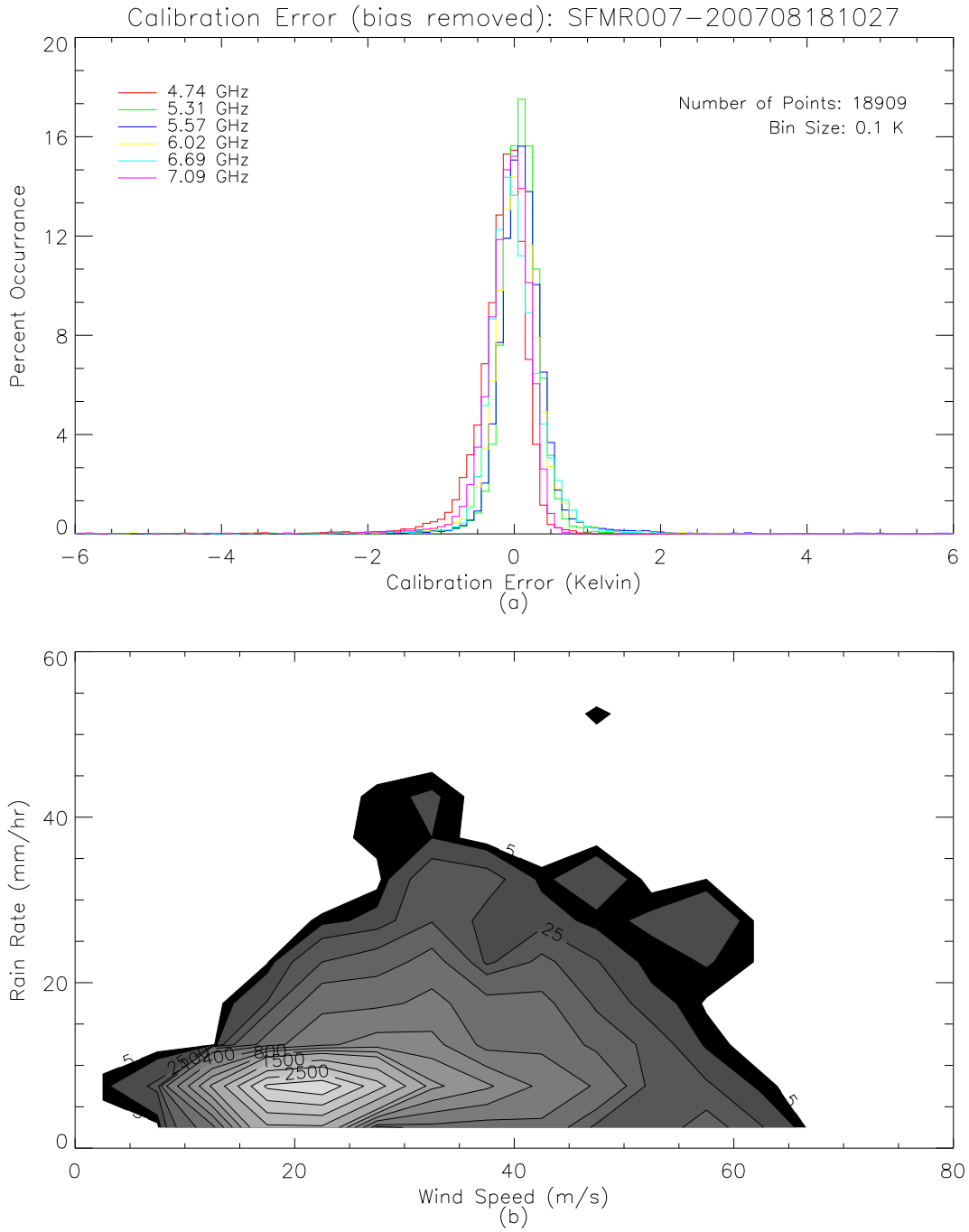

Figure 26 Same as Figure 24except the mean errors calculated from the 16 August 2007 flight are used to correct the measurements. The errors now have a zero mean for all channels.

2.5.1 SFMR Stability Issues

Applying the approach described above, NOAA SFMR measurements from 2008 were analyzed. The lower two channels were not included because of RFI issues. A few examples are shown, 20080720, 20080812, 20080831, 20080906 and 20080924. The general trend was that the SFMR degraded over the season. As these plots show, the error histograms begin to shift and widen.

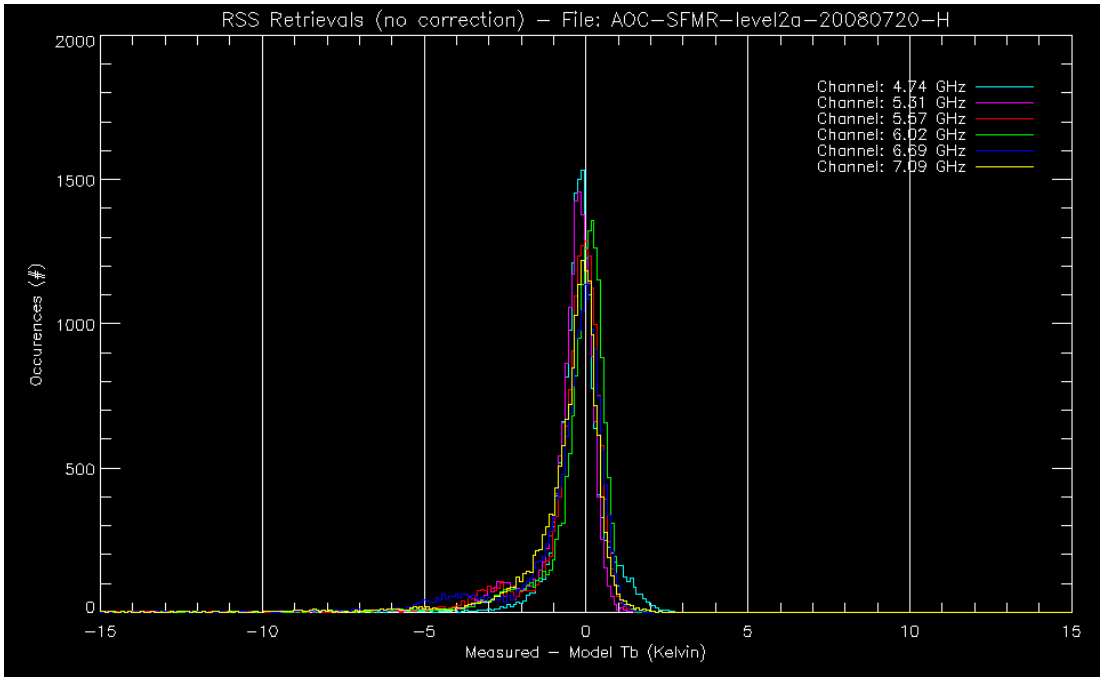

Figure 27: NOAA SFMR brightness temperature histogram for 20 July 2008.

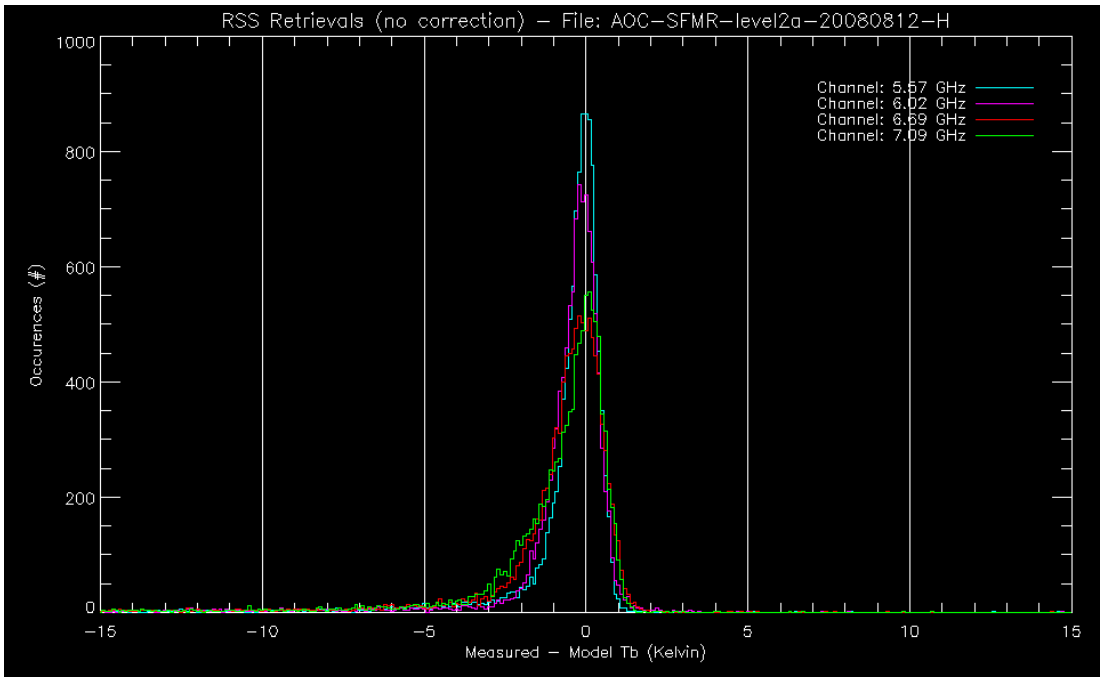

Figure 28: NOAA SFMR brightness temperature histogram for 12 August 2008.

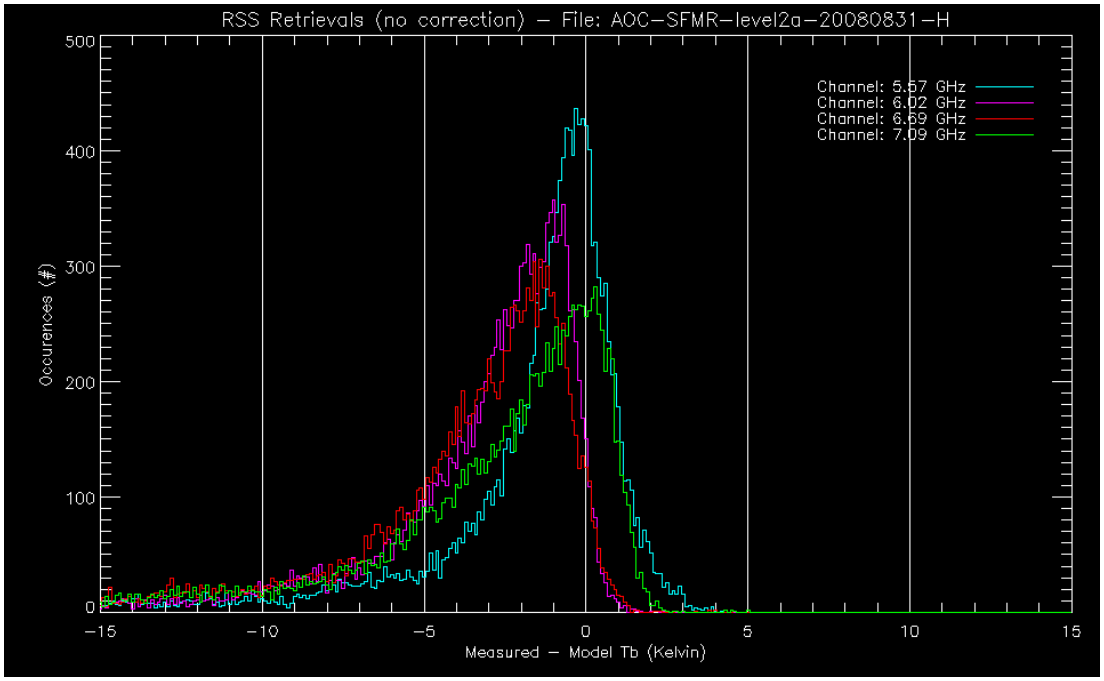

Figure 29: NOAA SFMR brightness temperature histogram for 31 August 2008.

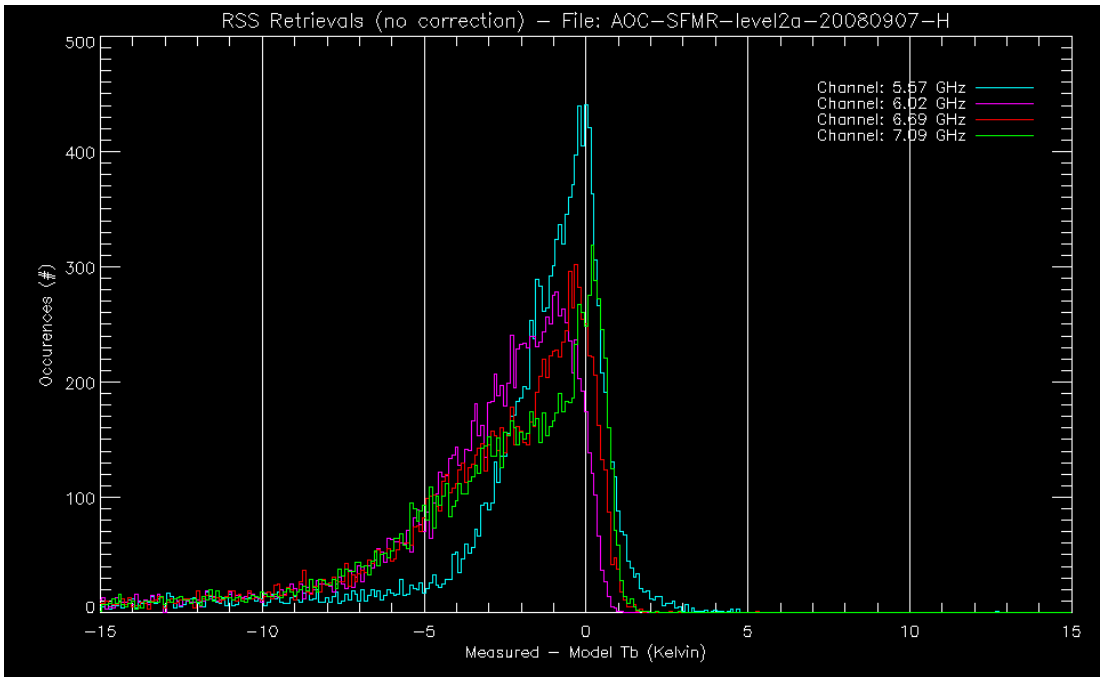

Figure 30: NOAA SFMR brightness temperature histogram for 7 September 2008.

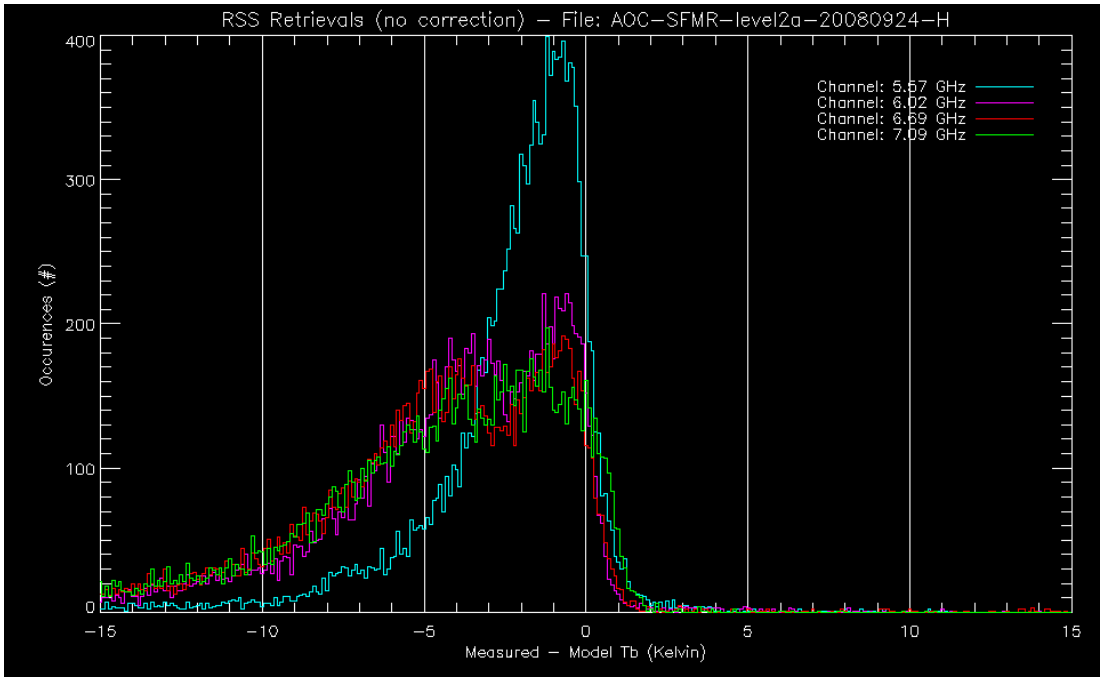

Figure 31: NOAA SFMR brightness temperature histogram for 24 September 2008.

Applying the tuning approach where we remove the relative channel biases whicle keeping the overall mean value the same, we were able to correct for these errors for most of the flights. The same data sets are shown below with the calibration biases removed. Note that as time progresses, the histograms start showing a bi-modal

response and no longer exhibit the sharp peak response that they should. This indicates the instrument is potentially drifting relative to the SFMR GMF within a flight. Note also that the calibration corrections are not constant from flight to flight.

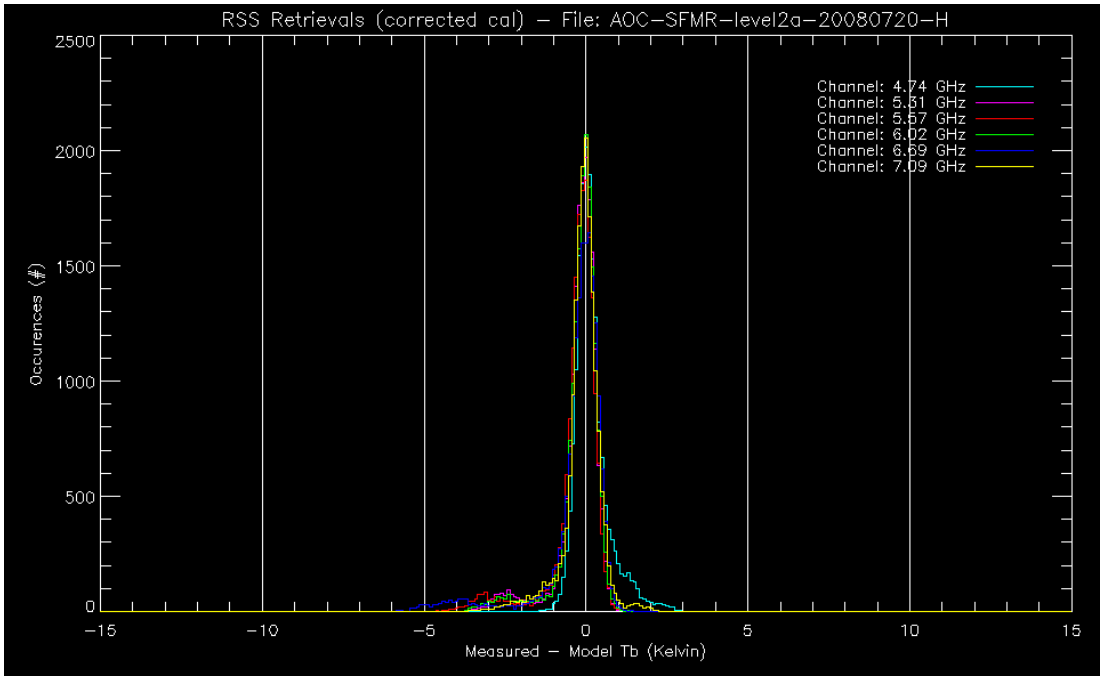

Figure 32: Same as above with calibration correction applied.

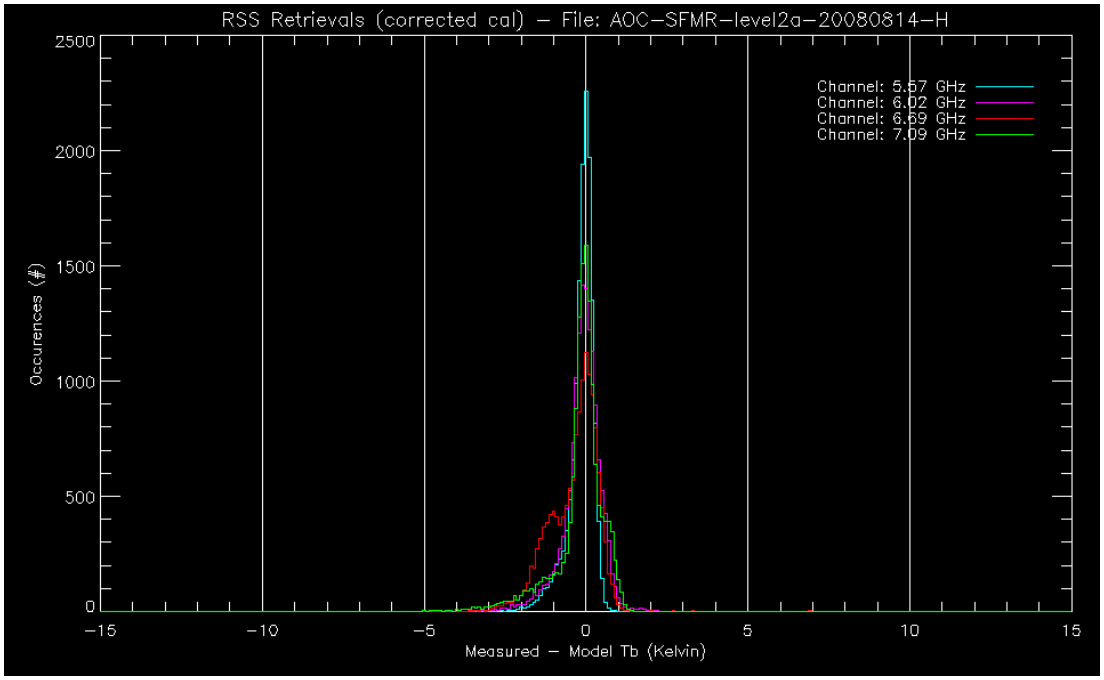

Figure 33: Same as above with calibration correction applied.

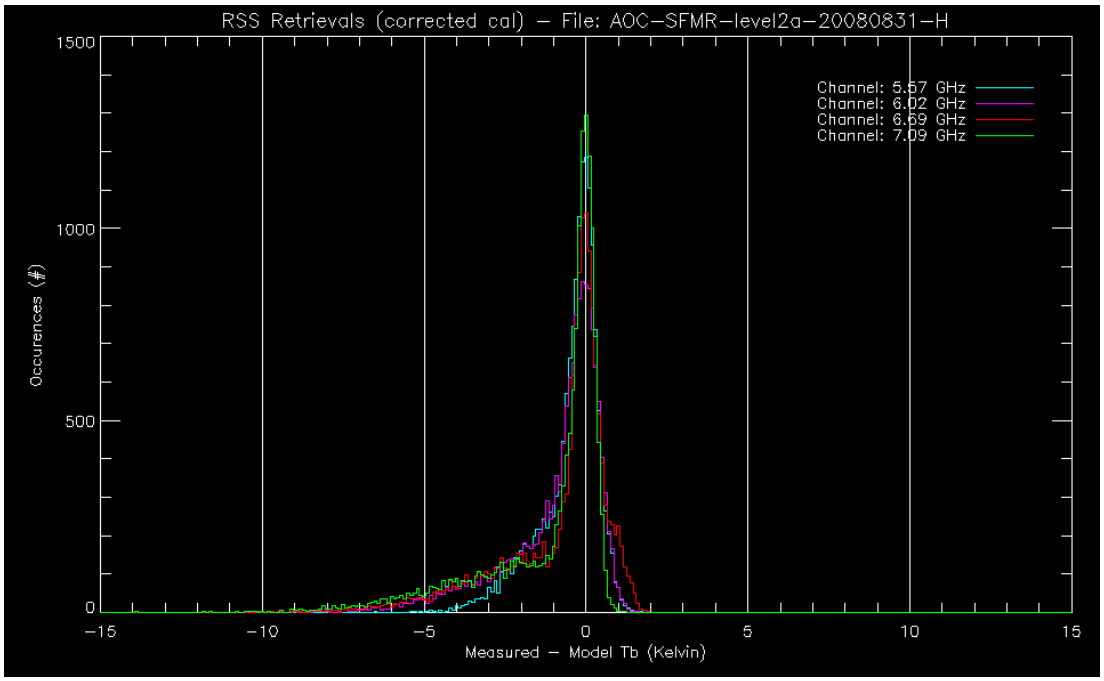

Figure 34: Same as above with calibration correction applied.

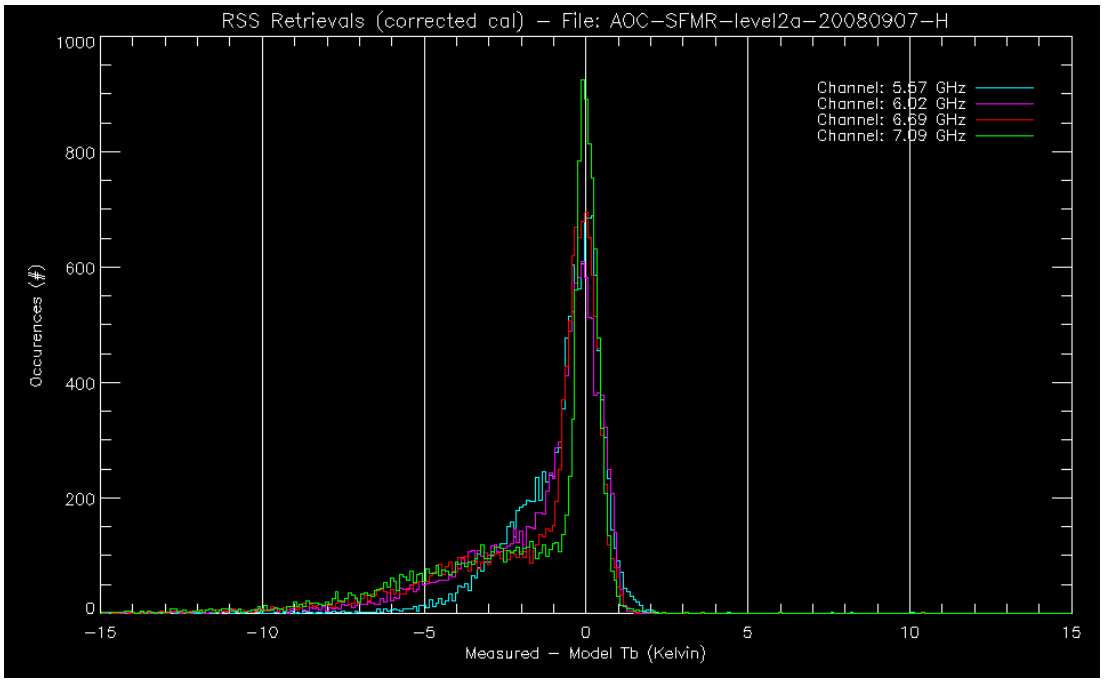

Figure 35: Same as above with calibration correction applied.

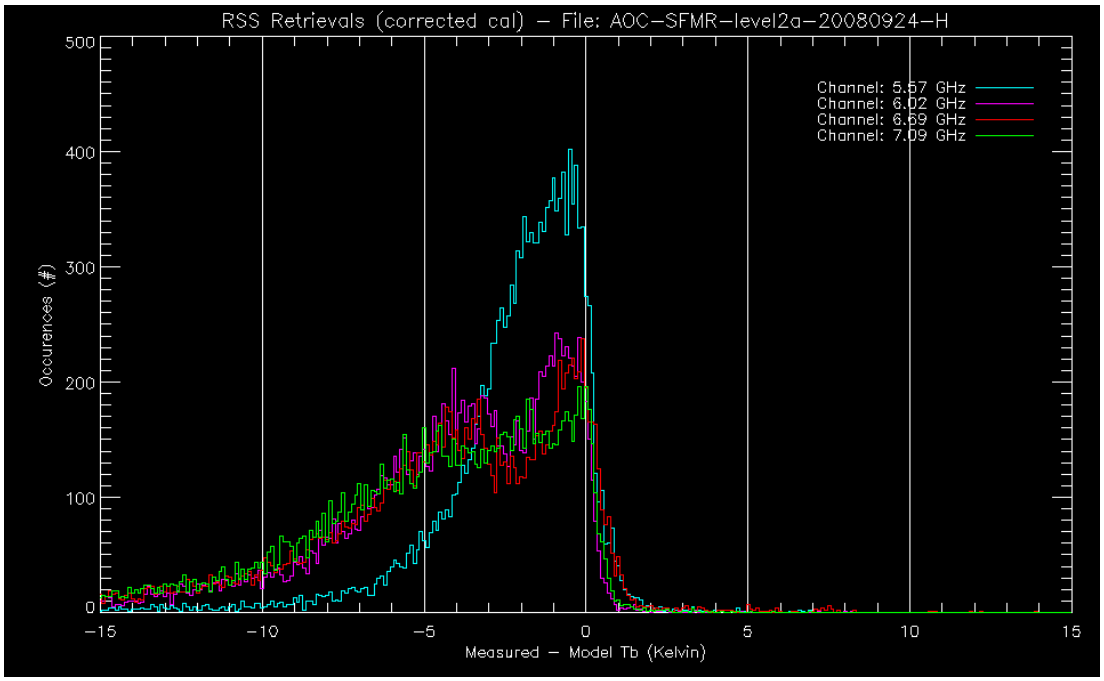

Figure 36: Same as above with calibration correction applied.

2.5.2 Hurricane Bill Example

Much discussion centered on Hurricane Bill in 2009. The AOC and Air Force SFMR units seem to disagree in terms of the maximum wind speeds reported. Applying the calibration analysis to the measurements collected, is not surprising that the instruments were not in agreement. Below the error histogram for the unit flown on the NOAA aircraft and on the Air Force at similar times on 20 August 2009 are shown. The retrievals for these data are also plotted versus time directly below the error histogram. In this case, the NOAA SFMR has large calibration errors and is reported a lower wind speed. The NOAA SFMR retrievals also exhibit more noise and do not show as low wind speeds in the eye. Much of this can be attributed to the calibration error or drift.

It should also be noted that for many Air Force flights, significant calibration errors (i.e. drifts with respect to the SFMR GMF) were noted. As a result, RSS recommends that the difference between the measured brightness temperature and the modeled value for each retrieval and channel be monitored to provide the user information as to the stability of the instrument and its calibration relative to the SFMR GMF. Further, NHC should apply this simple analysis during post analysis of a storm to provide quantified assessment as to the quality of the SFMR measurements for that mission.

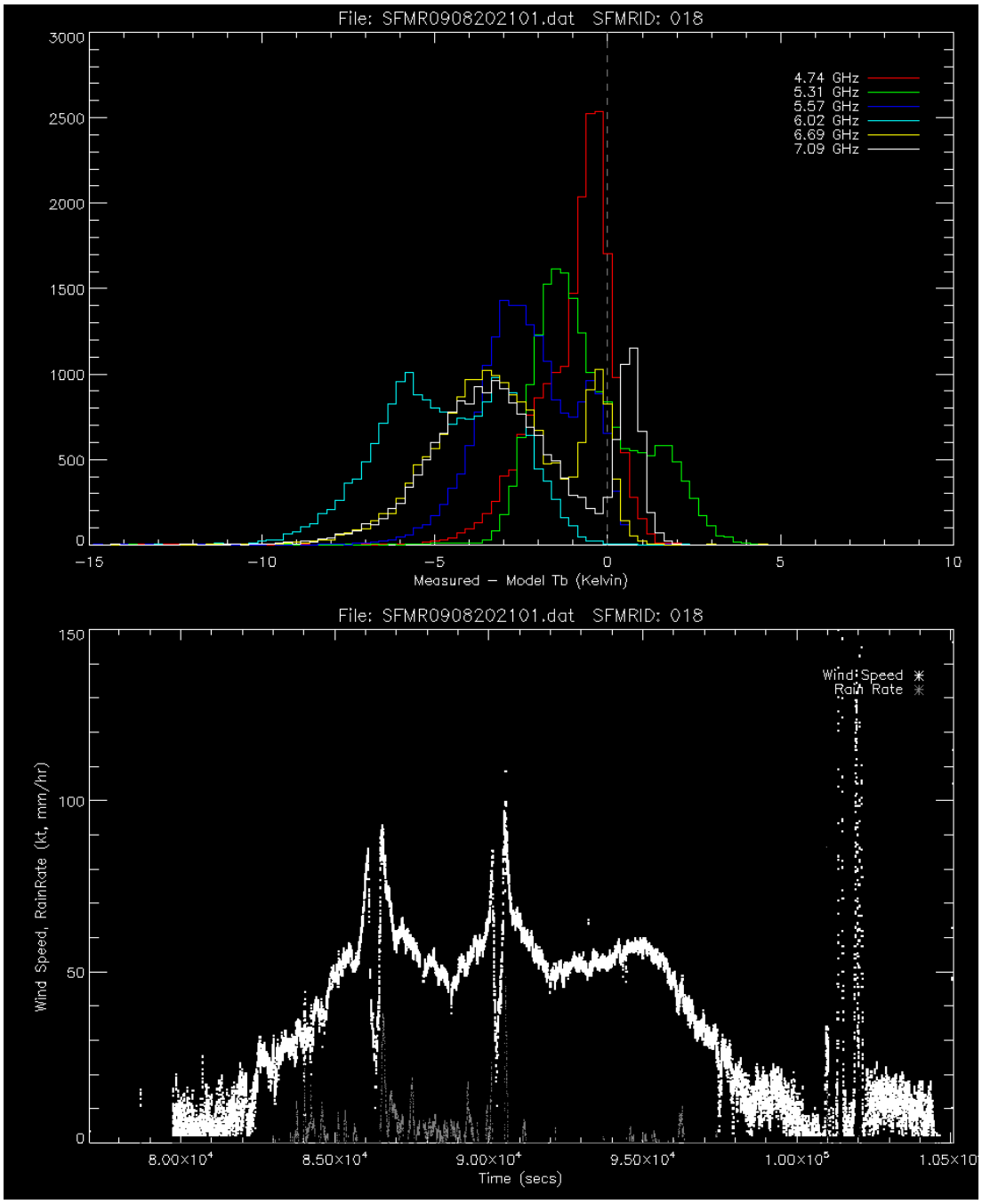

Figure 37: NOAA SFMR Measurements on 20 August 2009.

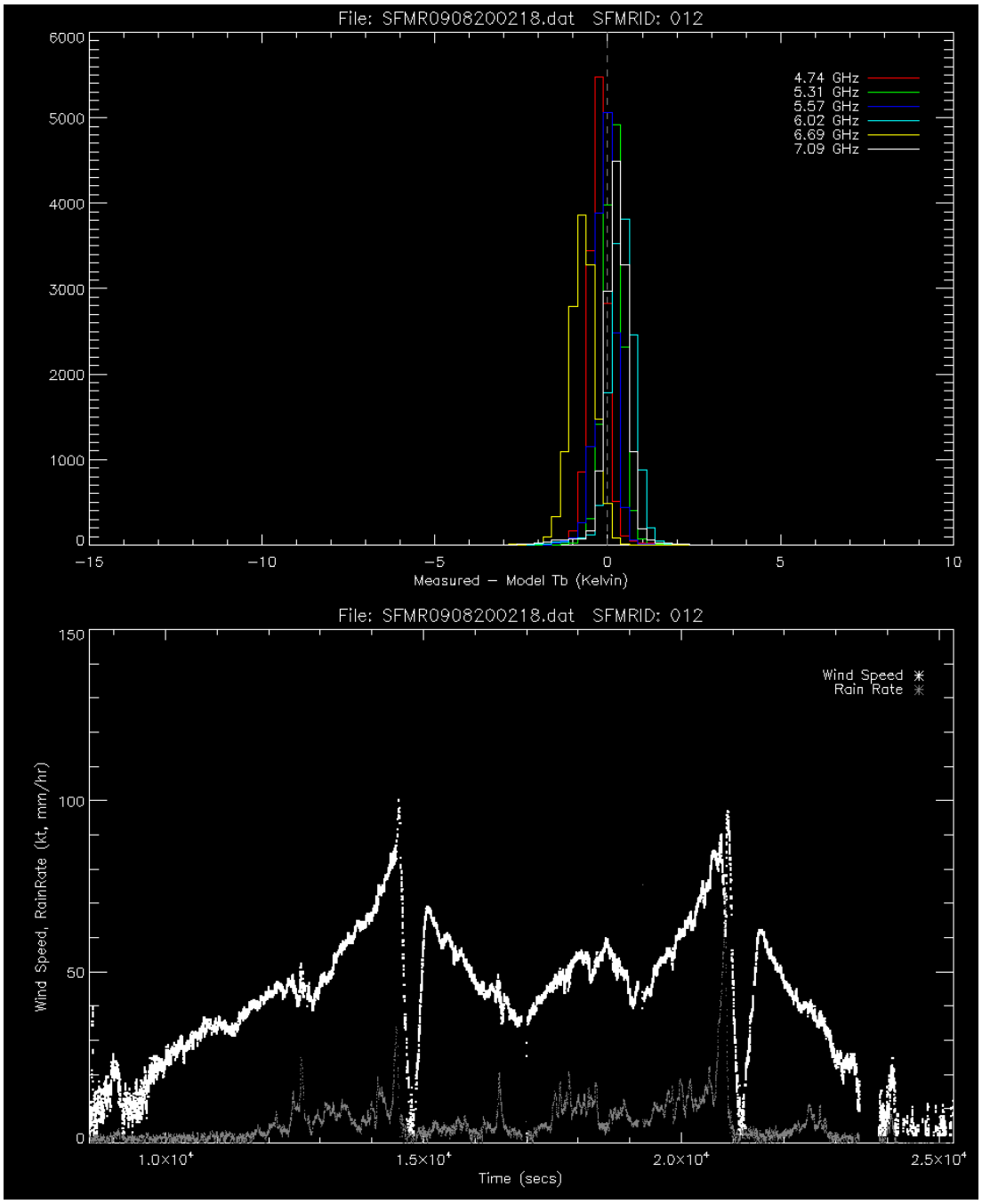

Figure 38: Air Force SFMR Measurements on 20 September 2009.

2.6 Azimuthal Variability

As found in Uhlhorn and Black (2003), SFMR surface winds show a tendency to be in error, relative to GPS dropwindsonde surface winds, as a function of storm-relative azimuth angle. In general, SFMR winds are found to be underestimated (overestimated) to the rear (fore) of the storm, with a clear single-harmonic modulation observed. There are potentially a couple of physical reasons for this observed variability:

1) Wind fetch-length and duration which varies azimuthally around a storm. Since the surface emissivity responds to foam produced by breaking waves, and not to the directly-applied stress, the retrieved SFMR wind speed may be modulated by the local wind wave development.

2) Sea surface temperature, which tends to cool to the rear of storms. The SST assumed for the SFMR radiative transfer model contains no information about this cooling, and therefore potentially differs from the the actual SST in some cases. An overestimated (underestimated) SST will produce an underestimated (overestimated) SFMR surface wind speed.

Whatever the reason, this error can be corrected based on a statistical relationship between SFMR/dropwindsonde wind differences as a function of azimuth angle, provided the storm motion direction is known. Powell et al. (2009) used a greatly expanded dataset to quantify this relationship. Based on 416 paired samples, they found the wind speed difference $S_{ws} - G_{ws}$ (m/s) varies according to:

$$S_{WS} - G_{WS} = 2.02\cos(\theta - 27),$$

where θ is the storm-relative azimuth angle in degrees, measured clockwise from the direction of motion. By assuming G_{ws} represents the true surface wind, this expression can be solved to correct the retrieved SFMR wind speed for this error.

2.7 Bathymetry-induced Error

As discussed in the previous section, SFMR winds do not respond directly to the surface wind stress, but to the resultant foam produced by breaking waves. In certain areas, particularly near coastlines, surface waves break due to shoaling, depending on the ratio of the wavelength to the local water depth. This may result in SFMR surface winds being in error, since it is necessarily assumed that wave breaking is due entirely to surface winds. The situation is complicated by wind direction, wave propagation direction, bathymetry gradient magnitude and direction, and relationships among these quantities.

Without accurate real-time information about the local surface wave energy spectrum, any possible error in SFMR winds must be corrected using statistical data. Due to the relative paucity of data obtained in land-falling storms, obtaining an adequate sample to accurately quantify this error has been difficult. To date, dropsonde surface winds have been obtained in sufficient quantity over a broad range of conditions, on two P-3 flights

in land-falling storms (Gustav and Ike in 2008). Since the advent of the operational SFMR in 2005, there have been several land-falling storms, but have generally lacked a large quantity of surface wind truth data to provide meaningful statistics. A sustained in situ observational effort over a number of cases can eventually help to achieve a desired result.

In lieu of quantitative results of the shoaling effects on SFMR winds, an approximate criterion that provides guidance on wind retrieval quality can be developed from linear wave theory and energy conservation principles. In terms of wave steepness (ratio of wave-height to wavelength H/L), deep water waves are found to become gravitationally unstable when the steepness exceeds 1/7, at which point breaking occurs. Another well-known shoaling-wave criterion states that breaking occurs when the wave height-to-water depth ratio (H/h_b) exceeds approximately 0.8. These relations are the two limits of the Miche (1944) criterion. Combining these provides a guide for depths at which wave breaking due to non-wind forcing may enhance surface emissivity, resulting in over-estimated surface winds:

H (m)	L (m)	h_b (m)
1	7	1
5	35	6
10	70	13
20	140	25

Furthermore, the Pierson-Moskowitz (1964) spectrum yields a relationship between significant wave height and wind speed. If the above height is taken to the be the significant wave height ($H = H_{1/3}$), then a wind speed vs. critical depth criterion can be estimated by the relation:

$$h_b \leq 0.033 V_{10}^2$$

V_{10} (m/s)	h_b (m)
10	3
20	12
30	27
40	48
50	75
60	108

These results are, of course, largely statistical and only suggest information on the probability of breaking, and do not indicate a simple on/off threshold for discarding data. However, they provide approximate guidance for questioning the validity of retrievals. In addition, as previously mentioned, bottom slope, and wind and wave direction will all act to modulate the breaking process. Further measurements will hopefully quantify the extent to which SFMR winds are in error under such conditions.

References

Esteban Fernandez, D., J.R. Carswell, S. Frasier, P.S. Chang, P.G. Black and F.D. Marks, “Dual-polarized C- and Ku-band ocean backscatter response to hurricane force winds.” JGR Oceans, Vol 111, pp 8013-8030, 2006.

Powell, Mark D; Uhlhorn, Eric W; Kepert, Jeffrey D Kepert, “Estimating maximum surface winds from hurricane reconnaissance measurements.” Weather and Forecasting, June, 2009.

Uhlhorn, E.W. and P.G. Black, “Verification of remotely sensed sea surface winds in hurricanes.” Journal of Atmospheric and Oceanic Technology, Vol. 20, pp 99-116, 2003.

Appendix 1

New SFMR Absorption GMF

One of the primary objectives of the 2nd year JHT effort was to improve the absorption geophysical model function (GMF) used by the SFMR retrieval process. This GMF predicts the absorption at C-band caused by precipitation. Since the brightness temperature measurements are affected by atmospheric absorption (i.e. it contributes to the measurements and attenuates the surface measurements), errors in the absorption GMF not only produce rain rate retrieval errors, but also produce ocean surface wind speed retrieval errors that depend on the rain rate, wind speed and altitude (see 1st year annual reports for more detail).

[Jiang et al, 2006] performed a comparison between the SFMR rain rate retrievals and those derived from the NOAA Lower Fuselage (LF) Radar and the NOAA Tail Doppler (TA) Radar. They reported a 5 mm/hr high bias in SFMR retrieved rain rates compared to the rain rate estimates derived from the LF and the TA radars, and found that the retrieved SFMR rain rates were approximately 60% lower than the collocated LF and TA rain rate estimates. The majority of their comparisons were for 5 to 30 mm/hr as derived by the radars. The authors concluded that the bias may be due to errors in the assumed height of the melting layer and in the way in which radar data are used to estimate average rain between the radiometer and the ocean surface. A representative measurement of rain by the TA and LF radars at one altitude was used to estimate the average mean rain rate for the vertical profile (i.e. SFMR volume). Without any other information, they argue that these two effects result in the systematic bias observed.

However, our analysis documented in the 1st year annual report and the results to follow, showed that biases in the SFMR rain rate retrieval can be caused by errors in the SFMR absorption GMF. This fact combined with the apparent under reporting of the rain rates and the anomalies in the SFMR retrievals, as noted in the previous section of this report, warranted a more thorough analysis and verification of the SFMR absorption GMF.

IWRAP Comparison

To gain a better understanding of this problem, the University of Massachusetts (UMass) Imaging Wind and Rain Airborne Profiler (IWRAP) [Esteban et al, 2005] was used to provide an independent, collocated estimate of the precipitation. This instrument was flown with the UMass SFMR on N42RF during the 2003 hurricane season and with the AOC SFMR (US002) during the 2005 hurricane season. It is a dual wavelength, conically scanning radar that simultaneously profiles the atmosphere and ocean surface at C and Ku-band and at two incidence angles. Because it conically scans, the volume it samples can be matched exactly to the SFMR volume. Using differential attenuation profile measurements, IWRAP can also directly measure the mean rain rate beneath the aircraft. Thus, the uncertainties in the assumptions that [Jiang et al, 2006] were required to make when deriving rain rate estimates from the LF and TA do not limit the IWRAP rain rate retrievals and their comparison to the SFMR rain rate retrievals.

Further, a single flight can realize thousands of collocated IWRAP-SFMR estimates providing the most thorough comparison data set.

Using the IWRAP measurements obtained in 2003 during flights through Hurricane Isabel, the Ku-band specific attenuation estimates were derived using differential attenuation techniques and collocated with the UMass SFMR rain rate estimates [Esteban, 2004]. Figure 39 (a) plots the Ku-band specific attenuation versus the UMass SFMR derived rain rate estimates. Note that the UMass SFMR acquires brightness temperature measurements at six frequencies over a very similar frequency range as the AOC SFMR. Further, it simultaneously measures all six frequency channels at 20 Hz resulting in a 0.06 K precision per channel over the same integration period as the AOC SFMR which has a 0.5 K precision. Overlaid on this plot is a power law model function that predicts the specific attenuation as a function of rain rate at two different temperatures. As this figure shows, the SFMR rain rates under predict the “true” rain rate, assuming the specific attenuation models are correct. Scaling the SFMR rain rates by a factor of 2.5 and subtracting an offset of 5 mm/hr, the specific attenuation measurements are plotted versus the “corrected” SFMR rain rate estimates in Figure 39 (b). The data now agrees well with the models. Figure 40 plots the corrected SFMR rain rate estimates and IWRAP rain rate estimates versus time. The agreement is excellent. The IWRAP rain rates show more variation only because the IWRAP spatial resolution is much greater. Note that the 5 mm/hr offset is the exact same bias as reported by [Jiang et al, 2006] even though they used a different approach and different instruments.

Following this comparison, rain rate estimates from IWRAP were derived from measurements collected from the NOAA N42RF WP-3D aircraft during a flight through Hurricane Rita on 22 September 2005. These estimates were collocated with the AOC SFMR rain rate estimates to within +/- 75 m in the along track direction (center of the pixels). More than 2000 collocated rain rate estimates (above 10 mm/hr) were found and these measurements spanned 10 mm/hr to 70 mm/hr. The collocated rain rate estimates were divided into 2.5 mm/hr bins, based on the IWRAP rain rate estimates, and averaged. Each bin contained a minimum of 30 pairs of collocated rain rate estimates. Figure 41 plots the results. A fit to this data set (linear regression) showed, once again, that the SFMR rain rates have an approximate bias of 5 mm/hr (4.6 mm/hr) and that they under estimate the rain rate by a factor of 2.5 compared to the IWRAP rain rate estimates. That is, the slope and offset of the linear regression between the SFMR and IWRAP rain rate estimates were 0.4 and 1.85 mm/hr, respectively.

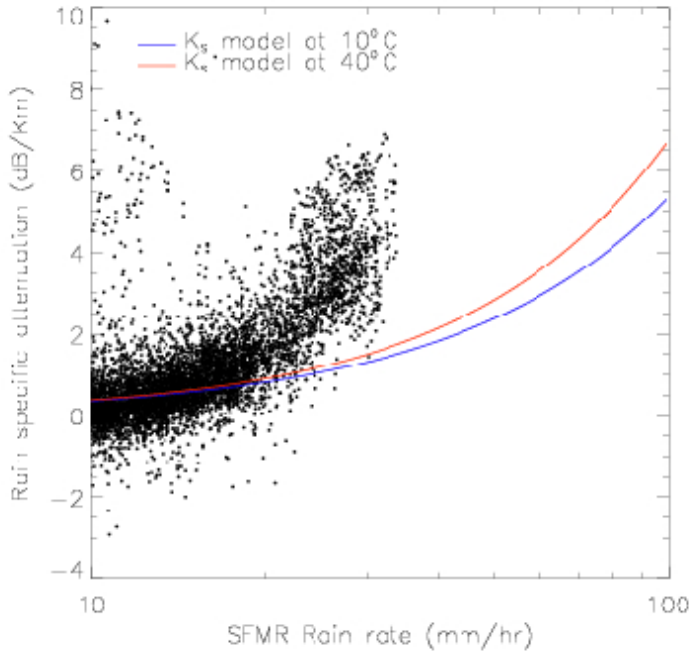

(a)

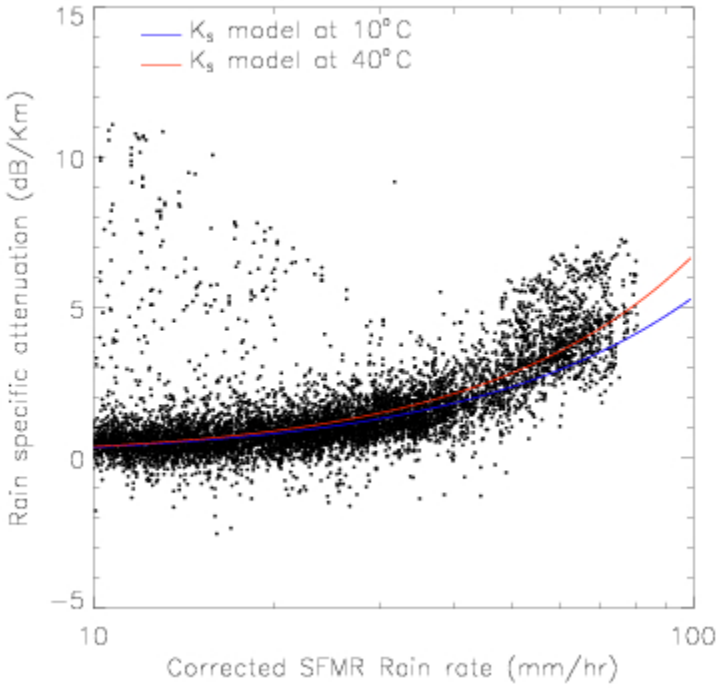

(b)

Figure 39: IWRAP derived specific attenuation plotted versus the UMass SFMR rain rate estimates (a) and corrected rain rate estimates (b). These observations were collected through a series of flights through Hurricane Isabel in 2003.

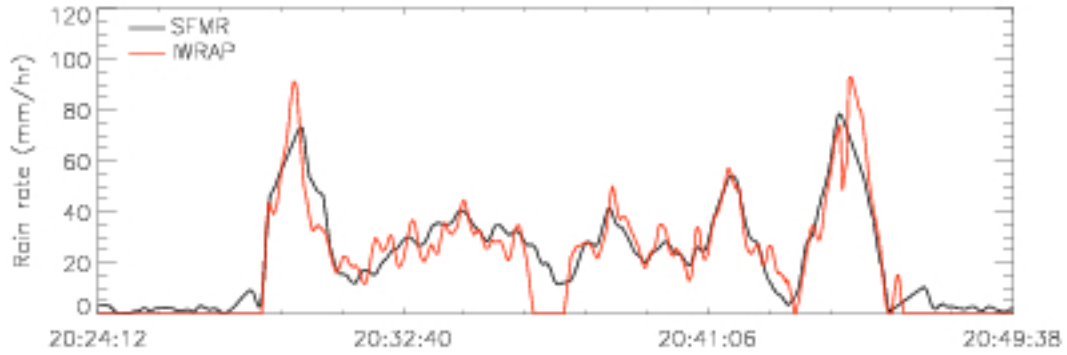

Figure 40: Time series plot of IWRAP (red) and corrected SFMR (black) rain rate estimates are shown. The corrected SFMR rain rates were derived by subtracting 5 mm/hr from the original SFMR rain rates and multiplying by 2.5.

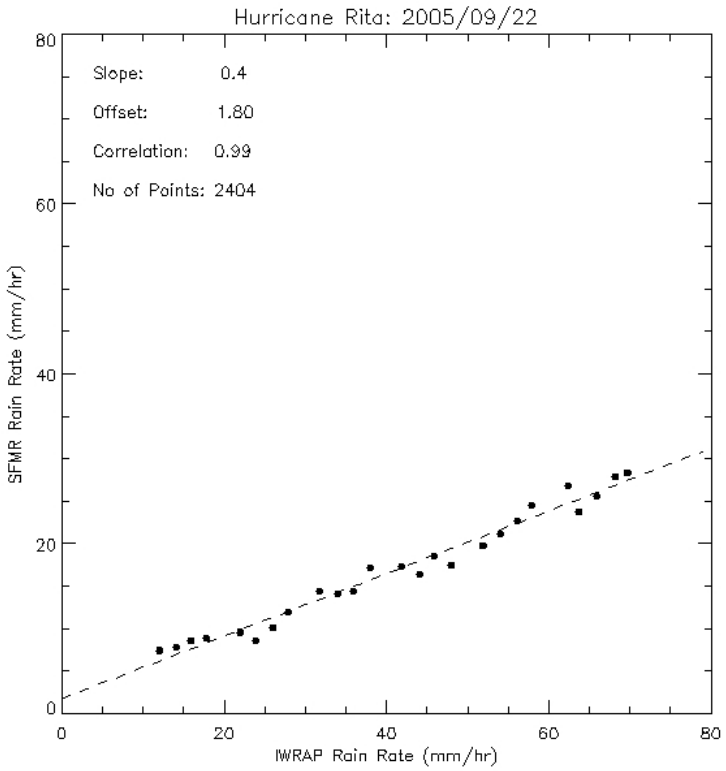

Figure 41: SFMR bin averaged rain rate estimates are plotted versus IWRAP rain rate estimates. The dashed line is a linear regression with the slope, offset and correlation coeffients given in the legend.

These independent results agree with those obtained from the 2003 data and are consistent with the results reported by [Jiang et al, 2006]. Furthermore, the correlation between these two sets of retrievals (IWRAP and the SFMR) is 98 percent. The high correlation shows that the precipitation sampled by these two instruments is the same, and the agreement between the comparison of the 2003 and 2005 data verifies that this approach is robust and consistent. Finally the difference between the IWRAP and SFMR rain rate estimates did not exhibit any dependence on the retrieved wind speed.

This is consistent with our simulations that show that modeling errors in the absorption GMF produce rain rate errors that are independent of wind speed

Deriving New SFMR Absorption GMF

The SFMR retrieval process currently uses an absorption model that was reported in [Jiang et al, 2006]. This model has three empirically derived parameters (R_m, R_e and F_e) and is given below:

$$K = \alpha\left(f^{R_m R_r^{F_e}}\right)\left(R_r^{R_e}\right) \quad (1)$$

where,

R_r = rain rate (mm/hr)
□ = 1.87×10^{-6} Np / km (constant)
f = frequency (GHz)
R_m = rain multiplier coefficient
R_e = rain exponent coefficient
F_e = frequency exponent coefficient

[Jiang et al, 2006] suggest that the parameter R_e should have a value of 1.15. Starting in 2005, all SFMR retrievals were derived using the 1.15 value for R_e. Using a Monte-Carlo analysis that is described below, the three empirically derived parameters were analyzed and found to not provide an optimal solution. New values were sought that would remove the bias in the SFMR rain rate retrievals, provide a stable solution and improve the accuracy of the SFMR wind speed and rain rate retrievals.

Monte-Carlo Analysis

As the equation (1) shows, the absorption increases with both rain rate and frequency. In order to assess the accuracy of different rain model parameters, RSS implemented a Monte-Carlo analysis that varied the empirically derived parameters, R_m, R_e and F_e, in equation (1) around their current values: 2.6, 1.15 and 0.0736, respectively, to seek a solution that would optimize the slope and offset between the comparison of the collocated IWRAP and SFMR rain rate estimates and maintain a correlation better than 97 percent between these two data sets. For each potential solution of R_m, R_e and F_e, the collocated SFMR rain rates were plotted versus the IWRAP rain rates and the slope and offset were calculated. Plotting the solutions in R_e, F_e and R_m space, we found a grouping for which the offset was less than 0.15 m/hr, the slope was greater than 0.9 and the correlation between the two retrieval data sets was greater than 97 percent. These solutions are given in Table 1.

Table 2: Solution set for absorption GMF coefficients.

Re	Fe	Rm	Slope (m)	Offset (b)
0.76	0.0676	2.75	0.947	0.110
0.74	*0.0696*	*2.75*	*0.950*	*0.138*
0.74	0.0716	2.8	0.900	0.015
0.72	0.0736	2.8	0.910	-0.109
0.7	0.0756	2.8	0.915	-0.074

Figure 42 plots the absorption GMF, as described by equation (1) and the coefficients in Table 1. The frequency was set to 6.02 GHz (middle SFMR channel) and each line represents a set of coefficients. The results were similar for the other SFMR frequencies as well. The blue curve represents the highlighted solution in Table 1. It is the chosen solution since it provides the lowest offset (-0.074 mm/hr) and represents roughly the average solution in Figure 42 . The green curve is the original solution (R_e = 1.15, F_e =0.0736 and R_m = 2.6), and as this plot shows, it significantly over estimates the absorption, and thus, the retrieval process under estimates the true rain rate and wind speed.

To validate these results, an independent collocated data set consisting of surface wind estimates from GPS dropsondes and the AOC SFMR deployed on N43RF WP-3D aircraft in 2005 were used. This is the same data set that was published by [Uhlhorn et al., 2006]. Note that the excess emissivity SFMR GMF (or wind GMF) was trained on this data set in [Uhlhorn et al, 2007]. The GPS dropsonde surface wind speed estimates were derived using the lowest 150-m averaged wind speeds reported from each drop profile and scaling the data according to [Franklin et al, 2003]. For details, see [Uhlhorn, et al, 2006]. The SFMR surface wind speeds were derived using the 2005 absorption GMF and the excess emissivity model as reported by [Uhlhorn et al, 2007].

Figure 43 plots a histogram of the retrieved rain rate for these data. Although rain rates greater than 40 mm/hr were sampled, the majority of the data was collected in lower rain conditions (approximately 70 percent of these data were acquired under rain conditions less than 20 mm/hr).

Figure 44 plots the GPS surface wind estimates versus the collocated SFMR surface wind estimates using the 2005 absorption GMF. The mean difference between the SFMR wind speed estimates and the GPS dropsonde surface wind estimates is approximately 1.0 m/s. The solid circles represent the bin averaged data (7 m/s bin size). A linear fit between these data is shown by the dashed curve and the slope and offset are given. The slope is consistent with that reported by [Uhlhorn et al, 2007]. Besides the SFMR slightly under reporting the surface wind speeds, the difference between the dropsonde surface winds and the SFMR error grows with wind speed.

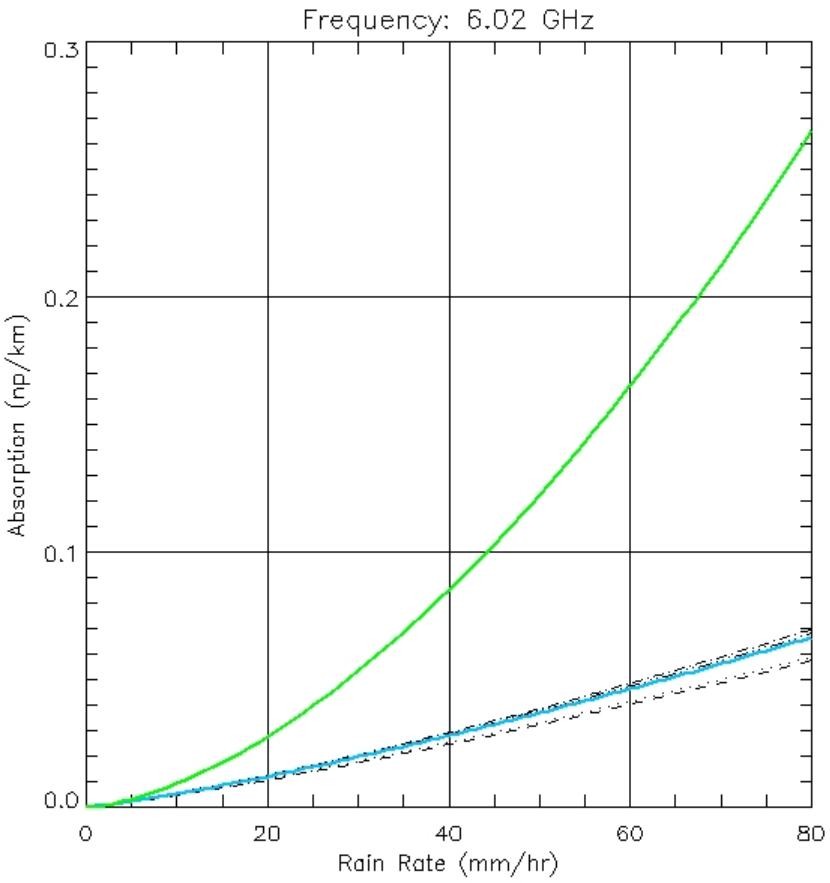

Figure 42: Absorption at 6.02 GHz plotted versus rain rate. The green curve is the original solution. The dashed dotted curves are from Table 2 and the blue curve is the selected solution.

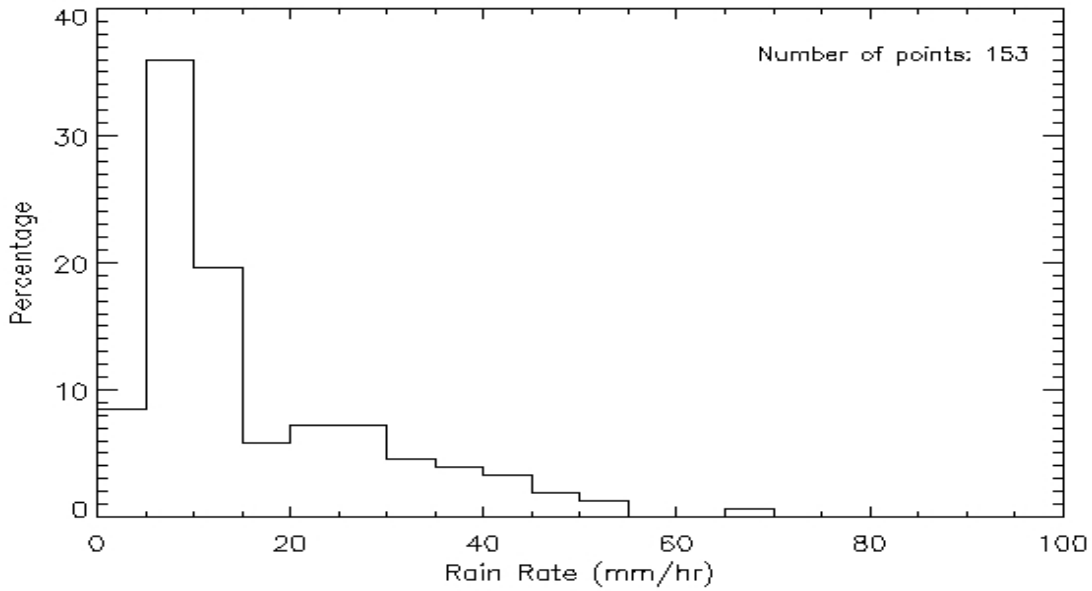

Figure 43: Histogram of rain rate measurements for figures 33 and 34. Bin size is 5 mm/hr.

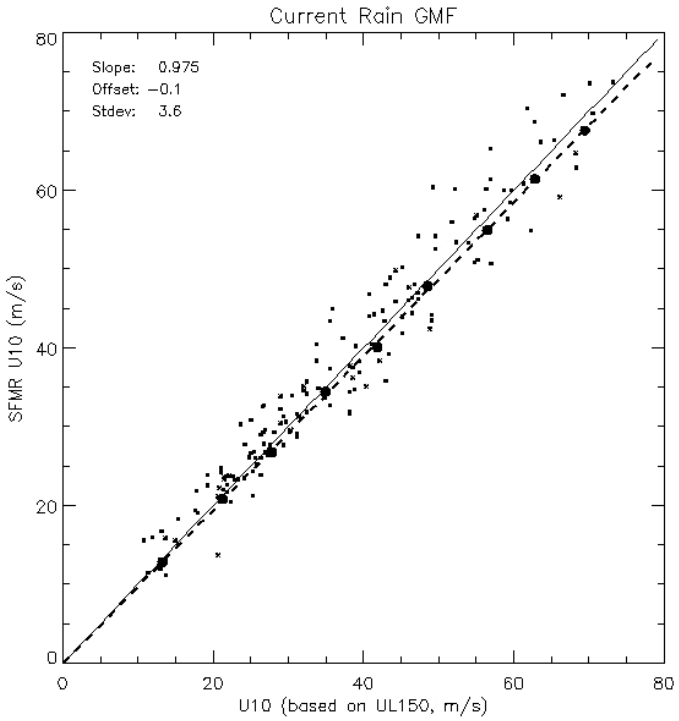

Figure 44: SFMR wind speed retrievals derived using the 2005 absorption GMF are plotted versus collocated GPS dropsonde surface wind speed estimates. See Uhlhorn et al, 2007 for details on processing of the dropsonde data and collocation scheme. The large solid circles represent the binned averaged data (7 m/s bins). The dashed line is a linear regression to the data.

Figure 45 plots this residual error (green circles) versus wind speed. It clearly shows a more negative value as a function of wind speed. Assuming that the errors in the 2005 absorption GMF are the cause, this error would be larger if higher rain rates had been experienced. The solid green curve is a linear fit to these data. The correlation of this fit is approximately -78 percent.

Using the new absorption GMF reported above (R_e = 0.7, F_e =0.0756, R_m = 2.8), new SFMR wind speed estimates are derived from the same set of SFMR measurements. Figure 46 plots the comparison between the GPS dropsonde surface wind speed estimates and these new SFMR surface wind speed estimates. The mean difference between the new SFMR surface wind speed estimates and those derived from the GPS dropsonde measurements is 0.087 m/s. Once again the data are averaged into 7 m/s bins shown by the solid circles. A linear fit to these data now shows a slope of 1.0. The residual error, shown in Figure 45 (blue dots), and the fit to this error (blue line), show no significant dependence on wind speed. Thus, the new absorption GMF better represents the true absorption due to rain, and this model has removed the errors (bias) in the wind speed retrieval caused by the errors in the 2005 absorption GMF.

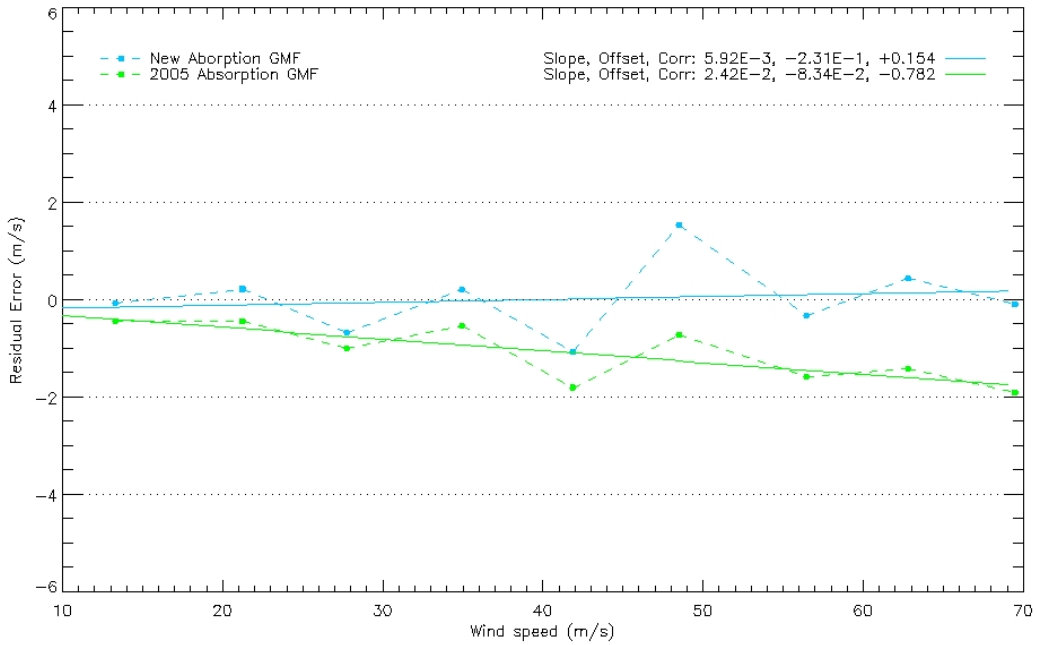

Figure 45: Residual error in retrieved wind speed. Blue and green lines are linear fits to the residual error when using the new absorption GMF and the 2005 absorption GMF, respectively.

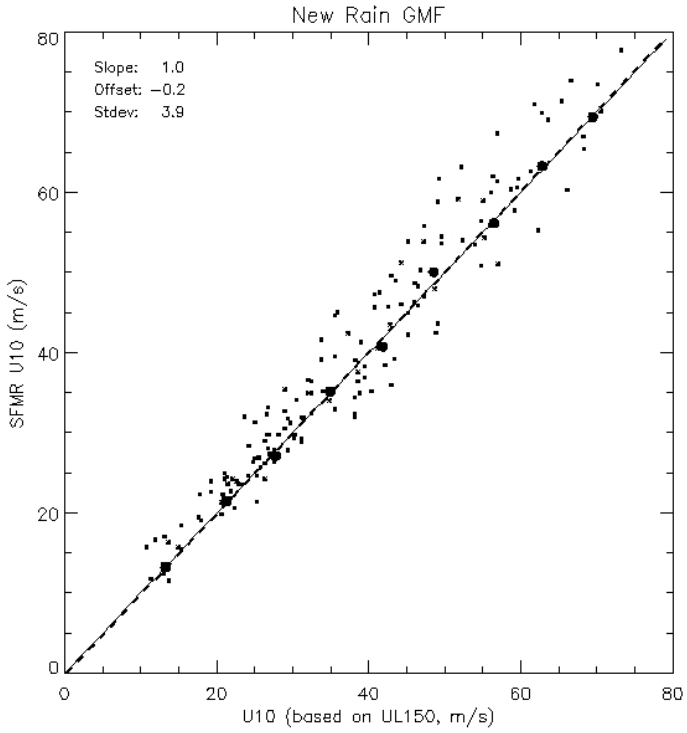

Figure 46: Same as Figure 44 except the new absorption GMF is used in the retrieval process (Re=.7, Rm=2.8, Fe=0.696)

Retrieval Error with 2005 Absorption GMF

Because the 2005 absorption GMF is incorrect, the SFMR wind speed and rain rate retrievals that were derived using this GMF are in error, and this error depends on wind speed, rain rate and altitude. At the 2007 IHC, the community requested that this error be determined. To accomplish this task, we simulated the brightness temperature measurements using the correct (new) absorption GMF over all rain and wind conditions and at two different altitudes. Using the 2005 absorption GMF in the retrieval process, the retrieved wind and rain rates are derived. Thus, this simulates the measurement and retrieval process for the 2005/2006 hurricane season. The error in the retrievals is simply the difference between the retrieved wind speed and rain rate and the actual wind speed and rain rate used to produce the simulated brightness temperature measurements.

Using the SFMR simulator, we derived a simulated brightness temperature data set over wind conditions from gale to category 5 hurricane force winds and rain rates from 0 to 100 m/hr. We assumed a 0.5 K measurement precision. For each wind speed and rain rate, we realized 1000 measurements at the six SFMR frequencies and a standard deviation of 0.5 K. The new absorption GMF was used in the SFMR brightness temperature model function to derive the mean values. A SST of 29 degrees, an ambient air temperature of 20 degrees C and an altitude of 1524 m were assumed. The SFMR retrieval process was run on each point using the 2005 absorption GMF. The mean errors between the retrieved wind speed and rain rate and the inputted wind speed and rain rate used to create the brightness temperature measurements were calculated and binned according to the wind speed and rain rate.

Figure 47 presents a contour of the wind speed retrieval error as a function of wind speed and rain rate assuming an altitude of 1524 m. The x-axis is the true wind speed in knots and the y-axis is the true rain rate in mm/hr. The SFMR retrievals under predict the true wind speed with the error growing with increasing rain rate and decreasing wind speed. For example if the true rain rate is 60 mm/hr, the SFMR using the 2005 absorption GMF would have reported 45 kt, 60.5 kt and 80 kt for a true wind speed of 50 kt, 64 kt and 83 kt, respectively.

As the aircraft flies higher, the error in the retrieved wind grows. Figure 49 presents the same contour except the assumed altitude is 3048 m. For the same example given above where the true rain rate was 60 mm/hr and the wind speeds were 50 kt, 64 kt and 83 kt, the retrieved SFMR wind speeds using the 2005 absorption GMF would have reported the surface wind speeds to be 43.2 kt, 59.4 kt and 88.9 kt. As these contour plots demonstrate, the uncertainty or error in the SFMR wind speed estimates, depends on altitude, wind speed and rain rate.

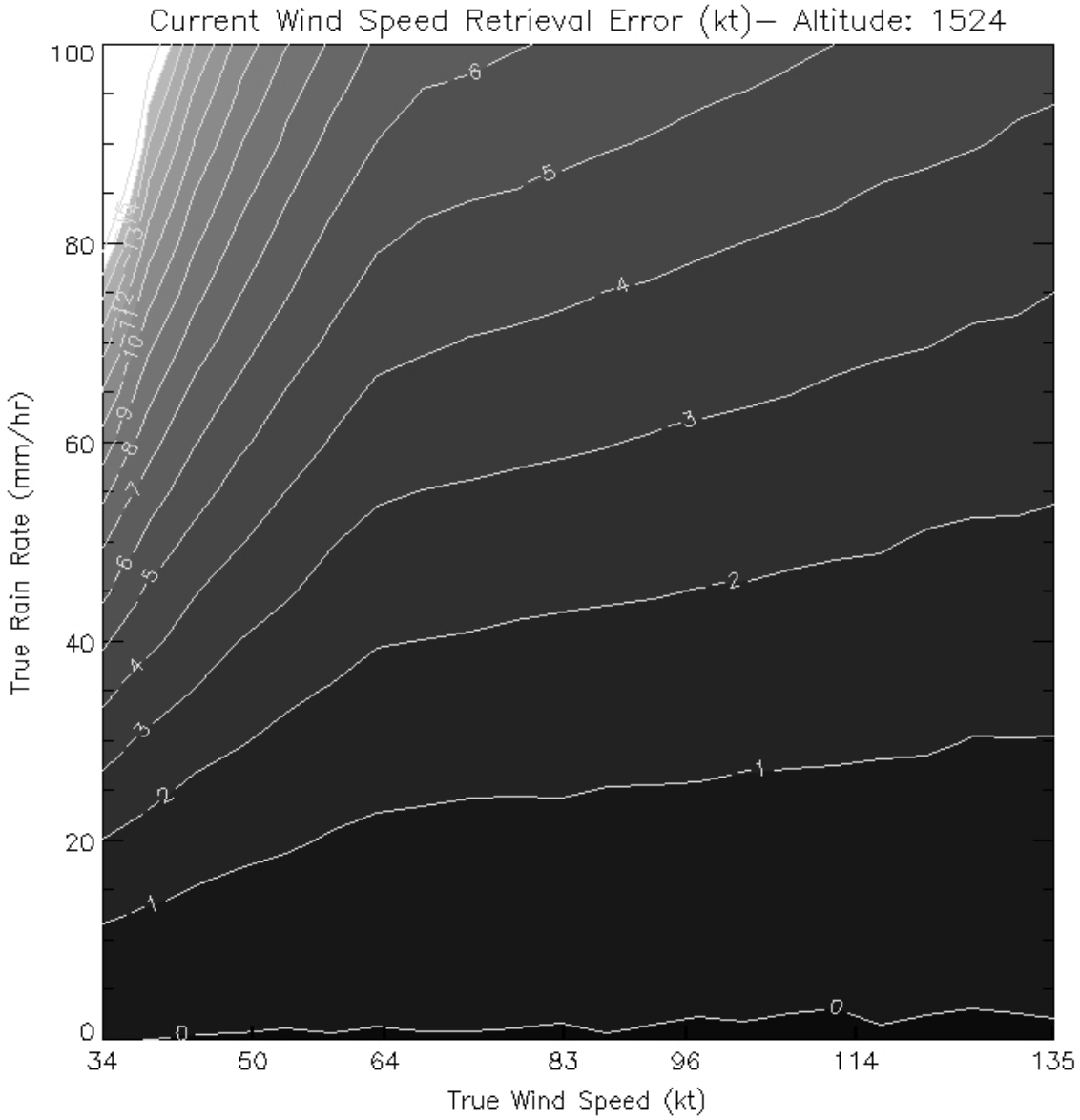

Figure 47: Contour of the SFMR wind speed retrieval error in knots using the 2005 absorption GMF in the retrieval process is shown over a range of wind speeds and rain rates. The reported error is calculated by subtracting the true wind speed from the retrieved wind speed. A negative value means that the SFMR retrieved winds under reports the true wind speed. A 1524-m altitude, 20 deg C ambient temperature and 29 deg C SST were assumed.

Likewise, the rain rate retrievals using the 2005 absorption GMF also under predict the true rain rates. However, unlike the wind speed retrieval error, the rain rate retrieval error is not dependent on wind speed or altitude. This is expected since it is a column averaged rain rate which accounts for the column height and the surface emissitivity is modeled correctly. Figure 49 and Figure 50 plot the contours for the SFMR rain rate retrievals for 1524 m altitude and 3048 m altitude. The rain rate retrieval error depends only on the true rain rate growing with increasing rain rate. This agrees with the results shown in the comparison between IWRAP and SFMR rain rate retrievals (Figure 41).

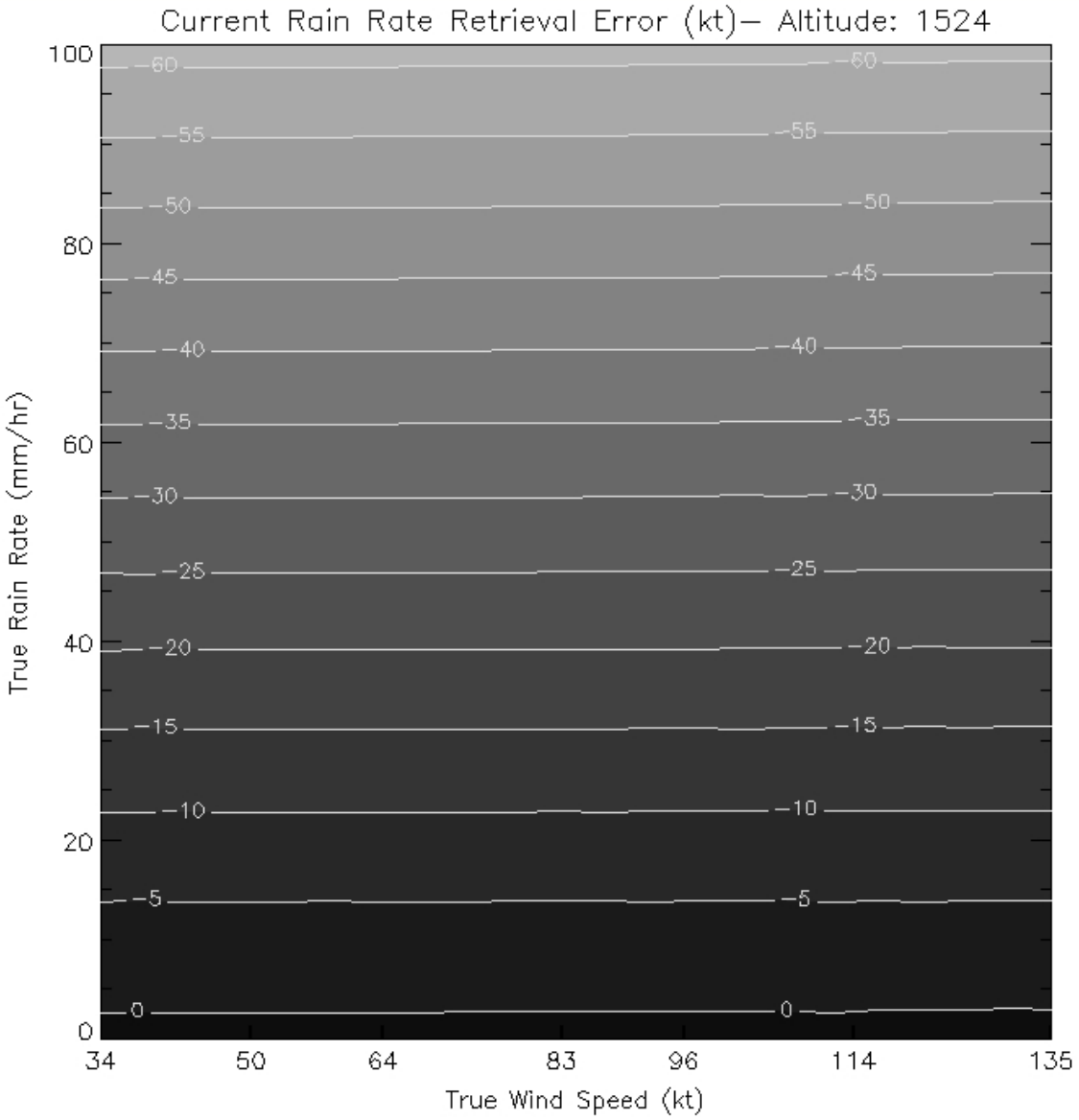

Figure 48: Contour of the SFMR rain rate retrieval error in mm/hr using the 2005 absorption GMF in the retrieval process is shown over a range of wind speeds and rain rates. The reported error is calculated by subtracting the true rain rate from the retrieved rain rate. A negative value means that the SFMR retrieved rain rate under reports the true rain rate. A 1524-m altitude, 20 deg C ambient temperature and 29 deg C SST were assumed.

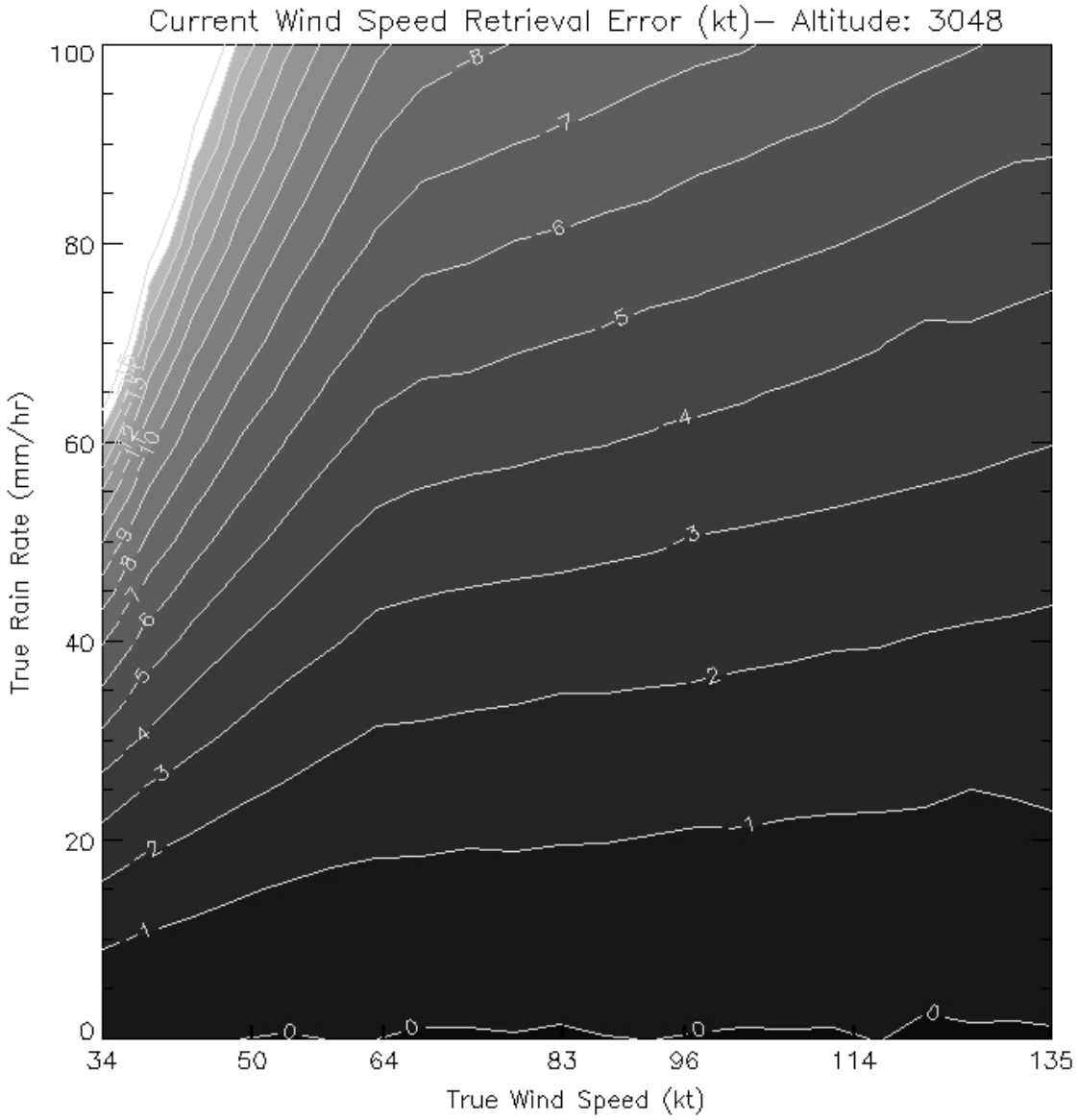

Figure 49: Same as Figure 47 except the altitude is now 3048 m.

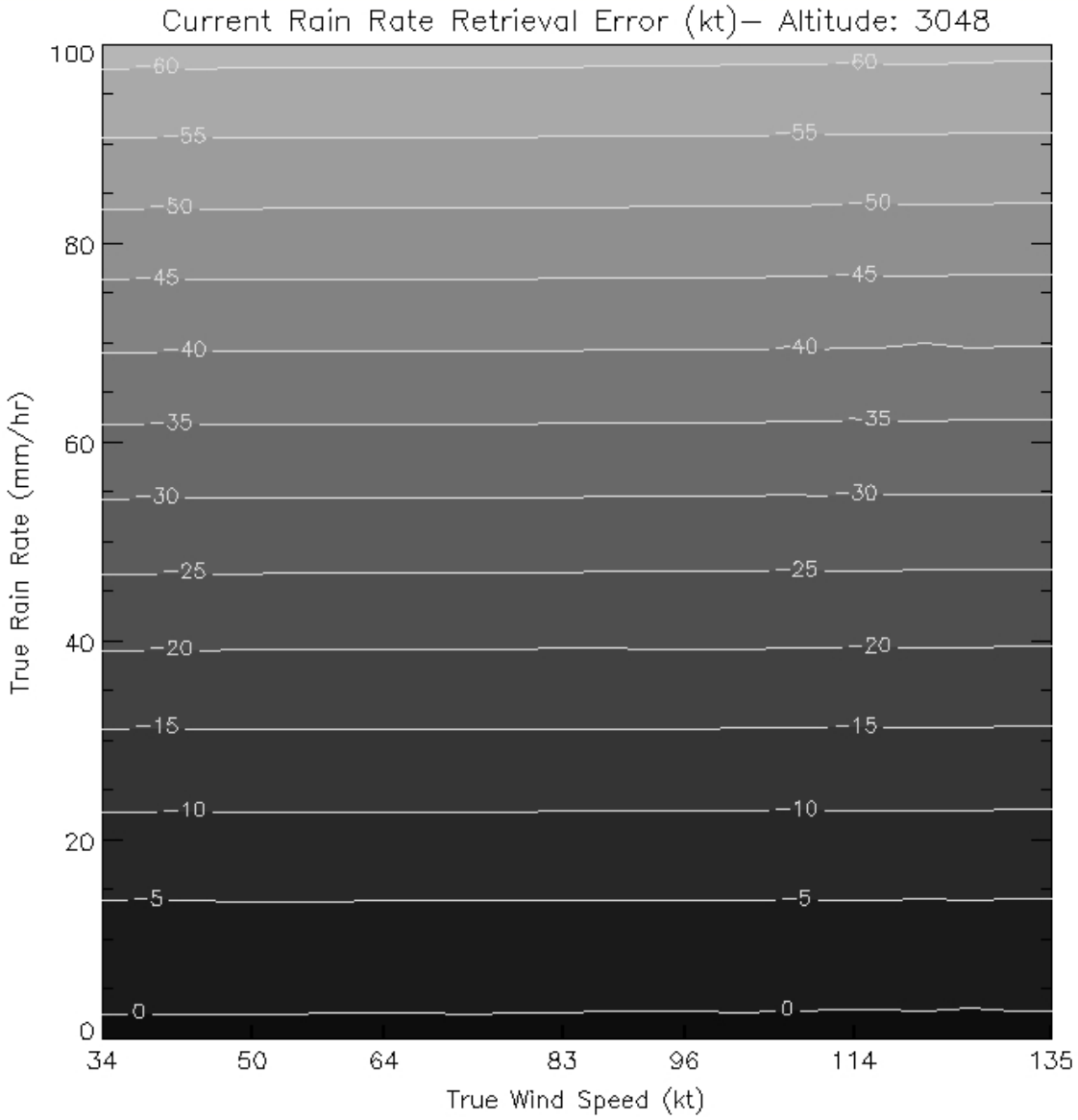

Figure 50: Same as Figure 48 except the altitude is now 3048 m.

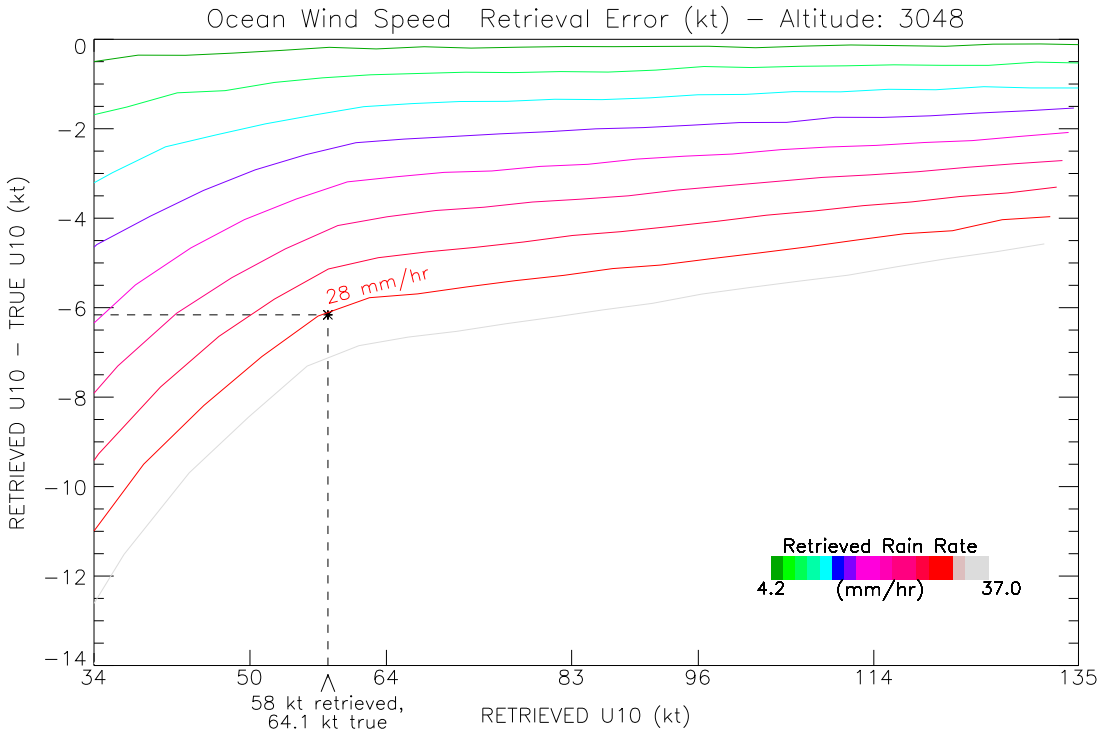

Figure 51: The error in the SFMR retrieved wind speed (retrieved – actual surface wind speed)

In order to determine the error in the 2005 and 2006 SFMR retrieval estimates from the retrievals themselves, a series of curves were generated. Each curve is at a constant SFMR retrieved rain rate and represents the error (SFMR retrieved surface wind – true surface wind) as a function of the SFMR retrieved surface wind speed. These curves are plotted in Figure 51. An altitude of 3048 m is assumed. From these curves the error in the retrieved SFMR wind speed can be determined based on the retrieved wind speed and rain rate. For example, if the retrieved rain rate was 28 mm/hr and the retrieved wind speed was 58 kt, the SFMR would have under estimated the true surface wind speed by 6.1 kt. That is, the true wind speed is really 64.1 kt, and the system is a category 1 hurricane rather than a tropical storm.

APPENDIX 2: Center Fix NetCDF file format.

```
netcdf centerFix-<storm name> {
dimensions:
        observationIndex = UNLIMITED ;
        stringWidth = 4 ;
        stringDepth = 16 ;
variables:
        double unixTime(observationIndex) ;
                unixTime:units = "seconds from 01/01/1970" ;
                unixTime:name = "Unix Time" ;
        float latitude(observationIndex) ;
                latitude:units = "degrees North" ;
                latitude:name = "Latitude" ;
        float longitude(observationIndex) ;
                longitude:units = "Degrees West" ;
                longitude:name = "Longitude" ;
        int eFlag(observationIndex) ;
                eFlag:units = "*0 - Source*10, 1 - Interpolated, 2 - Extrapolated" ;
                eFlag:name = "Flag Indicating Actual, Interpolated or Extrapolated Data" ;
        char fixSource(stringDepth, stringWidth) ;
                fixSource:name = "Center Fix Data Source. Index multiplied by 10 to get
eFlag value." ;

// global attributes:
                :dataType = "Center Fix data" ;
                :storm = "<storm name>" ;
                :creationTime = "yyyymmdd hh:mm:ss" ;
                :fileSize =  ;
                :deltaTime = 30. ;
                :startTime = ;
                :centerFixSource                                                    =
"AIRC,BEST,DVTS,AMSU,ANAL,SSMI,TRMM,AMSR,SSMS,WSAT,QSCT,ASCT,RDR
C,RDRD,MMHS,UDEF" ;
```

APPENDIX 3: URNT15 NetCDF file format.

```
netcdf URNT15-<STORM NAME> {
dimensions:
        observationIndex = UNLIMITED ;
variables:
        short aircraftAgencyTag(observationIndex) ;
                aircraftAgencyTag:name = "0 = Airforce, 1 = NOAA" ;
        short aircraftTailNumber(observationIndex) ;
                aircraftTailNumber:name = "Tail Number" ;
        int observationNumber(observationIndex) ;
                observationNumber:name = "Observation Number" ;
                observationNumber:units = "(same number as in original file)" ;
        double unixTime(observationIndex) ;
                unixTime:units = "seconds from 01/01/1970" ;
                unixTime:name = "Unix Time" ;
        float latitude(observationIndex) ;
                latitude:units = "degrees North" ;
                latitude:name = "Latitude" ;
        float longitude(observationIndex) ;
                longitude:units = "Degrees East" ;
                longitude:name = "Longitude" ;
        float staticAirPressure(observationIndex) ;
                staticAirPressure:units = "mbar" ;
                staticAirPressure:name = "Static Air Pressure" ;
        float geopotentialAltitude(observationIndex) ;
                geopotentialAltitude:units = "m" ;
                geopotentialAltitude:name = "Geopotential Altitude" ;
        float surfacePressure(observationIndex) ;
                surfacePressure:units = "mbar" ;
                surfacePressure:name = "SurfacePressure" ;
        float dValue(observationIndex) ;
                dValue:units = "m" ;
                dValue:name = "DValue" ;
        float airTemperature(observationIndex) ;
                airTemperature:units = "degrees Celsius" ;
                airTemperature:name = "Air Temperature" ;
        float dewPoint(observationIndex) ;
                dewPoint:units = "degrees Celsius" ;
                dewPoint:name = "Dew Point" ;
        float flightWindSpeed(observationIndex) ;
                flightWindSpeed:units = "kt" ;
                flightWindSpeed:name = "Flight Wind Speed" ;
        float flightWindDirection(observationIndex) ;
                flightWindDirection:units = "degrees wrt North" ;
                flightWindDirection:name = "Flight Wind Direction" ;
```

float maxFlightWindSpeed(observationIndex) ;
maxFlightWindSpeed:units = "kt" ;
maxFlightWindSpeed:name = "Max Flight Wind Speed" ;
float maxSFMRWindSpeed(observationIndex) ;
maxSFMRWindSpeed:units = "kt (max ten second average)" ;
maxSFMRWindSpeed:name = "Max SFMR Wind Speed" ;
float SFMRRainRate(observationIndex) ;
SFMRRainRate:units = "mm/hr" ;
SFMRRainRate:name = "Sfmr Rain Rate" ;
float qualityFlag(observationIndex) ;
qualityFlag:units = "" ;
qualityFlag:name = "Quality Flag" ;
float latDistTocenterFix(observationIndex) ;
latDistTocenterFix:units = "km" ;
latDistTocenterFix:name = "Latitude Distance to Center Fix" ;
float lonDistTocenterFix(observationIndex) ;
lonDistTocenterFix:units = "km" ;
lonDistTocenterFix:name = "Longitude Distance to Center Fix" ;
float centerFixLat(observationIndex) ;
centerFixLat:units = "km" ;
centerFixLat:name = "Center Fix Latitude" ;
float centerFixLon(observationIndex) ;
centerFixLon:units = "km" ;
centerFixLon:name = "Center Fix Longitude" ;
int centerFixVFlag(observationIndex) ;
centerFixVFlag:units = "*0 - Source*10, 1 - Interpolated, 2 - Extrapolated, 3 - No Data, 4 - Bad Data" ;
centerFixVFlag:name = "Flag Indicating Actual or Extrapolated Data" ;
float latDistTobestTrack(observationIndex) ;
latDistTobestTrack:units = "km" ;
latDistTobestTrack:name = "Latitude Distance to Best Track" ;
float lonDistTobestTrack(observationIndex) ;
lonDistTobestTrack:units = "km" ;
lonDistTobestTrack:name = "Longitude Distance to Best Track" ;
float bestTrackLat(observationIndex) ;
bestTrackLat:units = "km" ;
bestTrackLat:name = "Best Track Latitude" ;
float bestTrackLon(observationIndex) ;
bestTrackLon:units = "km" ;
bestTrackLon:name = "Best Track Longitude" ;
int bestTrackVFlag(observationIndex) ;
bestTrackVFlag:units = "*0 - Source*10, 1 - Interpolated, 2 - Extrapolated, 3 - No Data, 4 - Bad Data" ;
bestTrackVFlag:name = "Flag Indicating Actual or Extrapolated Data" ;
float latDistToaircraft(observationIndex) ;
latDistToaircraft:units = "km" ;

```
            latDistToaircraft:name = "Latitude Distance to Aircraft" ;
        float lonDistToaircraft(observationIndex) ;
            lonDistToaircraft:units = "km" ;
            lonDistToaircraft:name = "Longitude Distance to Aircraft" ;
        float aircraftLat(observationIndex) ;
            aircraftLat:units = "km" ;
            aircraftLat:name = "Aircraft Latitude" ;
        float aircraftLon(observationIndex) ;
            aircraftLon:units = "km" ;
            aircraftLon:name = "Aircraft Longitude" ;
        int aircraftVFlag(observationIndex) ;
            aircraftVFlag:units = "*0 - Source*10, 1 - Interpolated, 2 - Extrapolated, 3 -
No Data, 4 - Bad Data" ;
            aircraftVFlag:name = "Flag Indicating Actual or Extrapolated Data" ;
        float latDistToairc_best(observationIndex) ;
            latDistToairc_best:units = "km" ;
            latDistToairc_best:name = "Latitude Distance to Aircraft/Best Track" ;
        float lonDistToairc_best(observationIndex) ;
            lonDistToairc_best:units = "km" ;
            lonDistToairc_best:name = "Longitude Distance to Aircraft/Best Track" ;
        float airc_bestLat(observationIndex) ;
            airc_bestLat:units = "km" ;
            airc_bestLat:name = "Aircraft/Best Track Latitude" ;
        float airc_bestLon(observationIndex) ;
            airc_bestLon:units = "km" ;
            airc_bestLon:name = "Aircraft/Best Track Longitude" ;
        int airc_bestVFlag(observationIndex) ;
            airc_bestVFlag:units = "*0 - Source*10, 1 - Interpolated, 2 - Extrapolated,
3 - No Data, 4 - Bad Data" ;
            airc_bestVFlag:name = "Flag Indicating Actual or Extrapolated Data" ;

// global attributes:
            :storm = "URNT15-<STORM NAME>.nc" ;
            :dataType = "URNT15 message data." ;
            :creationTime = "<yyyymmdd hh:mm:ss" ;
            :cfFileSize =  ;
            :newData = 0 ;
            :centerFixSource =
"AIRC,BEST,DVTS,AMSU,ANAL,SSMI,TRMM,AMSR,SSMS,WSAT,QSCT,ASCT,RDR
C,RDRD,MMHS,UDEF" ;
}
```

APPENDIX 4: REPTN3 NetCDF file format.

```
netcdf REPNT3-<storm name> {
dimensions:
        observationIndex = UNLIMITED ;
        altitudeIndex = 10 ;
variables:
        short aircraftAgencyTag(observationIndex) ;
                aircraftAgencyTag:name = "0 = Airforce, 1 = NOAA" ;
        short aircraftTailNumber(observationIndex) ;
                aircraftTailNumber:name = "Tail Number" ;
        int observationNumber(observationIndex) ;
                observationNumber:name = "Observation Number" ;
                observationNumber:units = "(same number as in original file)" ;
        double unixTime(observationIndex) ;
                unixTime:units = "seconds from 01/01/1970" ;
                unixTime:name = "Unix Time" ;
        float aircraftLatitude(observationIndex) ;
                aircraftLatitude:units = "degrees North" ;
                aircraftLatitude:name = "Aircraft Latitude (Splash Point)" ;
        float aircraftLongitude(observationIndex) ;
                aircraftLongitude:units = "Degrees West" ;
                aircraftLongitude:name = "Aircraft Longitude (Splash Point)" ;
        float latitude(observationIndex) ;
                latitude:units = "degrees North" ;
                latitude:name = "Latitude (Splash Point)" ;
        float longitude(observationIndex) ;
                longitude:units = "Degrees West" ;
                longitude:name = "Longitude (Splash Point)" ;
        double splashTime(observationIndex) ;
                splashTime:units = "seconds from 01/01/1970" ;
                splashTime:name = "Splash Time (primary sort key)" ;
        float pressure(observationIndex, altitudeIndex) ;
                pressure:units = "mbar" ;
                pressure:name = "SurfacePressure" ;
        float airTemperature(observationIndex, altitudeIndex) ;
                airTemperature:units = "degrees Celsius" ;
                airTemperature:name = "Air Temperature" ;
        float dewpoint(observationIndex, altitudeIndex) ;
                dewpoint:units = "degrees Celsius" ;
                dewpoint:name = "Dewpoint" ;
        float windSpeed(observationIndex, altitudeIndex) ;
                windSpeed:units = "kt" ;
                windSpeed:name = "Surface Wind Speed" ;
        float windDirection(observationIndex, altitudeIndex) ;
```

```
        windDirection:units = "degrees wrt North" ;
        windDirection:name = "Wind Direction" ;
float altitude(observationIndex, altitudeIndex) ;
        altitude:units = "m" ;
        altitude:name = "Geopotential Altitude" ;
float wl150WindSpeed(observationIndex) ;
        wl150WindSpeed:units = "kt" ;
        wl150WindSpeed:name = "WL150 Wind Speed" ;
float wl150WindDirection(observationIndex) ;
        wl150WindDirection:units = "deg" ;
        wl150WindDirection:name = "WL150 Wind Direction" ;
float wl150WindHeight(observationIndex) ;
        wl150WindHeight:units = "m" ;
        wl150WindHeight:name = "WL150 Wind Height" ;
float mblWindSpeed(observationIndex) ;
        mblWindSpeed:units = "kt" ;
        mblWindSpeed:name = "Mean Boundary Layer Wind Speed" ;
float mblWindDirection(observationIndex) ;
        mblWindDirection:units = "deg" ;
        mblWindDirection:name = "MBL Wind Direction" ;
float dlmWindSpeed(observationIndex) ;
        dlmWindSpeed:units = "kt" ;
        dlmWindSpeed:name = "Deep Layer Mean Wind Speed" ;
float dlmWindDirection(observationIndex) ;
        dlmWindDirection:units = "deg" ;
        dlmWindDirection:name = "DLM Wind Direction" ;
int dlmTopPressure(observationIndex) ;
        dlmTopPressure:units = "mbar" ;
        dlmTopPressure:name = "DLM Pressure - Top of Layer" ;
int dlmBottomPressure(observationIndex) ;
        dlmBottomPressure:units = "mbar" ;
        dlmBottomPressure:name = "DLM Pressure - Bottom of Layer" ;
int lastWindHeight(observationIndex) ;
        lastWindHeight:units = "m" ;
        lastWindHeight:name = "Height of Last Reported Wind" ;
float latDistTocenterFix(observationIndex) ;
        latDistTocenterFix:units = "km" ;
        latDistTocenterFix:name = "Latitude Distance to Center Fix" ;
float lonDistTocenterFix(observationIndex) ;
        lonDistTocenterFix:units = "km" ;
        lonDistTocenterFix:name = "Longitude Distance to Center Fix" ;
float centerFixLat(observationIndex) ;
        centerFixLat:units = "km" ;
        centerFixLat:name = "Center Fix Latitude" ;
float centerFixLon(observationIndex) ;
        centerFixLon:units = "km" ;
```

centerFixLon:name = "Center Fix Longitude" ;
float centerFixVFlag(observationIndex) ;
centerFixVFlag:units = "*0 - Source*10, 1 - Interpolated, 2 - Extrapolated, 3 - No Data, 4 - Bad Data" ;
centerFixVFlag:name = "Flag Indicating Actual or Extrapolated Data" ;
float latDistTobestTrack(observationIndex) ;
latDistTobestTrack:units = "km" ;
latDistTobestTrack:name = "Latitude Distance to Best Track" ;
float lonDistTobestTrack(observationIndex) ;
lonDistTobestTrack:units = "km" ;
lonDistTobestTrack:name = "Longitude Distance to Best Track" ;
float bestTrackLat(observationIndex) ;
bestTrackLat:units = "km" ;
bestTrackLat:name = "Best Track Latitude" ;
float bestTrackLon(observationIndex) ;
bestTrackLon:units = "km" ;
bestTrackLon:name = "Best Track Longitude" ;
int bestTrackVFlag(observationIndex) ;
bestTrackVFlag:units = "*0 - Source*10, 1 - Interpolated, 2 - Extrapolated, 3 - No Data, 4 - Bad Data" ;
bestTrackVFlag:name = "Flag Indicating Actual or Extrapolated Data" ;
float latDistToaircraft(observationIndex) ;
latDistToaircraft:units = "km" ;
latDistToaircraft:name = "Latitude Distance to Aircraft" ;
float lonDistToaircraft(observationIndex) ;
lonDistToaircraft:units = "km" ;
lonDistToaircraft:name = "Longitude Distance to Aircraft" ;
float aircraftLat(observationIndex) ;
aircraftLat:units = "km" ;
aircraftLat:name = "Aircraft Latitude" ;
float aircraftLon(observationIndex) ;
aircraftLon:units = "km" ;
aircraftLon:name = "Aircraft Longitude" ;
int aircraftVFlag(observationIndex) ;
aircraftVFlag:units = "*0 - Source*10, 1 - Interpolated, 2 - Extrapolated, 3 - No Data, 4 - Bad Data" ;
aircraftVFlag:name = "Flag Indicating Actual or Extrapolated Data" ;
float latDistToairc_best(observationIndex) ;
latDistToairc_best:units = "km" ;
latDistToairc_best:name = "Latitude Distance to Aircraft/Best Track" ;
float lonDistToairc_best(observationIndex) ;
lonDistToairc_best:units = "km" ;
lonDistToairc_best:name = "Longitude Distance to Aircraft/Best Track" ;
float airc_bestLat(observationIndex) ;
airc_bestLat:units = "km" ;
airc_bestLat:name = "Aircraft/Best Track Latitude" ;

```
        float airc_bestLon(observationIndex) ;
                airc_bestLon:units = "km" ;
                airc_bestLon:name = "Aircraft/Best Track Longitude" ;
        int airc_bestVFlag(observationIndex) ;
                airc_bestVFlag:units = "*0 - Source*10, 1 - Interpolated, 2 - Extrapolated,
3 - No Data, 4 - Bad Data" ;
                airc_bestVFlag:name = "Flag Indicating Actual or Extrapolated Data" ;

// global attributes:
                :dataType = "REPNT3 message data - sorted by splash time." ;
                :storm = "REPNT3-<STORM NAME>" ;
                :creationTime = "<yyyymmdd hh:mm:ss" ;
                :cfFileSize =  ;
                :newData = 0 ;
                :centerFixSource =
"AIRC,BEST,DVTS,AMSU,ANAL,SSMI,TRMM,AMSR,SSMS,WSAT,QSCT,ASCT,RDR
C,RDRD,MMHS,UDEF" ;
}
```